AD NUMBER

AD857498

LIMITATION CHANGES

TO:

Approved for public release; distribution is unlimited.

FROM:

Distribution authorized to U.S. Gov't. agencies and their contractors; Critical Technology; JUN 1969. Other requests shall be referred to U.S. Army Aviation Material Laboratories, Fort Eustis, VA 23604. This document contains export-controlled technical data.

AUTHORITY

USAAMRDL ltr, 23 Jun 1971

AD

USAAVLABS TECHNICAL REPORT 68-90C

SINGLE-STAGE AXIAL COMPRESSOR COMPONENT DEVELOPMENT FOR SMALL GAS TURBINES

VOLUME III

SUPERSONIC COMPRESSOR STAGE DEVELOPMENT

By

Charles H. Muller

Leslie R. Cox

June 1969

U. S. ARMY AVIATION MATERIEL LABORATORIES
FORT EUSTIS, VIRGINIA

CONTRACT DA 44-177-AMC-392(T)
CURTISS-WRIGHT CORPORATION
WOOD-RIDGE, NEW JERSEY

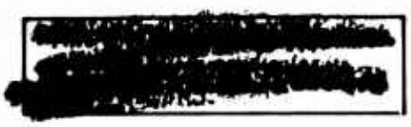

Disclaimers

The findings in this report are not to be construed as an official Department of the Army position unless so designated by other authorized documents.

When Government drawings, specifications, or other data are used for any purpose other than in connection with a definitely related Government procurement operation, the United States Government thereby incurs no responsibility nor any obligation whatsoever; and the fact that the Government may have formulated, furnished, or in any way supplied the said drawings, specifications, or other data is not to be regarded by implication or otherwise as in any manner licensing the holder or any other person or corporation, or conveying any rights or permission, to manufacture, use, or sell any patented invention that may in any way be related thereto.

Disposition Instructions

Destroy this report when no longer needed. Do not return it to the originator.

DEPARTMENT OF THE ARMY
U. S. ARMY AVIATION MATERIEL LABORATORIES
FORT EUSTIS, VIRGINIA 23604

Appropriate technical personnel of this Command have reviewed this report and concur with the conclusions contained herein.

The findings and recommendations outlined herein will be taken into consideration in the planning of future programs for compressors and gas turbine engines.

This is the third volume of a three-volume report.

Task 1G162203D14413
Contract DA 44-177-AMC-392(T)
USAAVLABS Technical Report 68-90C

June 1969

SINGLE-STAGE AXIAL COMPRESSOR COMPONENT DEVELOPMENT FOR SMALL GAS TURBINES

Volume III

Supersonic Compressor Stage Development

by

C. Muller
L. Cox

Curtiss-Wright Corporation
Wood-Ridge, New Jersey

for

U.S. ARMY AVIATION MATERIEL LABORATORIES
FORT EUSTIS, VIRGINIA

SUMMARY

The overall objective of this program is to advance small high-pressure ratio axial compressor technology to the point where an engine designer has sufficient design data to incorporate the axial compressor in a small gas turbine engine.

The design and analysis of a single stage supersonic compressor are reported in Volume I. The development and experimental evaluation of the rotor for this compressor design are reported in Volume II. The development and demonstrated performance of the complete axial stage, including exit stators and interstage connecting duct, are presented herein.

The compressor stage performance is as follows:

	Stage		
	Design Goals	Demonstrated	
Inlet Guide Vane Setting	Design	Design	-4 Degrees
Pressure Ratio	2.8:1	2.69:1	2.62:1
Adiabatic Efficiency (Percent)	82.2	73.9	74.7
Corrected Airflow (Pounds Per Second)	4.0	4.02	4.02
Corrected Speed (Revolutions Per Minute)	50,700	50,700	50,700

The relatively high degree of circumferential variation in rotor exit flow conditions, experienced during the rotor testing under phase II, was reduced to more nearly uniform conditions during the stage tests due to the addition of the exit stators. The rotor performance demonstrated during the stage test shows an improvement over that demonstrated in the rotor tests to the point where it is very close to all goals. The rotor performance is as follows:

	Rotor and Inlet Guide Vanes			
	Design Goals	Demonstrated		
		Phase II	Phase III	
Inlet Guide Vane Setting	Design	Design	Design	-7 Degrees
Pressure Ratio	2.89:1	2.77:1	2.91:1	2.85:1
Adiabatic Efficiency (Percent)	85.2	82.6	80.7	83.9
Corrected Airflow (Pounds Per Second)	4.0	4.01	4.02	3.94
Corrected Speed (Revolutions Per Minute)	50,700	50,700	50,700	50,700

The improvement in rotor and inlet guide vane performance is attributed to the improved circumferential uniformity of the flow conditions and to the advanced inlet guide vane design. The part-speed surge margin was increased significantly in the stage tests, as compared to that indicated by the rotor tests.

The demonstrated exit stator and interconnecting duct total pressure loss at design speed peak stage performance points ranged from 6.5 to 9 percent as compared to a goal of 3 percent and represents the primary performance deficiency for the stage. A flow acceleration, which occurred between the rotor trailing edge and the stator leading edge, caused higher stator losses and prevented the attainment of the desired flow conditions at the stator entrance. Fixed total pressure probes at the rotor exit appeared to introduce an effective aerodynamic blockage which was much greater than expected and thus contributed significantly to this acceleration. The lowest stator and duct loss occurred in a build with only 3 fixed rotor exit probes. The build which achieved the best rotor performance had 2 additional fixed probes at the rotor exit and exhibited higher stator and duct losses; thus, the best rotor performance and lowest stator and duct losses were not achieved in the same build. The design speed pressure loss of the tip section for the stator and duct was measured to be below 3 percent at certain test points, indicating that the design goal is feasible.

Based on the demonstrated rotor performance and the fact that under certain conditions the stator and duct losses at the tip section met the design goal, it is believed that the performance of this compressor stage can be met with further development.

FOREWORD

This work was performed under United States Army Contract DA 44-177-AMC-392(T) (Task 1G162203D14413) by Curtiss-Wright Corporation to advance and demonstrate high-pressure ratio axial compressor technology for small gas turbines. This contract is administered by the Propulsion Division of the U.S. Army Aviation Materiel Laboratories. The phase I effort consisted of the design of a single-stage supersonic axial compressor and test rig and an analytical evaluation of its performance potential as a boost stage for small gas turbine engine compressors. The rotor performance of this compressor was experimentally investigated and developed under phase II. The overall stage performance was experimentally investigated and developed under phase III and is reported herein.

The manager of the small gas turbine engine program was T. Schober, and the manager of this compressor technology contract was C. H. Muller. Principal contributing engineers were L. Cox, W. Litke, and A. Schmitter. The overall guidance and technical direction provided by Mr. A. Sabatiuk, and the direction of Mr. S. Lombardo, are gratefully acknowledged. The guidance of Mr. J. White, Mr. H. Morrow, Mr. E. Johnson and Mr. D. Cale of the U.S. Army Aviation Materiel Laboratories is also gratefully acknowledged.

TABLE OF CONTENTS

LIST OF ILLUSTRATIONS

LIST OF TABLES

LIST OF SYMBOLS

A/A^*	isentropic area ratio - dimensionless
A^*	area at which sonic flow would occur - square inches
A_{ann}	annular area - square inches
A_{flow}	flow area - square inches
a	acoustic velocity (based on static temperature) - feet per second
a_t	acoustic velocity (based on total temperature) - feet per second
C_p	specific heat for a constant pressure process - BTU per pound per degree Rankine
D	diameter - inches
D_m	mean diameter - inches
g	acceleration of gravity - feet per second squared
h	hub streamtube
IC	iron-constantan thermocouple
ID	inside diameter - inches
i	incidence angle - degrees
i'	modified incidence angle - degrees
J	work constant (778 foot-pounds per BTU)
K	continuity equation constant (0.26048 pound square root of degree Rankine per second per square inch per inch of mercury)
k	spring rate - pounds per inch
M	Mach number - dimensionless
m	mean streamtube
N	rotational speed - revolutions per minute
OD	outside diameter - inches
P_s	static pressure - inches of mercury

P_T total pressure - inches of mercury

R radius of curvature in meridional plane - inches; (or gas constant, 53.4 foot-pounds per pound per degree Rankine, when it occurs in the expression $\sqrt{KgRT_s}$)

REC total pressure recovery - ratio of total pressure remaining after losses through blade row passage to initial total pressure at blade row inlet - dimensionless

r radius from compressor axis - inches

T_s static temperature - degrees Rankine

T_T total temperature - degrees Rankine

t tip streamtube

t_c ratio of maximum blade thickness to the chord length

U rotor blade section speed - feet per second

V velocity - feet per second

V_{ax} axial velocity component - feet per second

V_{tan} tangential velocity component - feet per second

W airflow - pounds per second

α tangential airflow angle relative to the compressor axis - degrees

β tangential angle to blade camber line - degrees

β' tangential angle to blade suction surface - degrees

δ deviation angle - degrees (or ratio of local total pressure to a reference pressure, when occurs in $(W\sqrt{\theta})/\delta$ - dimensionless)

Δ change of a quantity across a blade row - dimensionless

ξ airflow slope angle in meridional plane - degrees

η_{ad} adiabatic efficiency - dimensionless

γ ratio of specific heats - dimensionless

ϕ blade camber angle - degrees

ρ density - pounds per cubic foot

θ air turning angle through a blade row - degrees (or ratio of local total temperature to a reference temperature, when it occurs in either $N/\sqrt{\theta}$ or $(W\sqrt{\theta})/\delta$ - dimensionless)

Subscripts

amb ambient conditions

0 station at entrance to inlet guide vanes

1 absolute conditions (relative to nonrotating reference) at a station representing exit of inlet guide vanes and inlet to rotor

2 entrance conditions to rotor relative to the rotating rotor blade

3 exit conditions from the rotor relative to the rotating rotor blade

4 absolute conditions (relative to nonrotating reference) at a station representing the rotor exit and inlet to the exit stator

5 absolute conditions at a station representing the exit of the exit stator and interconnecting duct

INTRODUCTION

The objective of the U.S. Army Aviation Materiel Laboratories in the field of small gas turbine engines is to advance the technology in the major component areas to the point where a small gas turbine engine can be designed to provide a nonregenerated engine with a specific fuel consumption of less than 0.460 pound per horsepower per hour. The compressor component required to make this performance goal possible must be capable of high pressure ratio (16:1 range) at good component efficiencies and, in addition, must be designed for simplicity, ruggedness, durability, and minimum cost.

The objective of this program is to advance high pressure ratio axial compressor technology to the level that, when matched analytically with advanced centrifugal compressor technology, will provide a 16:1 compressor which offers the desired engine performance. Specifically, this program is to develop a supersonic axial compressor to serve as the boost or supercharging stage. Since the part-power performance of these engines is also critical, several studies have been included in the program to gain some insight into the important off-design parameters and trade-offs which should influence the axial compressor development when considered in the overall compressor and engine operation.

The program was scheduled in three phases. Phase I involved (1) the design of the supersonic axial stage compressor and test rig; (2) an analytical study to evaluate the performance potential and characteristics of various compressor and engine configurations; and (3) the preliminary design of an advanced 16:1 axial/centrifugal compressor, an advanced gas generator incorporating this compressor, and a variable-geometry compressor rotor. In phase II the inlet guide vanes and compressor rotor were procured and developed through experimental testing. In phase III the exit stator and interconnecting duct design was finalized and fabricated, and the overall stage performance was evaluated through experimental testing, including a modification of the exit stator. Also in the final phase, an advanced inlet guide vane was designed and fabricated, and its effect on overall stage performance was evaluated in the testing of the compressor stage.

The supersonic axial compressor selected and designed under phase I of the program is a single-stage shock-in-rotor type of compressor with stage performance goals of 2.8:1 pressure ratio, 82.2 percent adiabatic efficiency, and 4.0 pounds per second corrected airflow. The performance goals for the rotor with inlet guide vanes, but without exit stators or interconnecting duct, are 2.89:1 pressure ratio, 85.2 percent adiabatic efficiency, and 4.0 pounds per second corrected airflow.

Phase I was completed in September 1966. The compressor design procedures, criteria, predicted performance, and results of various analytical studies performed are presented in Volume I of this report.*

* Single-Stage Axial Compressor Component Development for Small Gas Turbine Engines (U), Vol I, USAAVLABS Technical Report 68-90A, U.S. Army Aviation Materiel Laboratories, Fort Eustis, Virginia (Confidential report).

Phase II was completed in May 1967. The purpose of this phase was to evaluate the compressor rotor performance, when tested with the inlet guide vanes but without exit stators, and to develop the rotor to an acceptable performance level prior to finalizing the exit stator design. The results of the experimental testing and data analysis performed under the tasks of this phase are presented in Volume II of this report.* The rotor test results were used to finalize the exit stator design and to analyze the results of the initial experimental stage performance tests performed under phase III of the program.

Phase III was completed in December 1968. The purpose of this phase was to conduct experimental testing of the complete compressor stage in order to evaluate the performance of the exit stator and interconnecting duct, the performance of the rotor and inlet guide vanes when tested with the exit stator, the performance of an advanced inlet guide vane design, and the overall performance of the compressor stage. The design data for the finalized exit stator and interconnecting duct and for the advanced inlet guide vane, together with the results of the experimental testing, are reported herein.

* Single-Stage Axial Compressor Component Development for Small Gas Turbine Engines, Vol II, USAAVLABS Technical Report 68-90B, U.S. Army Aviation Materiel Laboratories, Fort Eustis, Virginia.

EXIT STATOR AND INTERCONNECTING DUCT FINAL CONFIGURATION AND FABRICATION

FINAL DESIGN

The preliminary design of the exit stator and interconnecting duct was performed under phase I of the program and is presented in Volume I of this report under the section entitled Supersonic Axial Compressor.[c] In this preliminary design, the overall exit stator and interconnecting duct configuration and inlet and exit dimensions were established. The flow path, blade angles, and area schedule were established to match the design point rotor exit conditions and airflow. The resultant flow path and blade section along the main streamline are presented in Figure 34 of Volume I; the area and Mach number schedules, in Figure 35 of Volume I. The total pressure loss was estimated to be 3 percent, and this was the performance goal for the stator and interconnecting duct.

The purpose of the subject task under phase III was to review and if necessary modify the stator and duct design after the rotor test data from phase II were available and to complete the detail design drawings of the blade sections, shroud contours, and rig attachment surfaces for fabrication.

Analysis of the rotor test results indicated that the circumferential variation in the back pressure level which occurred prevented the demonstration of the design flow angles and Mach number at the rotor exit. Figure 1 is a comparison of the measured flow angle radial distribution with the design flow angle radial distribution at the rotor exit and stator entrance. The measured angle is from 3 to 6 degrees lower than the design. It was concluded, however, that the design values could be met under uniform circumferential conditions and that the addition of the exit stator was expected to provide this uniformity. On this basis it was decided not to modify the preliminary design. The effect on the performance of the stator design for the measured flow angles was also analyzed in the event that the expected improvements did not occur. The air angles measured in the rotor testing are approximately 3.5 to 6.5 degrees below the design angles (an increase in angle would accompany the expected increase in performance in the stage tests). The leading-edge wedge angle of the exit stator airfoil is 6 degrees. The design incidence angle is 0 degrees with respect to the expansion surface of the blade (referred to as the modified incidence angle) or +3 degrees to the mean camber angle. Even though the average incidence angle (relative to the mean camber angle) indicated by the measured air angles is 5 degrees below the design incidence of +3 degrees, a positive flow incidence to the compression surface is still indicated. On this basis the exit guide vane design was expected to provide acceptable performance over the possible range of incidence angles and still maintain the desired margin for improved rotor performance.

The final stacking of the stator airfoils resulted in only a small deviation from the original area schedule. The final area schedule, Mach number, and static pressure distribution are presented in Figure 2.

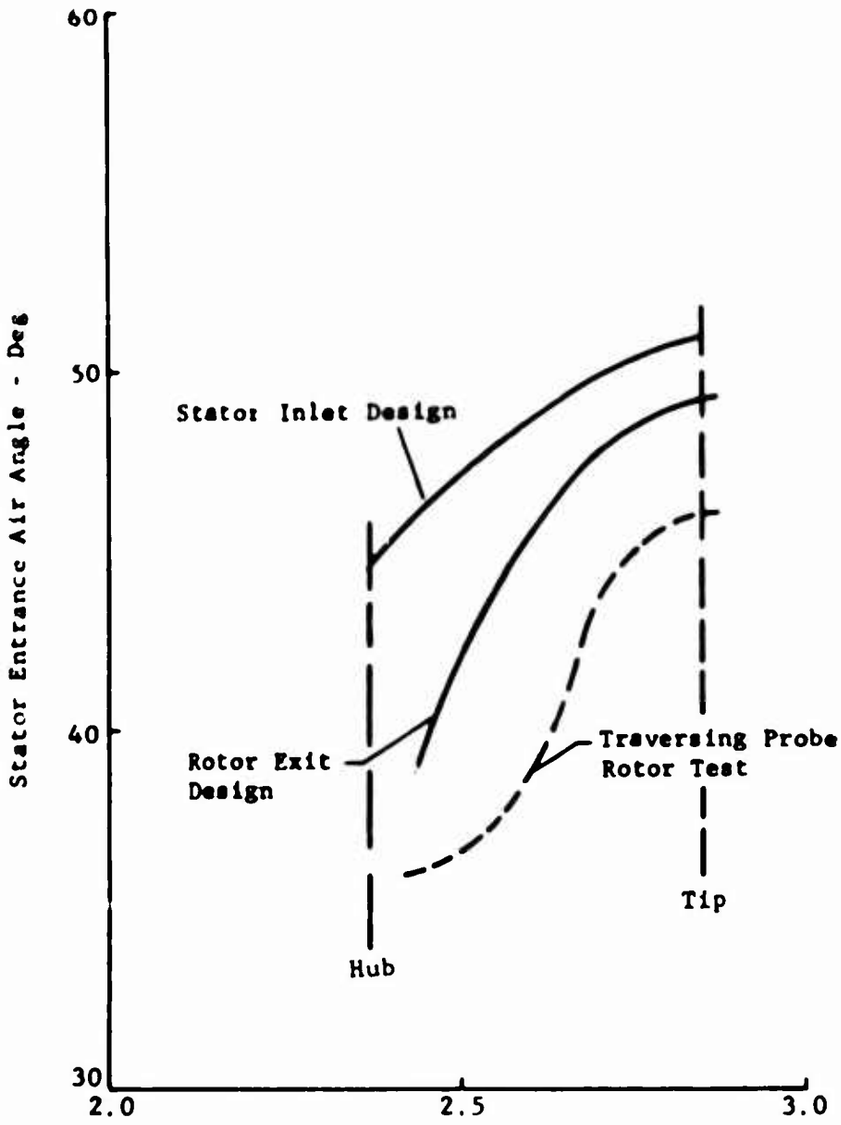

Figure 1. Measured Rotor Exit Air Angle Compared to the Design Angles.

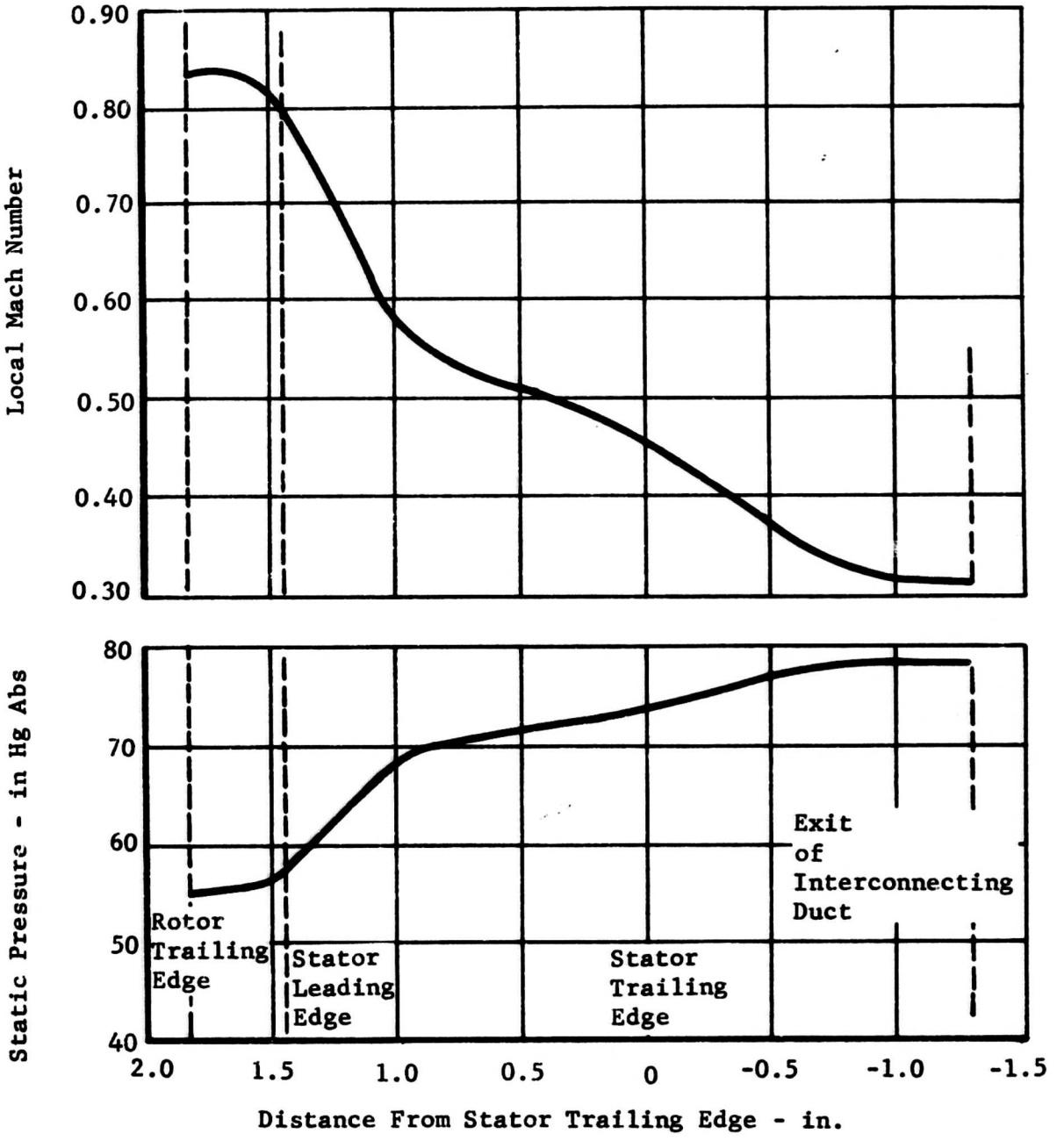

Figure 2. Final Design Mach Number and Static Pressure Schedule for the Exit Stator and Interconnecting Duct.

FABRICATION

The exit stator vanes were machined as an integral part of the inner shroud, and the outer shroud was brazed to the vane tips. Figures 3 and 4 show these components before brazing. This fabrication approach eliminates the pressure losses associated with airfoil end clearances and provides structural support through the stators which stiffens the spring rate of the rear bearing support system.

An oven silver braze process was used to join the outer shroud to the blade tips. This process satisfied the conditions of low enough temperatures, so as not to cause airfoil distortion, and extremely small airfoil to shroud fillets. The resulting fillets were of less than 0.010 inch radius. The small fillet size was considered to be critical in the stator passages since area reductions of 0.5 percent could lead to a choking of the flow when entrance Mach numbers in excess of 0.9 are possible. A .03-inch fillet represents an area reduction of .3 percent.

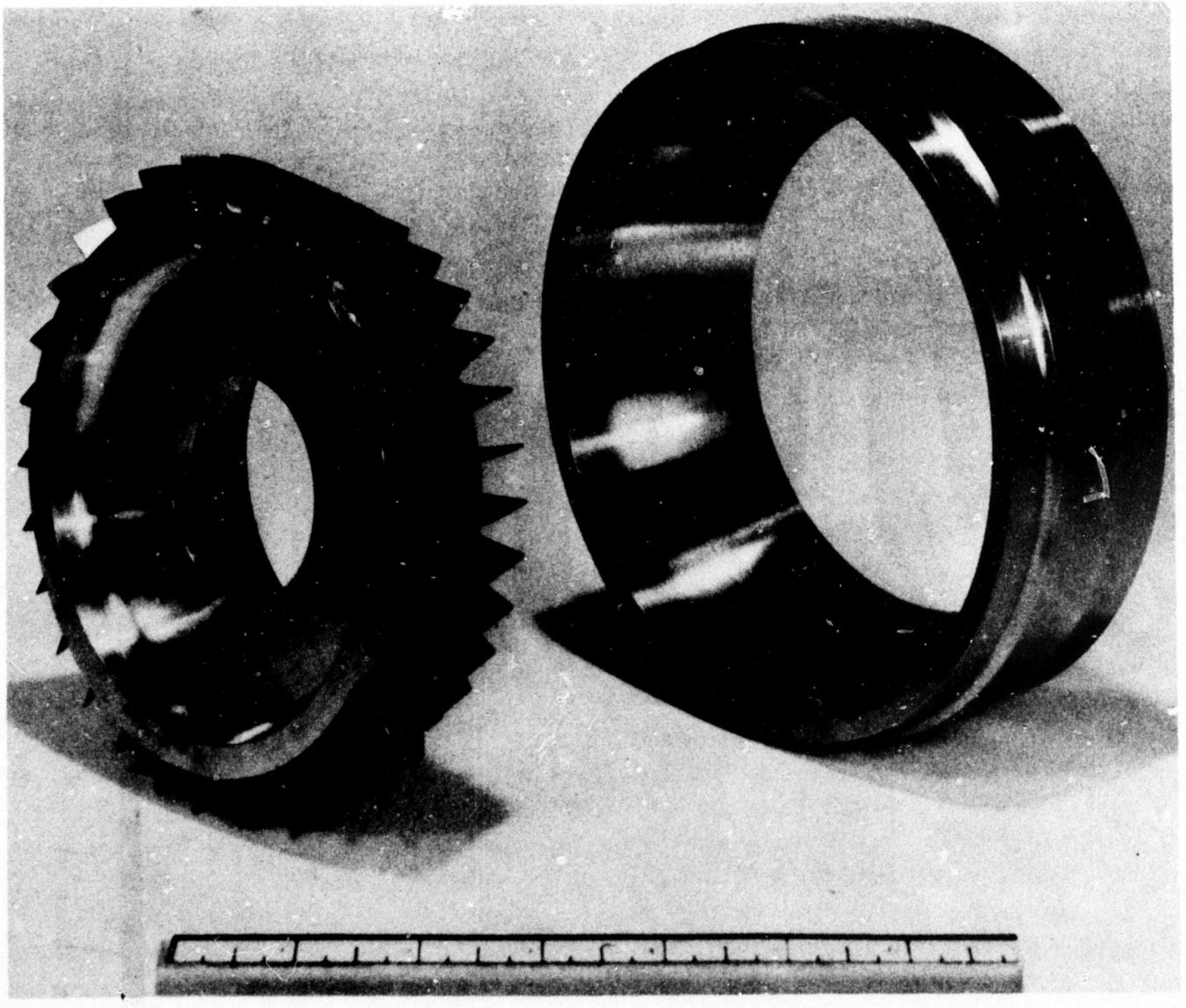

Figure 3. Exit Stator and Interconnecting Duct Assembly - Exploded View

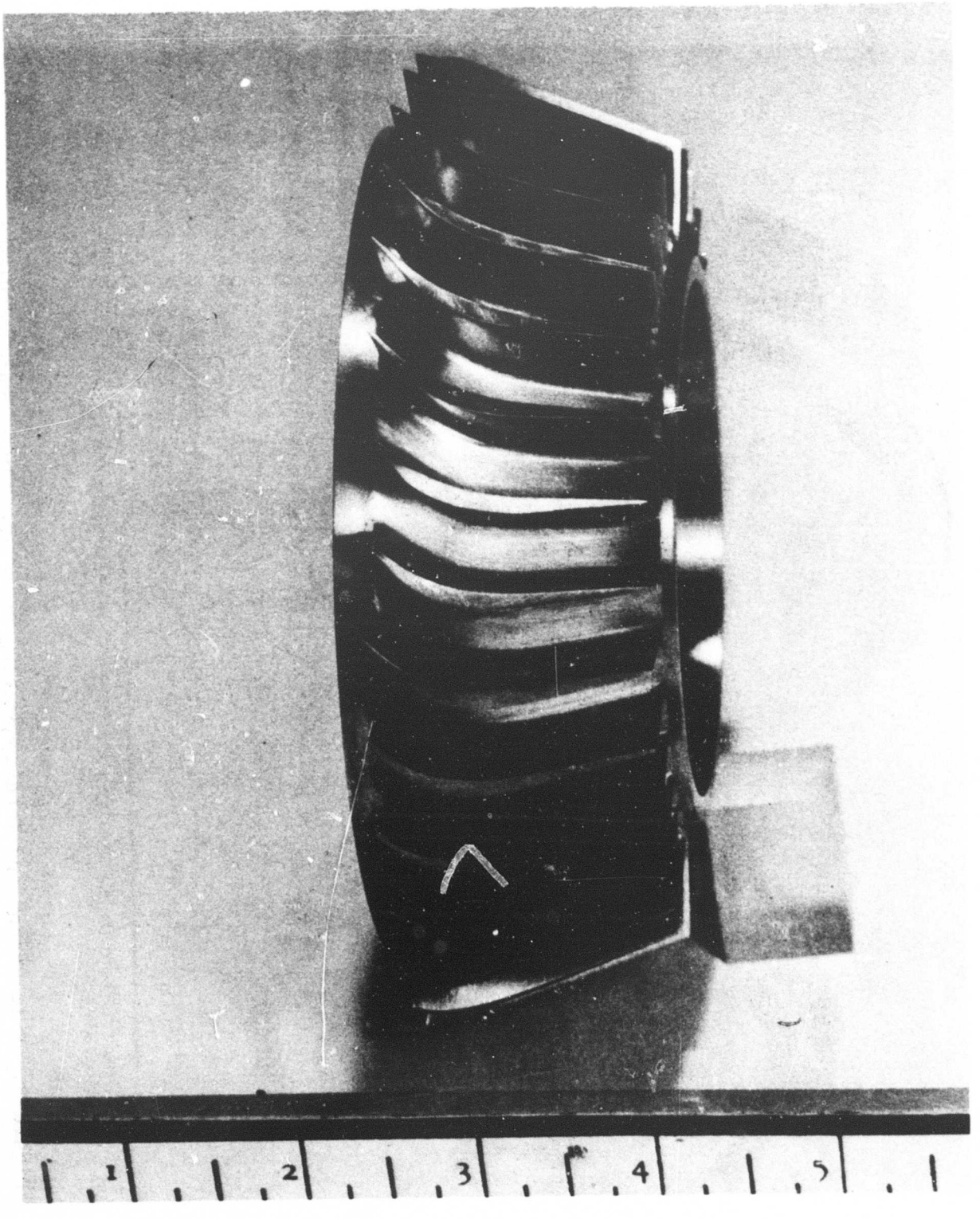

Figure 4. Exit Stator Vanes and Inner Shroud - Side View

STAGE TEST WITH NACA 65 SERIES INLET GUIDE VANES

Builds 6 and 6A of the compressor were tested under this task and included the first exit stator and interconnecting duct.

TEST CONFIGURATION

The compressor configuration for this test consisted of the inlet guide vanes, the compressor rotor, and the exit stator and interconnecting duct. The configuration is shown in Figure 5. The geometric data pertinent to the compressor aerodynamics are summarized in Table I for each compressor build.

Inlet Guide Vanes

The inlet guide vanes (IGV) were the same NACA 65 airfoil series vanes used in the phase II rotor testing and were positioned at the design setting.

Rotor

A new rotor (S/N 3) was fabricated for this test. The airfoil geometry of this rotor was made to the same specifications as the first rotor (S/N 1) tested in phase II. The angle of the leading edge expansion surface was reworked to the specifications of configuration 2, as was rotor S/N 2; however, the inspection data indicated that this angle was from .3 to .6 degree smaller than that of the first rotor (S/N 1). The tip diameter at the leading edge was 6.308 inches.

Shroud

The rotor shroud used in these builds was made to the same specifications as that in build 2 and had an abradable coating on the inner surface.

Tip Clearance

The nominal static tip clearance was set at .012 inch, which is constant from leading to trailing edge. The circumferential variation in tip clearance was less than .0015 inch.

Instrumentation

The test instrumentation is described in Appendix I, the Phase III Test Plan. The radial traversing probe at the 157 degree circumferential location was not installed for the initial testing in this build. Subsequent to the preparation of the test plan, the decision was made to include the following two sets of additional instrumentation:

1. Three fixed single-element probes to measure rotor pressure ratio. The probes were equally spaced every 120 degrees circumferentially and were located at station 4 between the trailing edge of the rotor and the leading edge of the exit stator. Their radial distance from the outer wall was .220 inch (mid streamtube) and set at approximately the design flow angle (α = 50°).

2.8:1 Supersonic Compressor

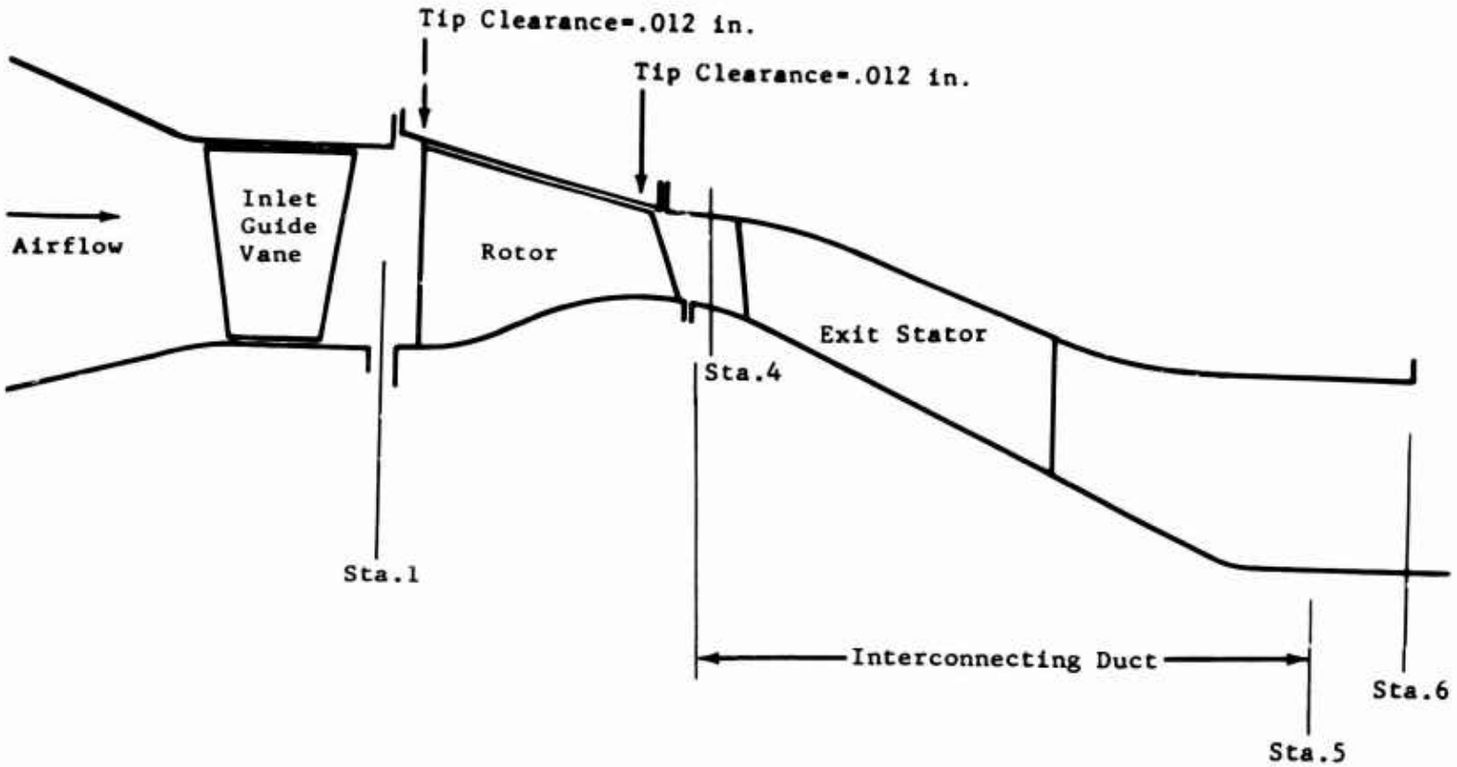

Figure 5. Compressor Flow Path for Builds 6 and 6A.

TABLE I. 2.8:1 SUPERSONIC COMPRESSOR EXPERIMENTAL HARDWARE DATA

	Build No.					Build No.								
	1	2	3	4	5	6	6A	7	8	9	10	10A	11	12
	← PHASE II →					← PHASE III →								
IGV:														
Type	NACA 65 Series							Developed Airfoil						
Setting	Design	Design	Design	+6°	-8°	Design	Design	Design	-4°	+7°	-4°	-4°	-7°	Design
Rotor														
Serial No.	S/N 1	S/N 2				S/N 3	S/N 3	S/N 4			S/N 5			
Configuration No.	1	2	3			4	4	5			6			
Leading Edge:														
Expansion Angle	1° Design	0.6° < Design				1° > Design					0.6° - 1.3° < Design			
Thickness	.007 - .015	.006 - .010				.005 - .010	.005 - .010	.008 - .010			.006 - .012			
Condition	New	New	3 Blades Cut Back			New	New	New	Nicked Blades		New			
Tip Clearance (Static)														
Leading Edge	.008	.008	.020			.012	.012	.013			.013			
Trailing Edge	.018	.018	.017			.012	.012	.011			.011			
Stator														
Serial No.	None					S/N 1		S/N 2						
Configuration No.						1		1			2			

2. Three fixed nine-element pitot rakes were installed at the stage exit plane (station 5) to measure the stator blade wakes. The elements of each rake were aligned along a direction tangential to a circle about the compressor axis and were equally spaced so that the total width was slightly more than the exit width of two blade passages (twice the blade-to-blade pitch) of the exit stator. The rakes were located at each of three radial distances (.220 inch, .420 inch, and .500 inch) from the outer shroud wall to represent tip, mean, and hub streamtube locations.

DESCRIPTION OF TEST

Data points were obtained along speed lines of 50, 60, 72, 80, 85, 90, and 95 percent for build 6. High vibrations were encountered at that point; they were later found to be due to a loose bearing race. The rig was disassembled, and the loose fit of the race was corrected. The compressor configuration was not changed in the subsequent build, 6A.

Data points were obtained for build 6A along the 80, 90, 95, and 100 percent speed lines. The compressor was throttled all the way to surge at 80 and 90 percent speeds only. The plan was to obtain performance data at all speeds before investigating the complete surge line. Testing was terminated before the 100-percent speed line was completed. Following the last data point, an excessive throttle change was made in attempting to set a higher pressure ratio, and the compressor was driven into surge. At that point, a failure occurred in the front support strut joints of the test rig.

TEST RESULTS

The performance data obtained during the testing of builds 6 and 6A included a complete set of measurements from the fixed total pressure pitot probes, the stagnation thermocouples, and the static pressure taps at each test point, and the traversing probe data at selected test points. With the exception of the surge line at the high speeds and the peak performance at design speed, a complete performance map was developed.

The results provided an adequate baseline of stage performance with the NACA 65 series airfoil IGV for evaluating the effects on performance of the advanced developed airfoil IGV scheduled for testing in the following build.

The overall performance of the exit stator and interconnecting duct was also established.

The key performance and parametric design speed data are summarized in Table II for each build.

TABLE II. 2.8:1 SUPERSONIC COMPRESSOR PERFORMANCE DATA SUMMARY

Build	IGV Setting	IGV Type	% $N/\sqrt{\theta}$	Max. $W\sqrt{\theta}/\delta$	Rotor + IGV P_T/P_T A	H	M	T	η	Rotor + IGV $\Delta T/\theta$ H	M	T	P_s/P_s Rotor Shroud	Sta. 1 O.D.	Sta. 1 I.D.	Exit M_m	Stator $\Delta P_T/P_T$ A	H	M	T	Exit Mach No. A	H	M	T	Stage P_T/P_T	η
Design Pt.	Design		100	4.016	2.89	2.86	2.91	2.90	85.2	207.2	217	223		2.38	2.31	.847	.03				.315				2.8	82.2
1	Design	NACA 65 Series	90	3.49	2.37	2.41	2.39	2.32	84.3	165	172	177														
2	Design	NACA 65 Series	90	3.66	2.31	2.34	2.33	2.27	82.8	161	172	174														
3	Design	NACA 65 Series	90	3.66	2.28	2.36	2.30	2.17	81.2	165	173	181														
3	Design	NACA 65 Series	100	4.02	2.77	2.92	2.78	2.62	82.6	201	212	225	1.87	1.93	1.96	.956										
4	+6°	NACA 65 Series	100	3.80	2.78	2.96	2.72	2.66	79.0	203	220	228														
5	-8°	NACA 65 Series	90	3.45	2.18	2.27	2.15	2.11	79.2	142	153	160														
6A	Design	NACA 65 Series	100	3.79	2.795		2.795		80.0		223.6		2.28	2.24	2.20	.857	.065				.335				2.61	73.7
7	Design	Developed Airfoil	100	3.73	2.82	2.95	2.74	2.82	79.6	219	224	228	2.16	2.06	2.06	.93	.078	0.11	.062	.057	.340	.36	.32	.40	2.60	72.4
8	-4°	Developed Airfoil	100	3.70	2.79	2.89	2.71	2.77	82.0	211	215	218	2.09	1.98	1.93	.94	.081	.095	.08	.070	.340	.37	.30	.41	2.57	74.4
9	+7°	Developed Airfoil	100	3.72	2.82	3.00	2.80	2.67	74.4	235	240	243	2.18	2.11	2.20	.93	.078	.13	.09	.01	.340	.32	.32	.43	2.60	67.6
10A	-4°	Developed Airfoil	100	4.08	2.87	2.96	2.80	2.84	82.7	215	217	224	2.25	2.01	2.0	.99	.085	.099	.075	.079	.41	.42	.38	.44	2.62	74.7
11	-7°	Developed Airfoil	100	4.02	2.85	2.95	2.81	2.82	83.9	210	214	220	2.21	1.91	1.98	.98	.091	.104	.096	.085	.40	.40	.37	.44	2.59	74.8
12	Design	Developed Airfoil	100	4.07	2.91	3.05	2.83	2.85	80.7	225	227	232	2.34	2.11	1.97	.99	.075	.091	.065	.068	.44	.47	.42	.45	2.69	73.8
12	Design	Developed Airfoil	101	4.09	2.97	3.10	2.90	2.91	80.5	230	233	237	2.38	2.12	1.99	1.03	.090	.081	.075	.074	.41	.40	.40	.44	2.70	72.6

Stage Performance

The predicted stage performance map is shown in Figure 6. Figure 7 is the experimental stage performance map. These data represent the performance from the inlet duct to the stage exit plane (station 5). The peak stage performance demonstrated at each speed is presented in Table III and compared to the design predictions.

TABLE III. STAGE PERFORMANCE DEMONSTRATED IN BUILDS 6 AND 6A COMPARED TO PREDICTED PERFORMANCE

	Percent Speed						
	50	60	70	80	90	95	100
Stage Pressure Ratio							
Predicted Peak	1.27	1.41	1.60	1.84	2.26	2.56	2.80
Data Peak	1.27	1.45	1.65 (72%)	1.92	2.27	2.43	2.61*
Efficiency							
Predicted Peak	80.2	83.5	83.3	82.7	82.5	82.4	82.2
Data Peak	75.5	79.7	73.8	76.6	77.3	75.3	73.2*

*Performance degraded by nickled blades

The predicted pressure ratios were met through 90 percent of design speed. The adiabatic efficiencies ranged from 6 to 11 points below the design predictions. The highest stage pressure ratio and adiabatic efficiency demonstrated at design speed was 2.61:1 at 73.2 percent.

The design speed airflow was 5 percent below the design goal of 4.0 pounds per second as expected. The results of the rotor testing under phase I had established the relationship between the leading edge expansion surface angle of the rotor and the induced airflow. The airflow induced in the build 6A stage test was consistent with that relationship for the expansion surface angles of the unmodified rotor. The results establish that the exit stator and interconnecting duct do not limit the airflow capacity of the rotor and IGV.

Figure 8 presents the distribution of measured static pressure rise through the compressor stage.

Inlet Guide Vane Performance

The performance of the NACA 65 airfoil series guide vanes in this test was consistent with that established in the phase I rotor testing. The static pressure data measured at the exit of the guide vanes are compared to the design values in Figure 9 and are seen to be only slightly higher. The measured airflow was 5 percent low at design speed,which should have resulted in a static pressure level .9 inch of mercury higher than the

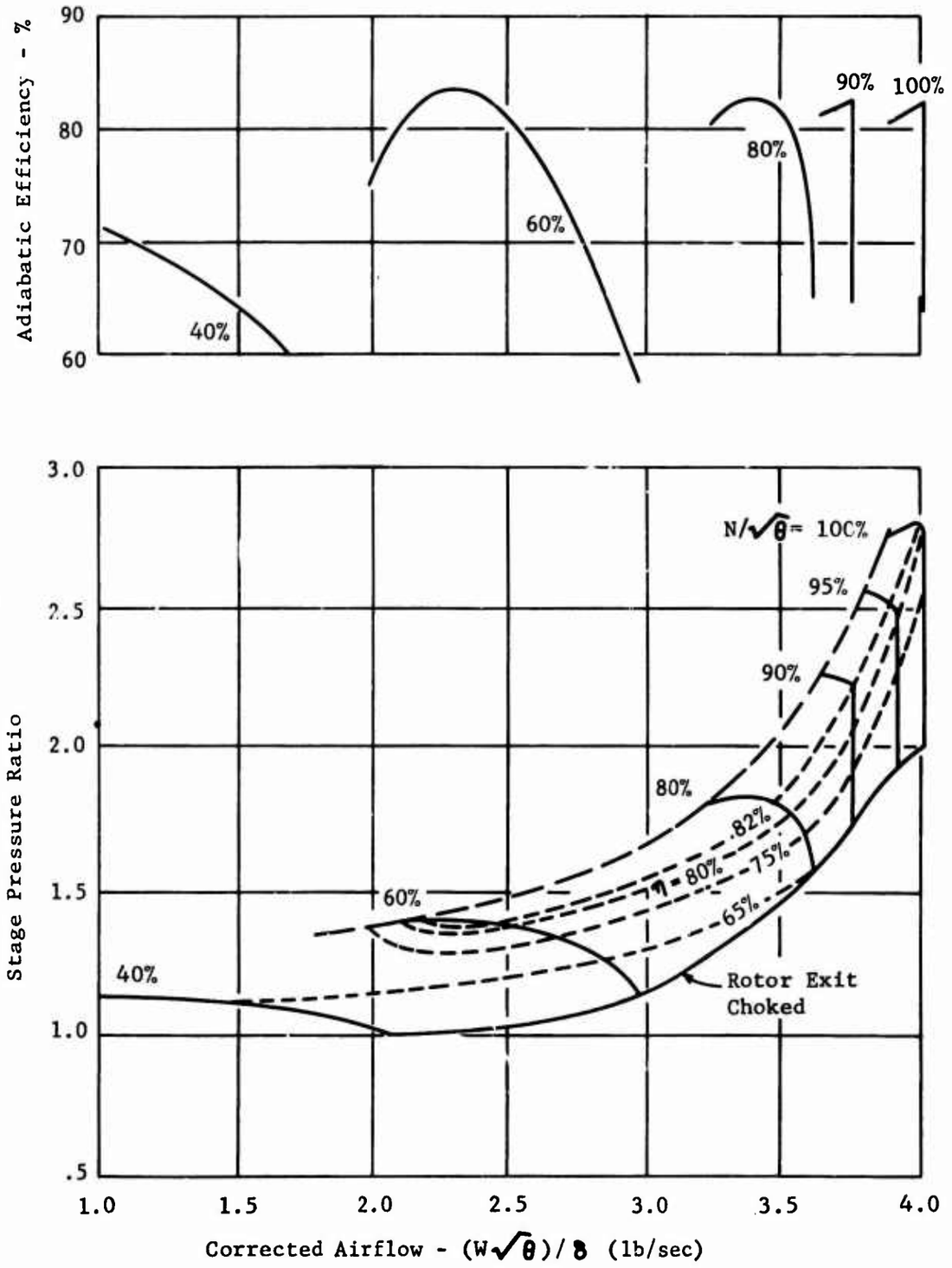

Figure 6. 2.8:1 Supersonic Compressor Predicted Stage Performance Map.

Rotor Configuration 4, Stator Configuration 1

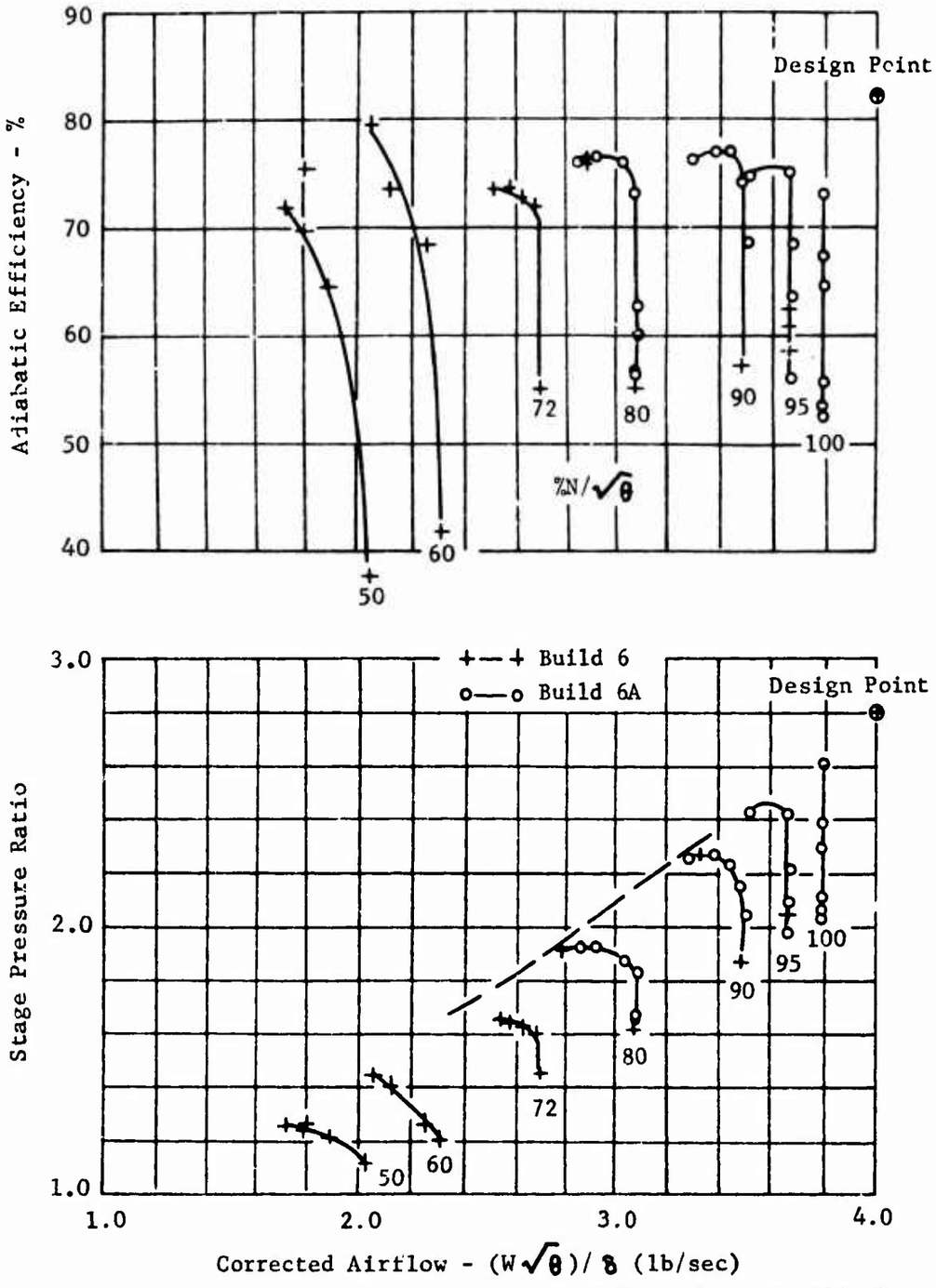

Figure 7. 2.8:1 Supersonic Compressor Test Stage Data, Builds 6 and 6A, NACA 65 Series IGV at Design Setting.

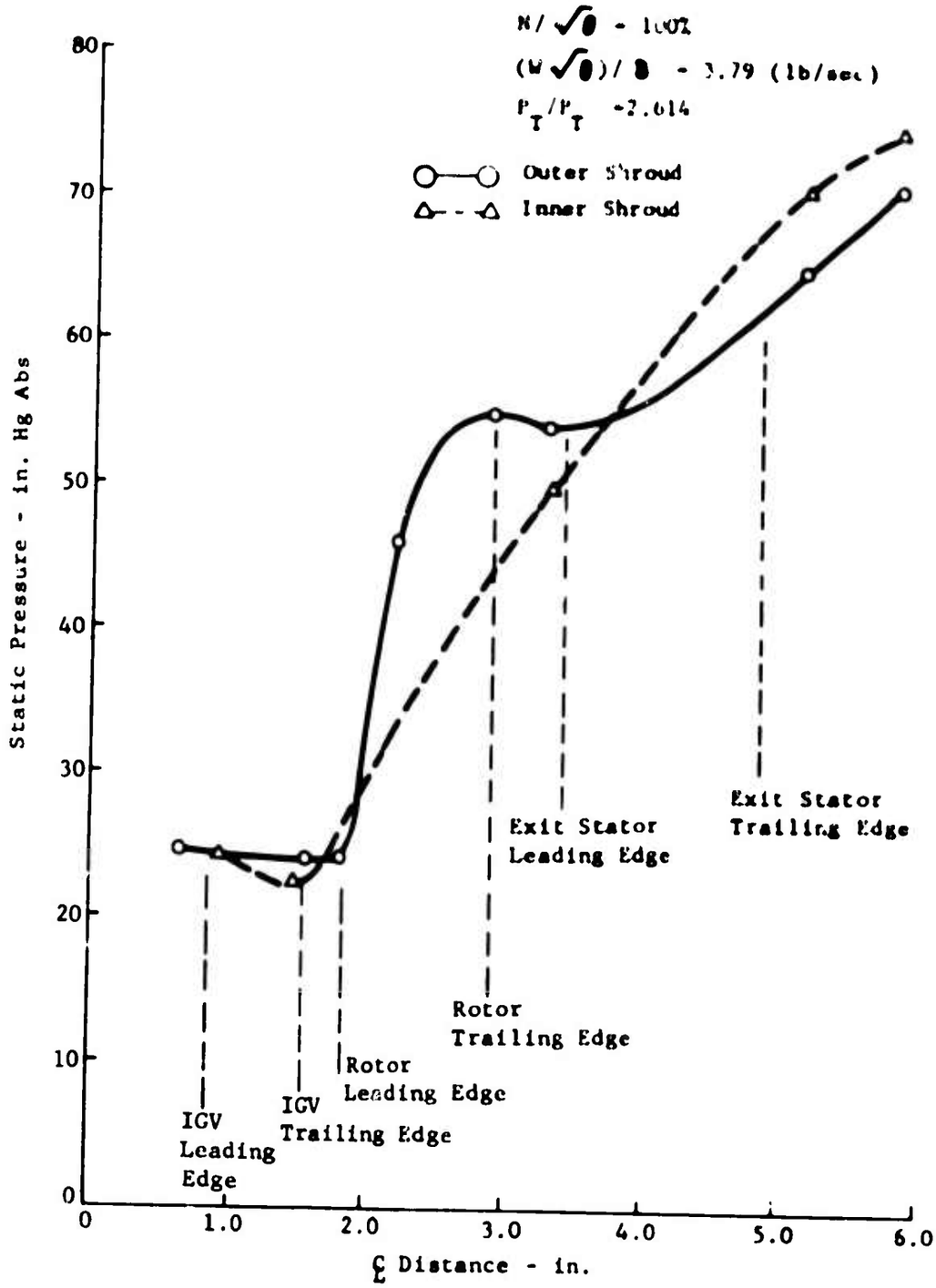

Figure 8. Build 6A Test Data, Static Pressure Distribution Versus Axial Distance Through Compressor.

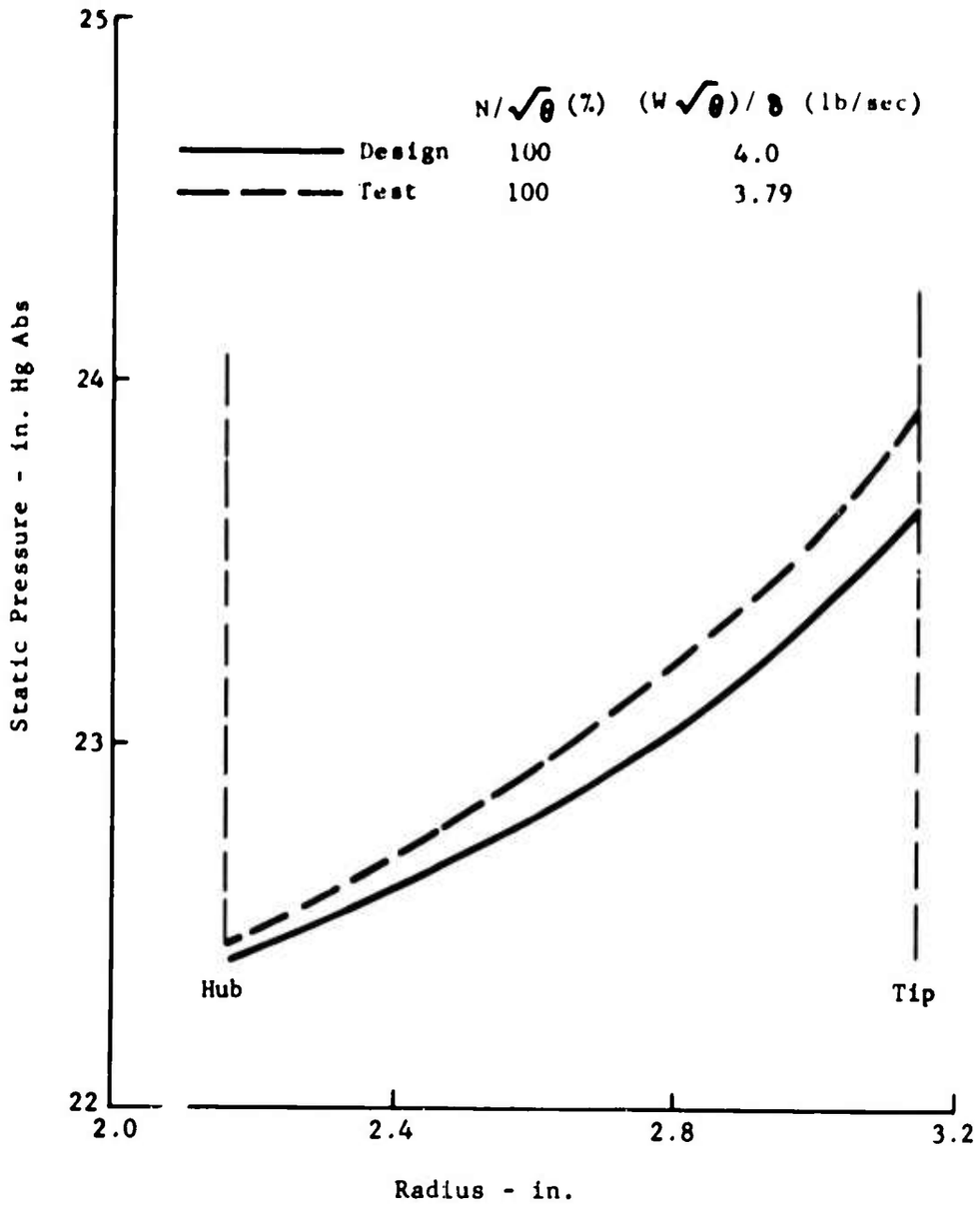

Figure 3. Build 6A Test Data, Static Pressure at IGV Trailing Edge Compared to Design.

design value. The lower level of the data indicates that the boundary layer and blade wake effects are higher than accounted for in the design.

Rotor Performance

The experimental performance map for the rotor and inlet guide vane is presented in Figure 10. A design speed pressure ratio of 2.79:1 at an 80 percent adiabatic efficiency was demonstrated. The rotor exit total pressure was measured at the mid streamtube only, and this value was used to compute the average rotor pressure ratio. The results of the rotor testing in phase II showed that the mid streamtube pressure ratio was a close approximation of the average rotor pressure ratio. The peak rotor pressure ratios for each speed line were equal to or slightly higher than those demonstrated in phase II. The 2.79:1 pressure ratio at design speed, which was not yet at the peak, was also slightly above the phase II peak value of 2.77:1. The peak adiabatic efficiencies for speeds of 80 percent through 95 percent were within 1.0 point of the phase II data. The design speed efficiency of 80 percent was 2.5 points below the phase II peak but had not reached the peak. At speeds of 70 percent and below, peak efficiencies were 5 to 10 points lower than those in phase II.

The data analysis computer program, described in the Phase III Test Plan (Appendix I), was run to evaluate the vector diagrams. The solutions from this program resulted in static pressure differences between the inner and outer shroud at the rotor exit that were considerably higher than the measured differences. The streamline flow paths established by the program and the corresponding static pressure gradients which satisfied radial equilibrium were, therefore, not a valid representation of the actual flow conditions. An alternate computer program was used subsequently to establish the vector diagrams. The inputs for this latter program are the rotor absolute inlet and outlet Mach numbers at given radii for each of three streamtubes, the IGV exit flow angle distribution, and the exit temperature profile. The streamtube radii at the rotor inlet and outlet were defined as established for the design case. The streamline paths of the phase II data analysis computer solutions indicated that the relationships between the inlet and outlet radii for the three respective streamtube locations do not differ significantly from the design values. The rotor exit Mach numbers at each of the streamtube radii were determined from the ratio of the measured static pressure to the measured total pressures at station 4. A linear static pressure gradient was used between the measured inner and outer shroud values to obtain the values of the streamtube radii. For the data from Build 6A, the total pressure was extrapolated to the streamtube radii by passing a profile through the measured mid streamtube pressure, which was assumed to follow the profile established in the phase II testing. The total temperature radial distribution at the rotor exit was assumed to be the same as that measured at the stage exit. This latter assumption implies negligible heat loss from, or heat transfer within, the airflow as it passes through the exit stator and interconnecting duct. The inlet Mach numbers were also determined from the ratio of static to total pressure at the three streamtube radii. The measured static pressures were assumed to have a linear radial gradient between the inner and outer

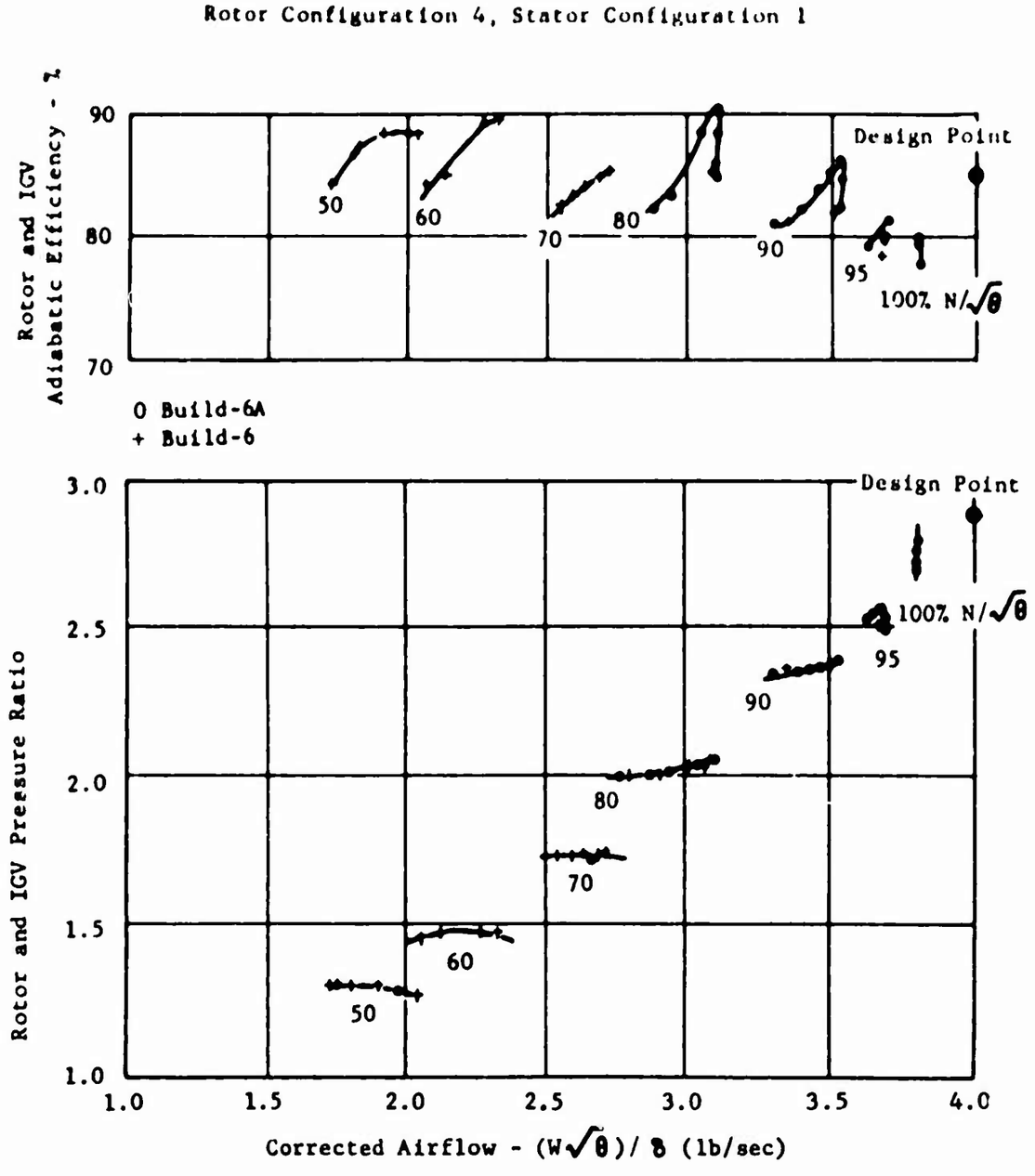

Figure 10. 2.8:1 Supersonic Compressor Stage Test, Build 6A Rotor Performance Data, NACA 65 Series IGV at Design Setting.

shroud. The total pressure was calculated from the design loss coefficient and the measured airflow.

Figure 11 shows the vector diagrams for the design speed test point and compares them to the design point vectors. The modified incidence for the inlet test data is 1.6 degrees, which is within .7 degree of the 2.3-degree value established in phase II for an attached supersonic flow condition. The accuracy of the calculated incidence can account for .7 degree difference when the accumulated tolerances of the metal angle measurement, the IGV setting, and the flow angle calculations are considered.

The rotor exit absolute flow angles at the hub and mid sections are within 1.5 degrees of the design values, while the tip is 6 degrees higher than design. The outer shroud static pressure at the rotor trailing edge is about 1.0 inch of mercury higher than at station 4, which indicates a slightly lower Mach number at that point and a slightly higher flow angle. The exit Mach number at the mid streamtube is within .01 of the design value, while the hub is .03 higher and the tip is .02 lower than their design value.

The demonstrated static pressure ratio across the rotor to station 4 was 2.24:1 at the outer shroud and 2.20:1 at the inner shroud. This was a significant increase from the phase II results but still short of the goals of 2.38:1 and 2.31:1 respectively. The static pressure ratio to the trailing edge of the rotor was 2.29:1 at the outer shroud which is closer to the design value. The decrease in static pressure between the rotor trailing edge and station 4 indicates that some reacceleration occurs. It should be noted that the test was terminated before the design speed peak performance had been reached and therefore the static pressure ratio is not the peak value.

The rotor exit conditions were much nearer to being circumferentially uniform than in the phase II rotor tests. The improvements in rotor static pressure ratio, total pressure ratio, and increased surge margin are a result of the more uniform flow.

Exit Stator and Interconnecting Duct Performance

The parameter used to evaluate the performance of the exit stator and interconnecting duct is the ratio of total pressure loss through this component to the entering total pressure $\frac{\Delta P_T}{P_T}$. The difference between this ratio and a value of 1.0 is referred to as the total pressure recovery of the component.

Figure 12 shows the variation of the loss with stage pressure ratio along constant speed lines. In this case the loss is the difference between the pressure of the mid streamtube entering the stator and the average pressure at the stage exit (station 5). The individual hub, mean, and tip performance is not indicated, as no total pressures were measured at the hub and tip locations of the rotor exit. The loss was plotted against the stage

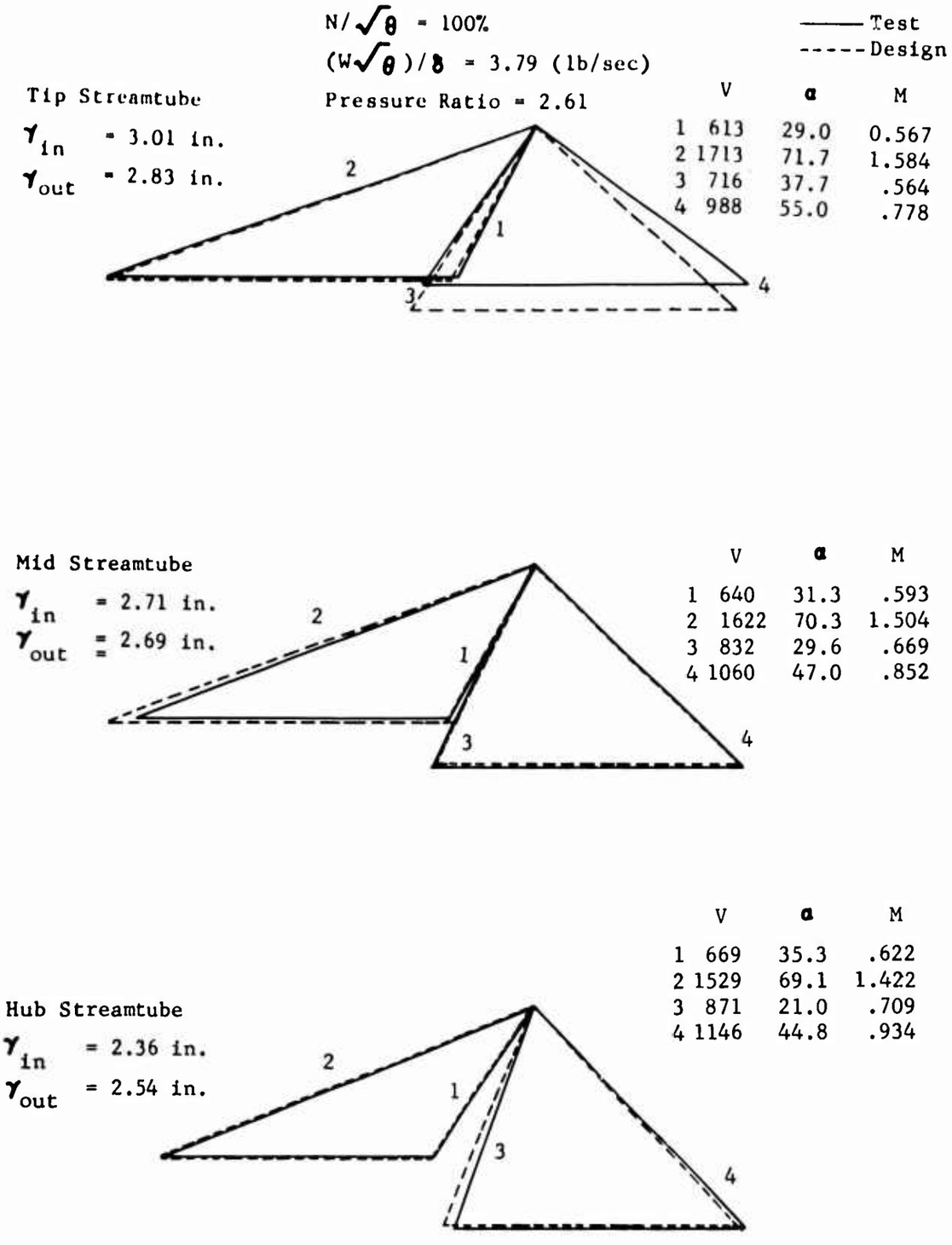

Figure 11. Build 6A Test Data, Vector Diagrams.

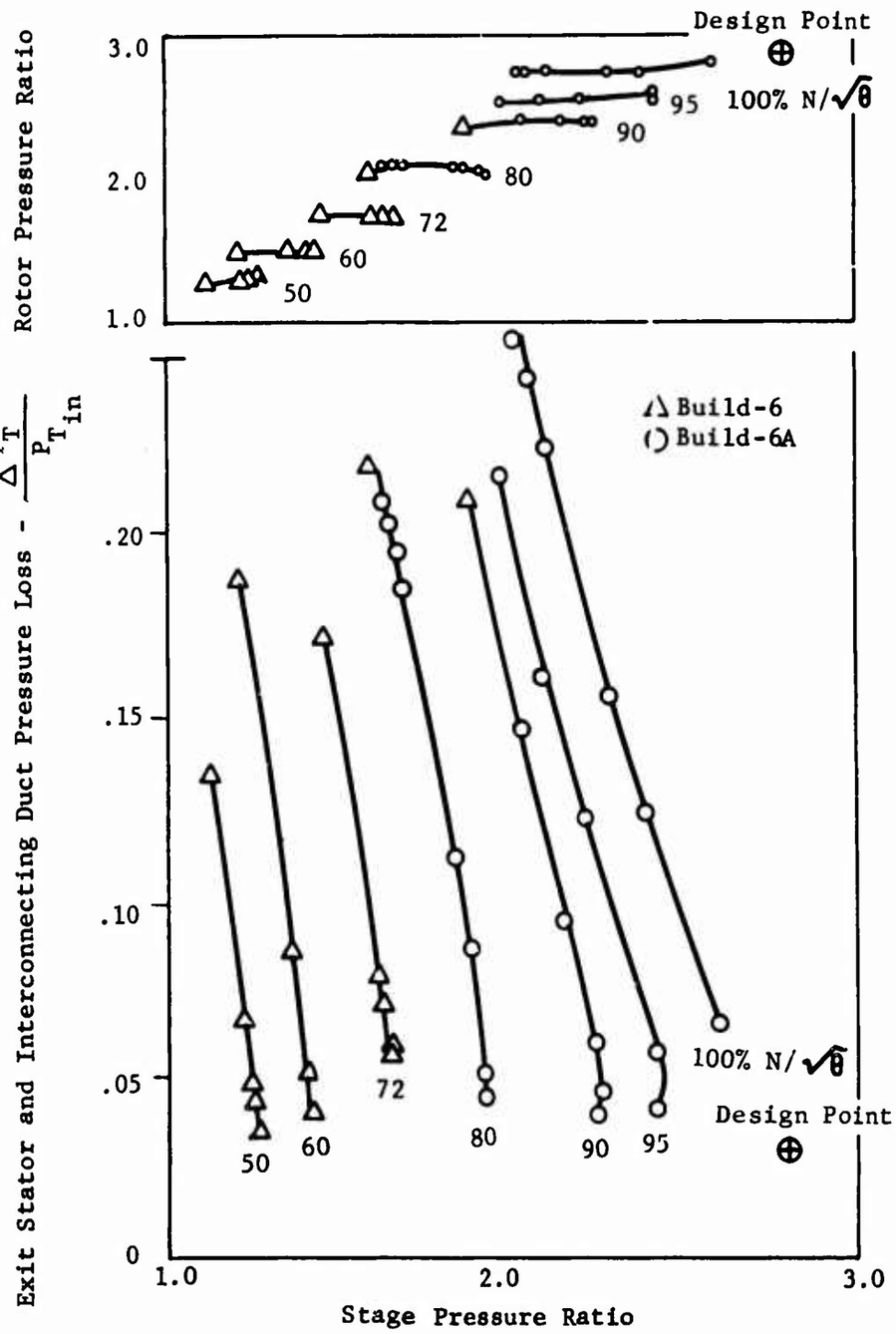

Figure 12. Build 6A Test Data, Pressure Loss for Exit Stator and Duct.

pressure ratio, since the flow characteristic is near vertical at the higher speeds. The results show that the losses continued to decrease along a given speed line all the way to the last most throttled test point. At design speed, the lowest loss demonstrated was .065 as compared to a goal of .03. At speeds of 95 and 90 percent, a loss of .04 was measured at the most throttled points.

When the throttle setting is wide open at the higher speeds, the stator and interconnecting duct passage are operating as a convergent/divergent supersonic nozzle, and the predominant losses are from the shock system which exists. As the throttle is closed, the shock moves upstream to a lower supersonic Mach number region and the associated losses decrease. At this stage of throttling, no change occurs in the flow conditions at the rotor exit. These flow conditions reflect a negative incidence to the leading edge of the exit stator. Once the degree of throttling has progressed to the point where the stator flow is completely subsonic from the leading edge on, the static pressure at the rotor exit responds to further throttling by increasing. The stator and duct losses beyond this throttle setting are primarily a function of the stator incidence and the entering stator Mach number since no shocks are present. As the static pressure at the rotor exit increases, the Mach number decreases and the flow angle increases (more positive stator incidence). The loss data from this test indicate that the stator incidence at which minimum loss occurs was not reached. The design speed rotor vector diagrams indicate that the incidence angles at the most throttled point were -3.3 degrees for the hub streamtube, -1.9 degrees for the mid streamtube, and +5.6 degrees at the tip streamtube.

Figures 13 and 14 compare the measured static pressures and computed Mach numbers through the stator and duct with the design values. The Mach numbers were computed from the ratio of the measured static pressure to the total pressure at the respective station. The total pressure is extrapolated from the measured conditions at the rotor exit. The extrapolation was performed by distributing the measured losses versus distance in the same proportion as calculated in the design. The Mach numbers agree quite well with the design values. The static pressure distribution compares favorably with the prediction, but the pressure level is low, as is the stage pressure ratio. No major deficiency in the passage design is evident from these data.

The total pressure profiles across the blade wakes at the stage exit (station 5) are shown in Figure 15. They indicate a maximum variation from the average value of $\pm$5.5 percent. The radial total pressure and Mach number profiles at this station are shown in Figure 16. The average total pressure at the stage exit was computed as the value which was consistent with both the radial and transverse profile data and satisfied continuity at the exit station using the measured static pressure, airflow, and total temperature. The continuity check was satisfied for a flow with zero whirl and a flow area equal to 97 percent of the geometric annulus area.

2.8:1 Supersonic Compressor Stage Test Data
Design IGV Setting
Rotor Configuration 4, Stator Configuration 1

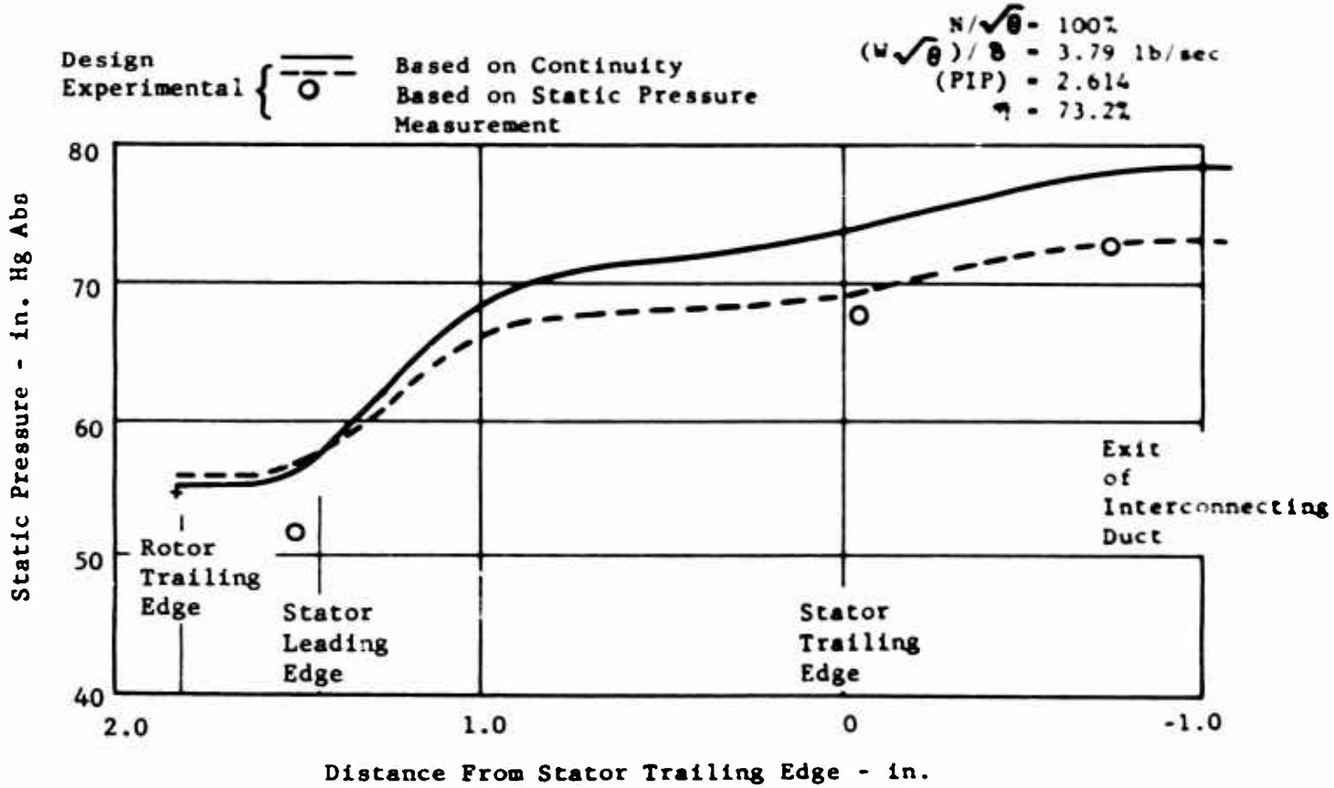

Figure 13. Build 6A Test Data, Static Pressure Distribution Through Exit Stator and Duct.

Rotor Configuration 4, Stator Configuration 1

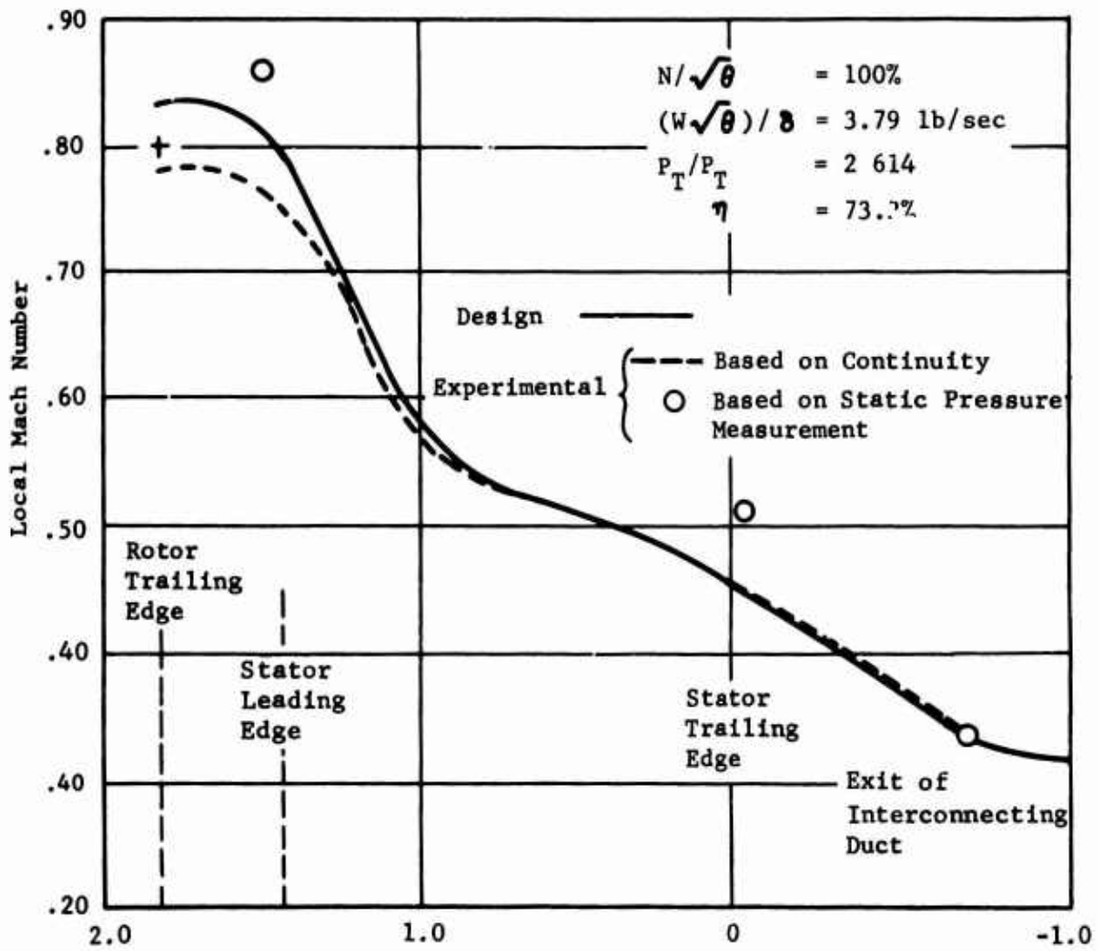

Figure 14. Build 6A Test Data, Mach Number Distribution Through the Exit Stator and Duct.

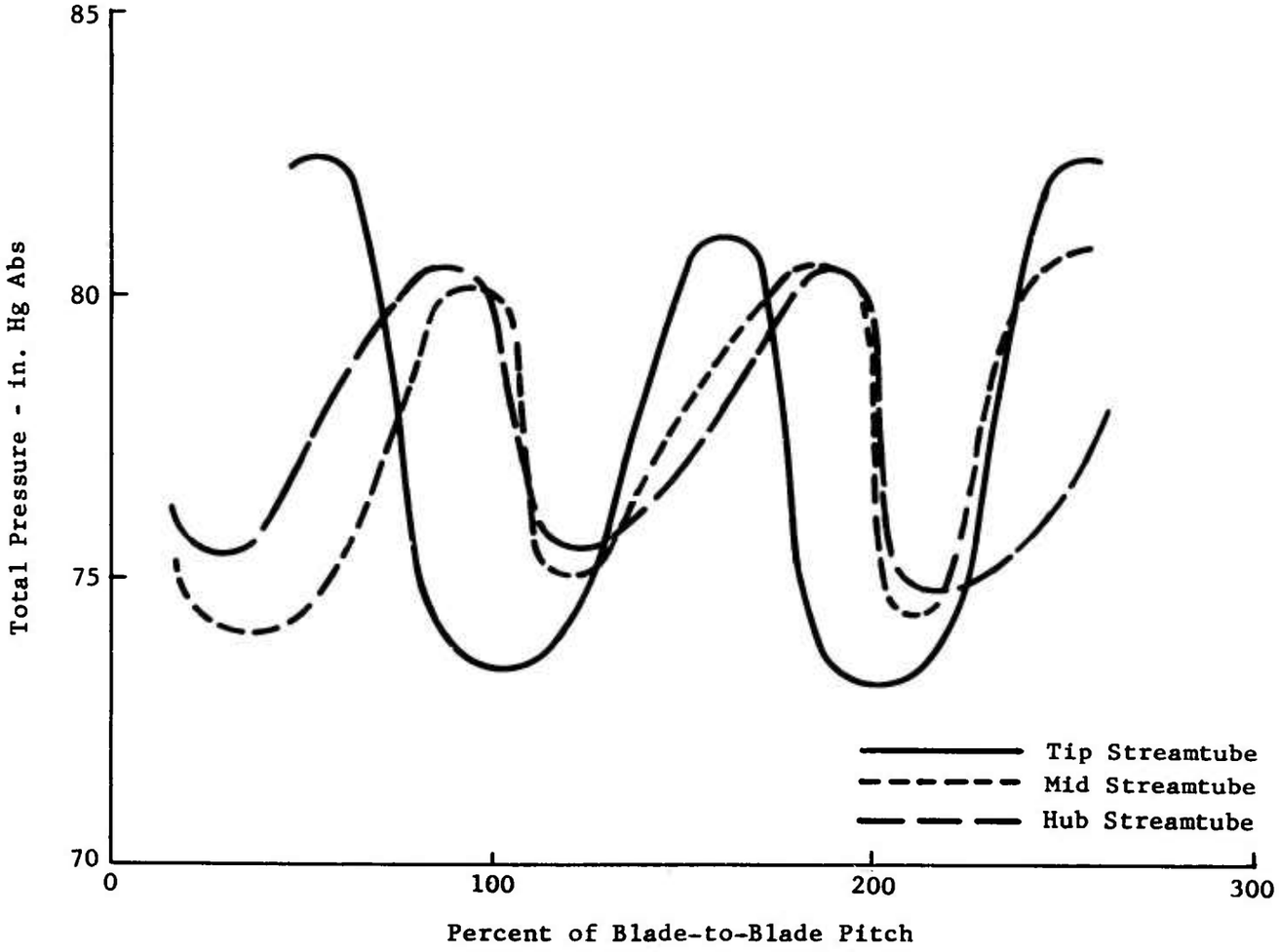

Figure 15. Build 6A Test Data, Exit Stator Pressure Profiles Across Exit Stator Blade Wakes at Stage Exit Station 5 for $N/\sqrt{\theta}$ = 100%, $(W\sqrt{\theta})/\delta$ = 3.661 lb/sec, P_T/P_T = 2.56:1.

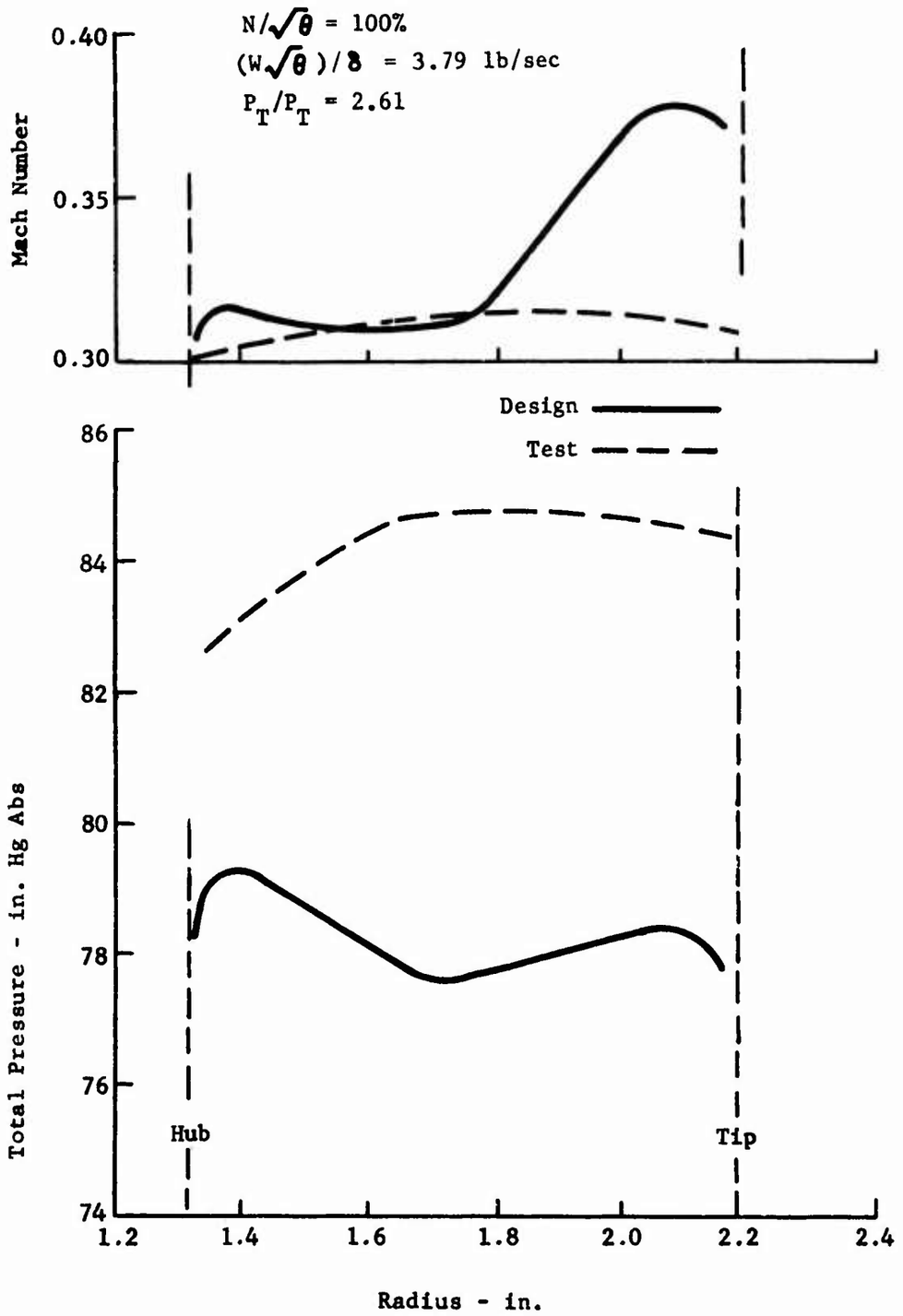

Figure 16. Build 6A Test Data, Stage Exit Conditions.

Figure 17 shows the measured flow angle (α) as a function of radius. The angle is within $\pm$2.0 degrees of the axial design goal except at the extreme hub, where it deviates up to 5.0 degrees.

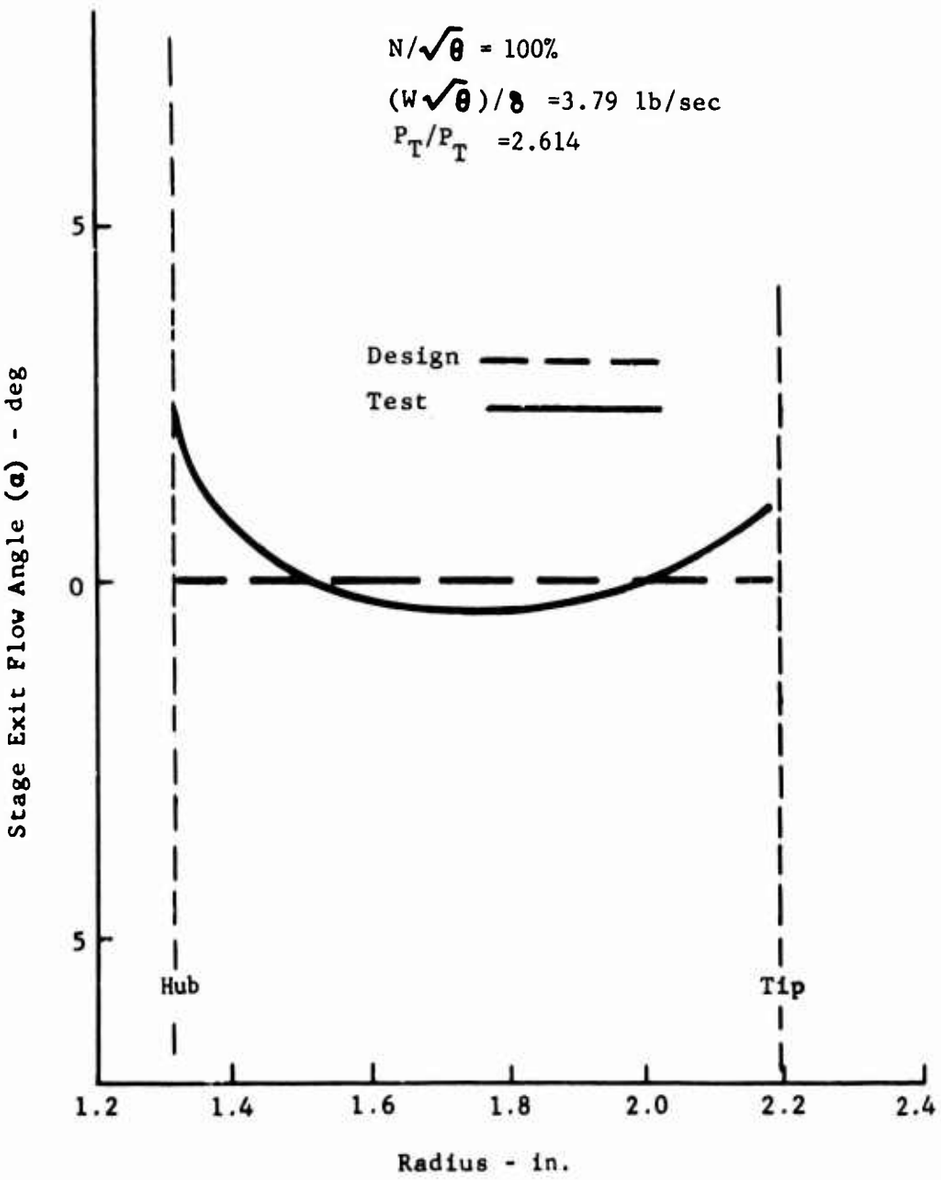

Figure 17. Build 6A Test Data, Flow Angle at Stage Exit.

STAGE TEST WITH DEVELOPED AIRFOIL INLET GUIDE VANES

Builds 7, 8, and 9 were tested under this task. The tests for these builds were conducted with new inlet guide vanes of an advanced design. The new guide vane assembly was the only design change to the compressor aerodynamic configuration. Due to the damage experienced in build 6A, a number of components had to be replaced with new hardware. A new front support housing with inlet strut assembly was fabricated with welded strut joints instead of brazed joints. The welded joints provided a strength several times that of the brazed joints and were expected to correct the conditions that led to the failure in build 6A.

Build 7 represented a design setting for the new IGV. The IGV setting was changed to -4° open in build 8 and +7° closed in build 9.

ADVANCED INLET GUIDE VANE DESIGN

The supersonic compressor design being developed under this program requires counterrotational prewhirl to the rotor leading edge. When counterrotational prewhirl is employed, failure to achieve the desired guide vane turning (excessive deviation) results in a decreased flow capacity and reduced pressure ratio capability. This is opposite to the consequences in conventional machines, where guide vanes introduce whirl in the direction of rotor rotation. Recognizing the importance of proper guide vane performance, an alternate guide vane was designed. This vane was a developed airfoil which utilized turbine nozzle design techniques. This guide vane design was expected to result in lower deviation and smaller blade wakes. Although lower guide vane losses were projected, the primary benefit was expected to be improved rotor performance as a result of a guide vane exit flow which meets the design Mach number profile and radial angle variation more accurately. The new vanes were designed to meet the same exit flow conditions [illegible]d in the design of the NACA 65 series vanes.

The blade airfoils were developed in a manner similar to the rotor and exit stator airfoil designs. Hub and tip shroud contouring was used to satisfy a continuously convergent area schedule while meeting other desired airfoil characteristics. The flow turning was completed in the first 40 percent of the blade chord so as to provide straight blade sections aft of the 40 percent chord point in order to insure minimum deviation. An annulus area which is considerably higher at the guide vane entrance results in a design point Mach number of 0.31, as compared to 0.47 for the NACA 65 series vanes. Figure 18 compares the Mach number schedule for the advanced guide vane design to that for the NACA 65 series vanes. The solidity of the advanced vane design ranges from 1.4 to 2.0. The solidity of the NACA 65 series vanes was 1.0. Figure 19 shows a typical airfoil section for the advanced design. The trailing edge angle of the blade was designed with the compression surface angle equal to the flow angle, which represents a 3-degree deviation for the 6-degree trailing edge wedge angle. Figures 20 and 21 are photos of the developed airfoil vane. Figure 22 is a photo of the developed airfoil inlet guide vane assembly. The flow path through the guide vane assembly is illustrated in Figure 23.

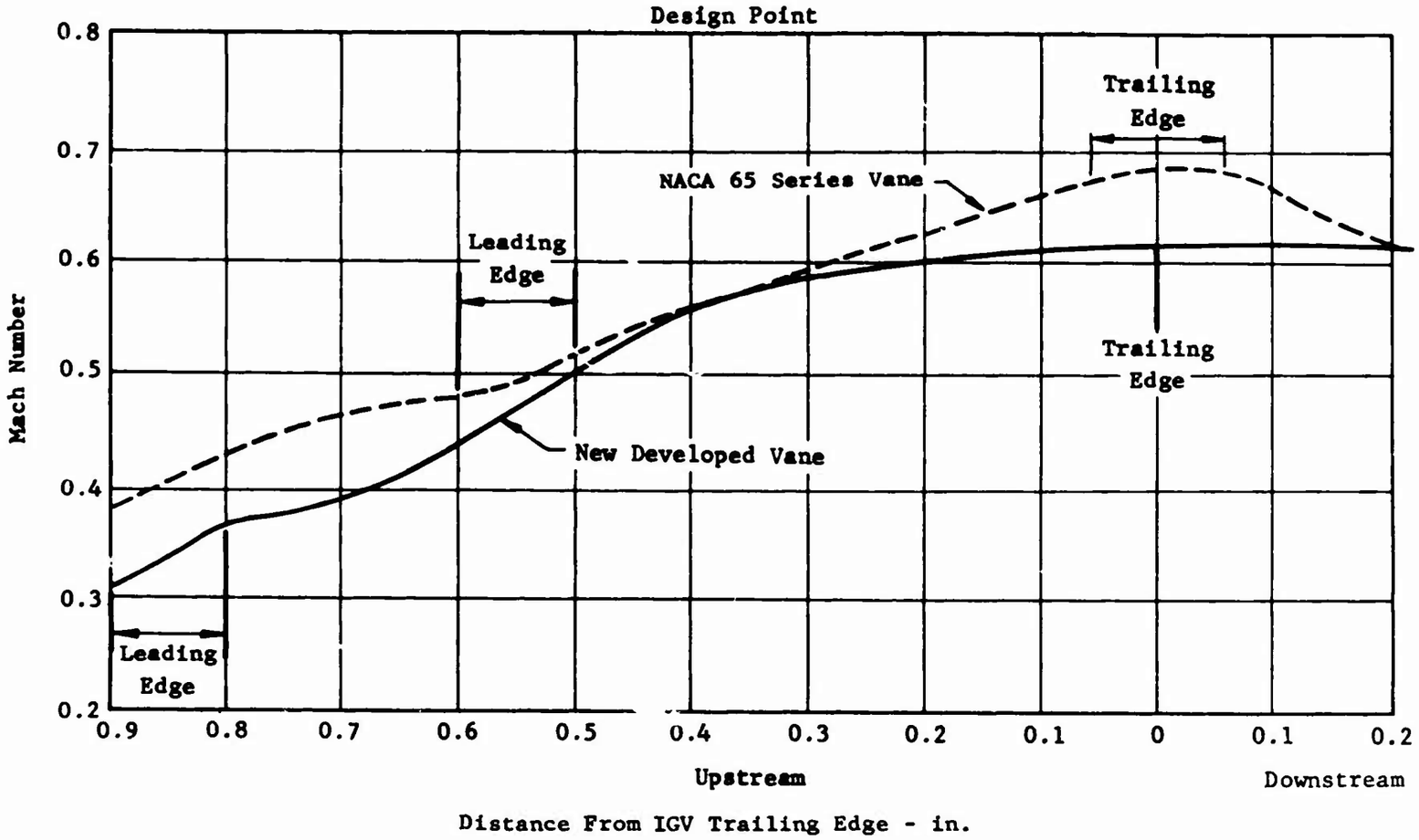

Figure 18. Inlet Guide Vane Mach Number Schedule; Comparison of New Developed Vane to NACA 65 Series Vane.

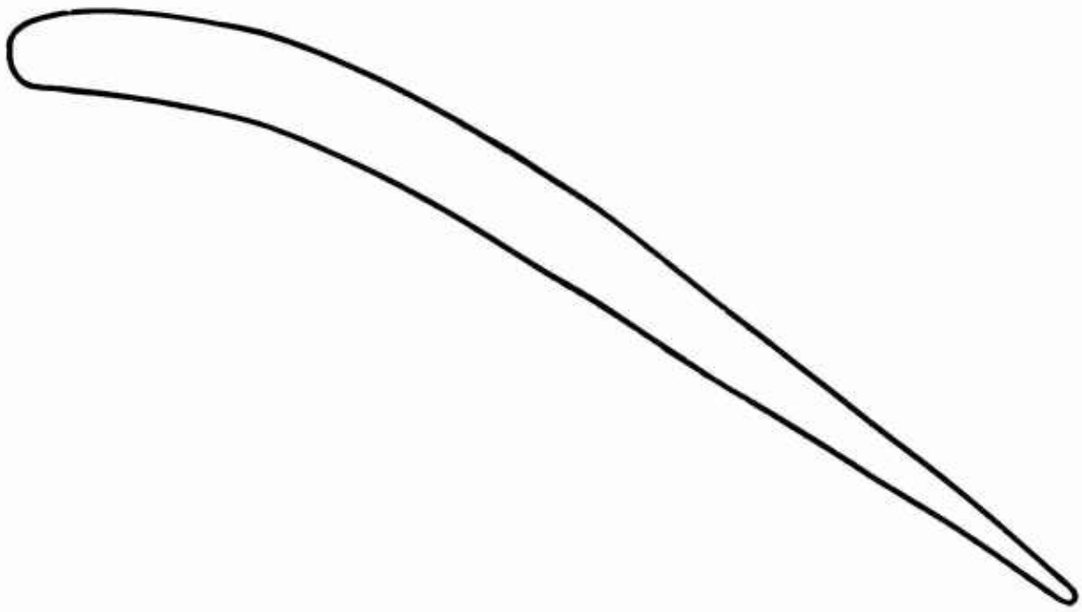

Figure 19. Typical Airfoil Section for Developed Airfoil Inlet Guide Vane.

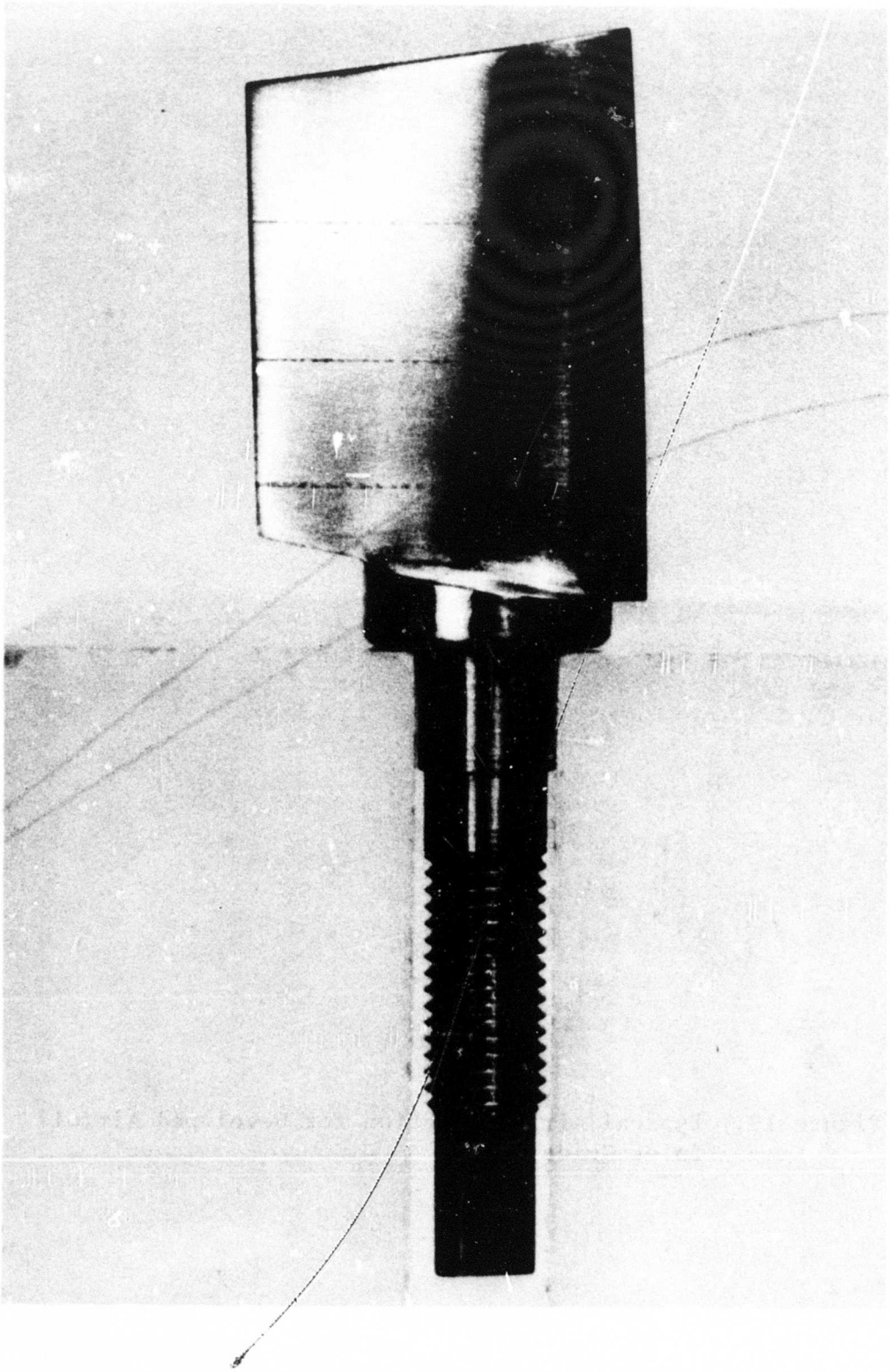

Figure 20. Developed Airfoil Inlet Guide Vane - Side View

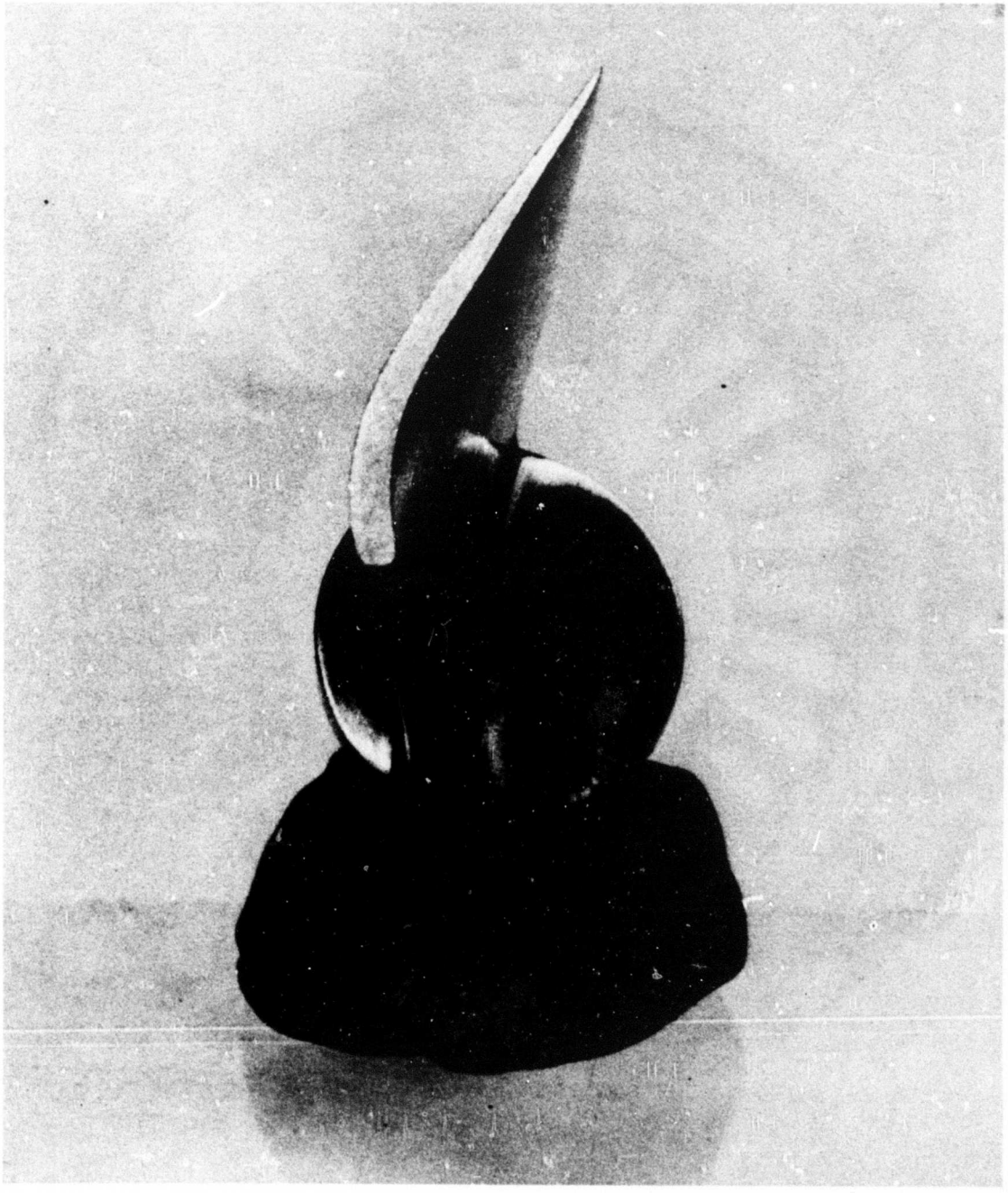

Figure 21. Developed Airfoil Inlet Guide Vane - Top View

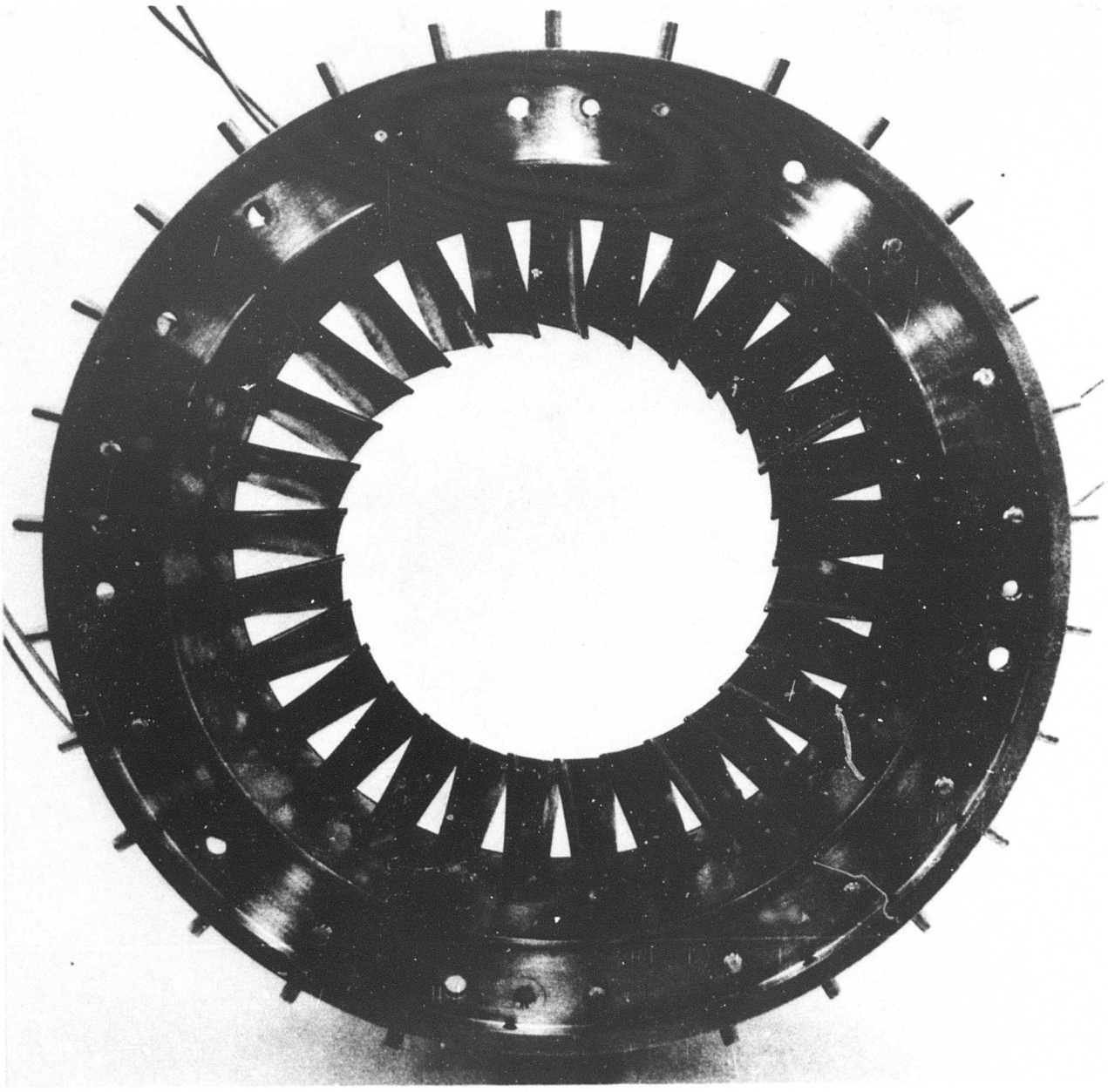

Figure 22. Developed Airfoil Inlet Guide Vane Assembly - Front View

2.8:1 Supersonic Compressor

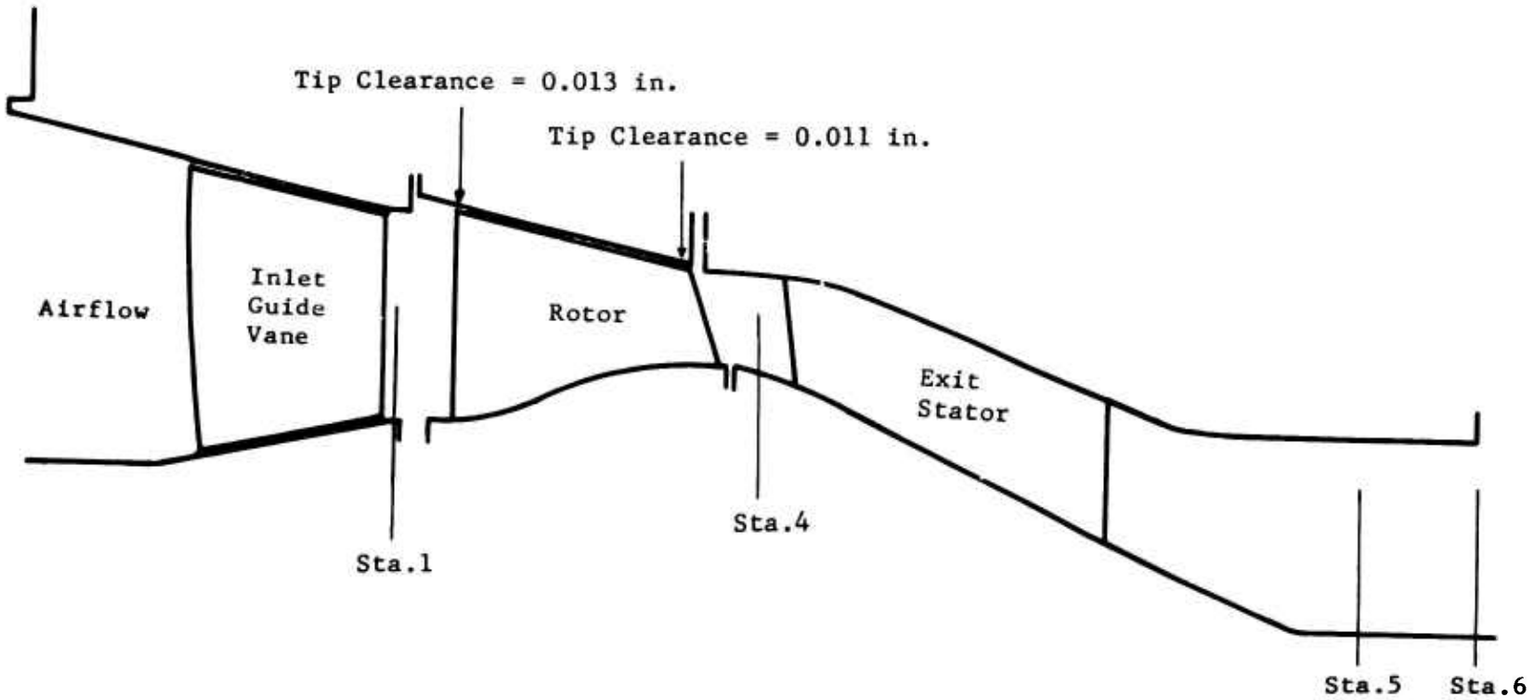

Figure 23. Compressor Flow Path for Builds 7, 8, and 9.

FABRICATION OF ADVANCED INLET GUIDE VANES

The inlet guide vane housing and the inner shroud were redesigned, in addition to the vanes themselves, as a part of the advanced inlet guide vane assembly. The hub and tip shroud contours are essentially conical in the area of the vanes. The potential tolerance buildup of this configuration, when providing for some vane angle variation, results in high blade-to-shroud clearances. In order to minimize the clearances, the blades were fabricated to an oversize span and finished as an assembly. The actual dimensions from measurements of the finished inner shroud and housing were used to establish the desired matching radii and angle of the cone at the blade ends for minimum clearance. The blade ends were then machined as an assembly with the outer housing. A variation of IGV setting from -4 degrees to +7 degrees was specified. The machining to the cone dimensions was first performed with the vane at the +7-degree angle setting and then repeated with the vane at a -5-degree angle setting to permit a variation between those limits. This procedure resulted in a blade to inner shroud clearance at the trailing edge of .010 for the design vane setting, .001 for the -5-degree setting, and .026 at the +7-degree setting.

TEST CONFIGURATION

The test configuration for build 7, which is shown in Figure 23, differs from build 6 by two changes. The new inlet guide vane assembly is one change. The other change is a difference in the rotor tip diameter and axial position relative to the shroud. A new rotor (S/N 4) was required and was fabricated to the same specifications as rotor S/N 3 in build 6. The inspection results for this rotor (S/N 4) indicate that the only significant variation from rotor S/N 3 is a .002-inch-thicker blade leading edge. The final tip grind of the blades resulted in a tip diameter of 6.280 inches, which was .028 inch undersized relative to rotor S/N 3. The rotor shroud was positioned .056 inch forward relative to the rotor to establish the desired tip clearance of .011 inch at the trailing edge and .013 inch at the leading edge. As a result, the gap between the rear face of the rotor shroud and the front face of the outer exit guide vane shroud was .061 inch, and the rotor trailing edge at the tip was just aft of the shroud trailing edge.

The new exit stator (S/N 2) was made to the same specifications as the one in build 6 (S/N 1), and inspection data indicated negligible deviations.

The IGV were at design setting for build 7. Builds 8 and 9 differed from build 7 only by a change in inlet guide vane settings, which were -4 degrees open and +7 degrees closed, respectively.

INSTRUMENTATION

All of the instrumentation that was included in build 6 was retained in builds 7, 8, and 9, and the instrumentation listed in Table IV was added.

TABLE IV. INSTRUMENTATION ADDED TO BUILDS 7, 8, AND 9

Instrumentation	Location			Operating Range
	Axial	Circumferential (deg)	Radial Distance from Flow Path O.D. (in.)	
1 Pitot $\alpha = 50^{\circ}$	Station 4	258	0.080	0 to 60 in. Hg. gage
1 Pitot $\alpha = 50^{\circ}$	Station 4	242	0.370	0 to 60 in. Hg. gage
3 Pitot $\alpha = 0^{\circ}$	Station 6	211, 207, 204	0.693	0 to 60 in. Hg. gage
3 Pitot $\alpha = 0^{\circ}$	Station 6	200, 196, 191	0.385	0 to 60 in. Hg. gage
3 Pitot $\alpha = 0^{\circ}$	Station 6	188, 184, 180,	0.120	0 to 60 in. Hg. gage
4 Total Thermos $\alpha = 0^{\circ}$	Station 6	33, 38, 45, 115	0.693	50° to 500°F
1 Total Thermos $\alpha = 0^{\circ}$	Station 6	56	0.385	50° to 500°F
2 Total Thermos $\alpha = 0^{\circ}$	Station 6	106, 108	0.120	50° to 500°F

The two fixed pitot probes added to station 4 were provided to measure the hub and tip streamtube total pressures at the rotor exit. The geometric blockage of these two probes was 0.2 percent of the design flow area and was not expected to cause a significant difference in the average flow conditions at this station. The instrumentation added to station 6 was to supplement the existing instrumentation and to serve as a backup for probes which become faulty.

DESCRIPTION OF TEST

Builds 7, 8, and 9 were tested through 100 percent speed for each of three IGV settings (design setting, -4° and $+7^{\circ}$). The rig operated well within vibrational limits and without mechanical difficulty throughout the testing. A total testing time of 34:25 and 243 data points were accumulated.

Post-test inspection of the rig revealed that the rotor blade leading edges had sustained a number of nicks (Figure 24). The nicks apparently were caused by an ingested particle or particles. It has been noted

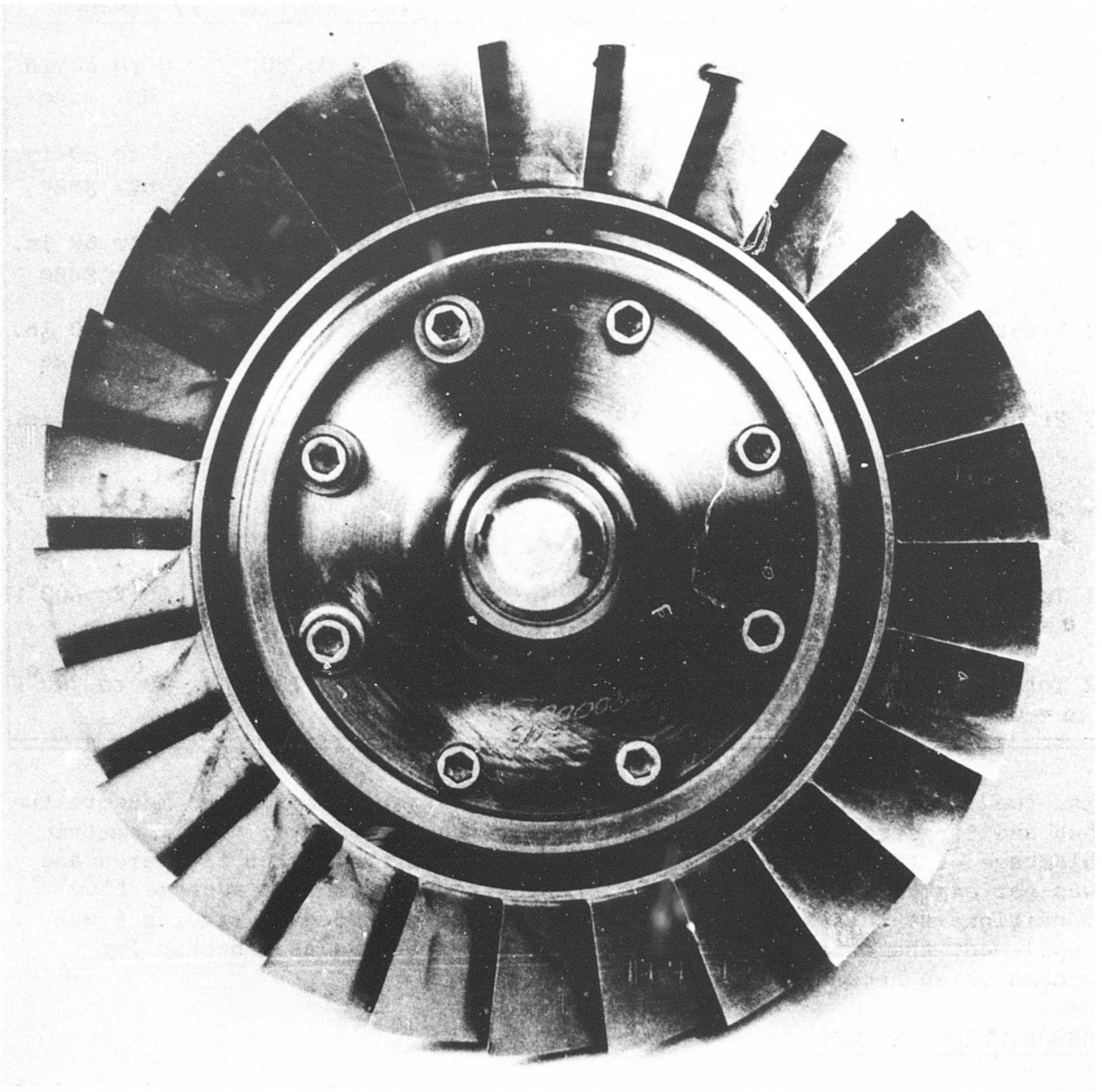

Figure 24. Builds 7, 8, and 9 - Post-Test Photo of Compressor Rotor Indicating Nicks on Leading Edge of Blades.

that following the completion of testing at the 95-percent speed line for the design IGV setting, a check point at this speed showed a degradation in efficiency from 75.8 percent to 73.6 percent. It is therefore believed that the nicks occurred at that time and that all subsequent performance data, including 100 percent speed at the design IGV setting and all points at the -4-degree and +7-degree settings, are degraded due to the nicks.

The surge line was established through 95 percent speed for builds 7 and 8. At 100 percent speed, the compressor was throttled to a point very close to the extrapolated surge line. The data indicated that little or no gain in performance would occur prior to surge, and it was decided that this additional data did not warrant the risk of possible damage to the rig at this point in the program. The build 9 surge line was established through 85 percent speed. Above 85 percent speed, the peak performance data for build 9 offered no advantage over that for builds 7 and 8 and the surge investigation at these speeds was not done, as it was not expected to contribute significant data.

TEST RESULTS

Stage Performance

The three stage-performance maps for each of the IGV settings of design, -4 degrees open, and +7 degrees closed are shown in Figures 25, 26, and 27, respectively. Table V summarizes the demonstrated peak pressure ratio and effeciency at each speed.

The highest peak stage pressure ratios were demonstrated at the design and +7-degree IGV settings, with the pressure ratios below 90 percent speed higher for the +7-degree setting than for the design setting. The peak design speed pressure ratio was 2.60:1. However, it should be noted that all design speed testing was subsequent to the performance degradation attributed to the nicked blades. The -4-degree guide vane setting showed the best peak stage efficiencies with a design speed peak of 74.4 percent at a pressure ratio of 2.57:1.

The part-speed pressure ratios and efficiencies for the design IGV setting were higher than those demonstrated in builds 6 and 6A. The pressure ratios of build 8 (-4-degree IGV setting) peaked at slightly lower values than those for builds 6 and 6A, but the pressure ratio versus corrected airflow relationship for constant speed lines agreed quite closely, indicating that the exit flow conditions of the developed airfoil IGV at the -4-degree setting are equivalent to those of the NACA 65 series IGV at the design setting.

The design speed corrected airflow at the -4-degree IGV setting of build 8 was 2 percent lower than that for build 6A, which is attributed to the undersized rotor tip diameter and the higher rotor leading edge thickness. Through 80 percent speed, however, the maximum airflow is higher than or equal to that of build 6A.

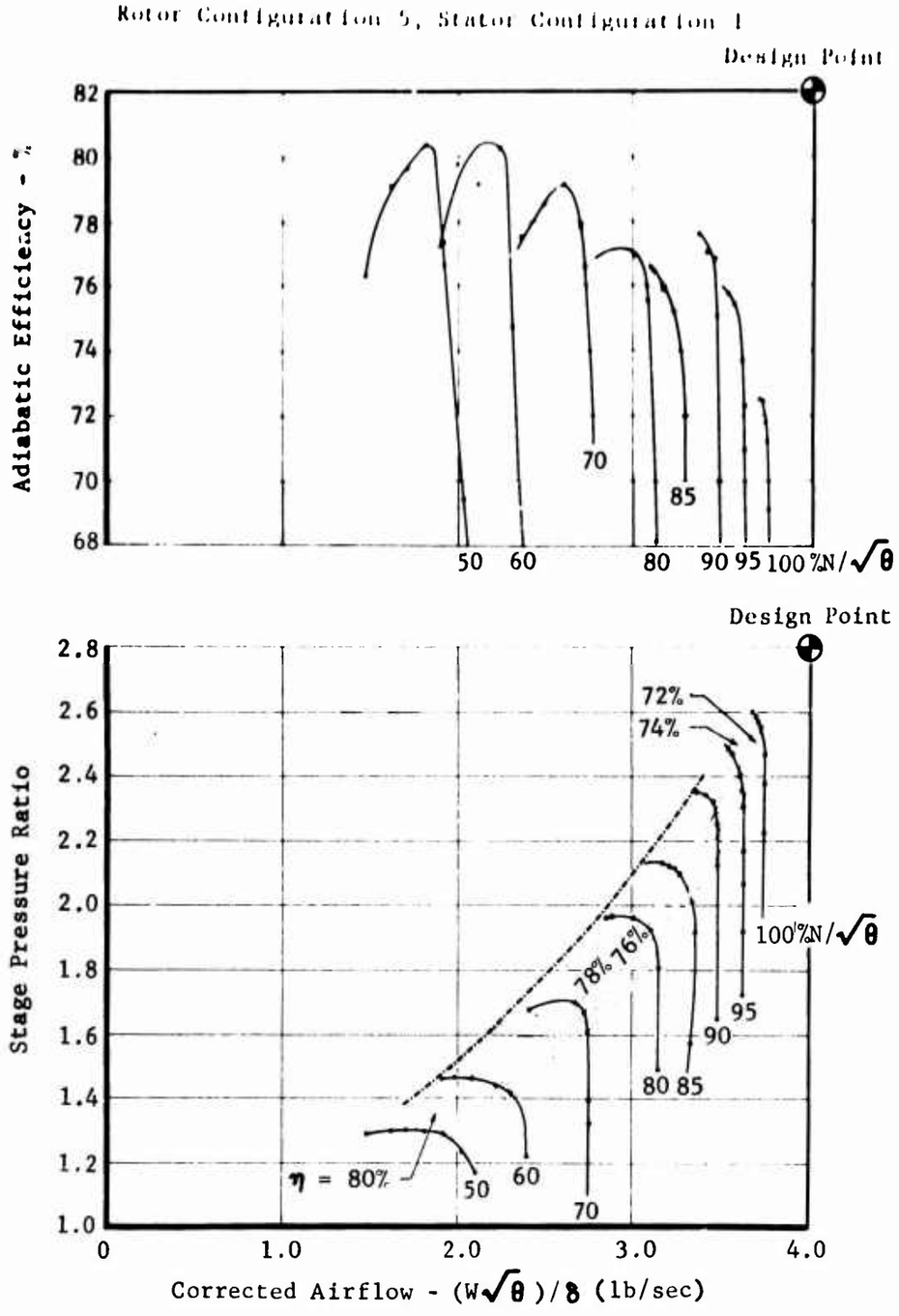

Figure 25. Supersonic Compressor Test Stage Data, Build 7, Developed Airfoil IGV at Design Setting.

Rotor Configuration 5, Stator Configuration 1

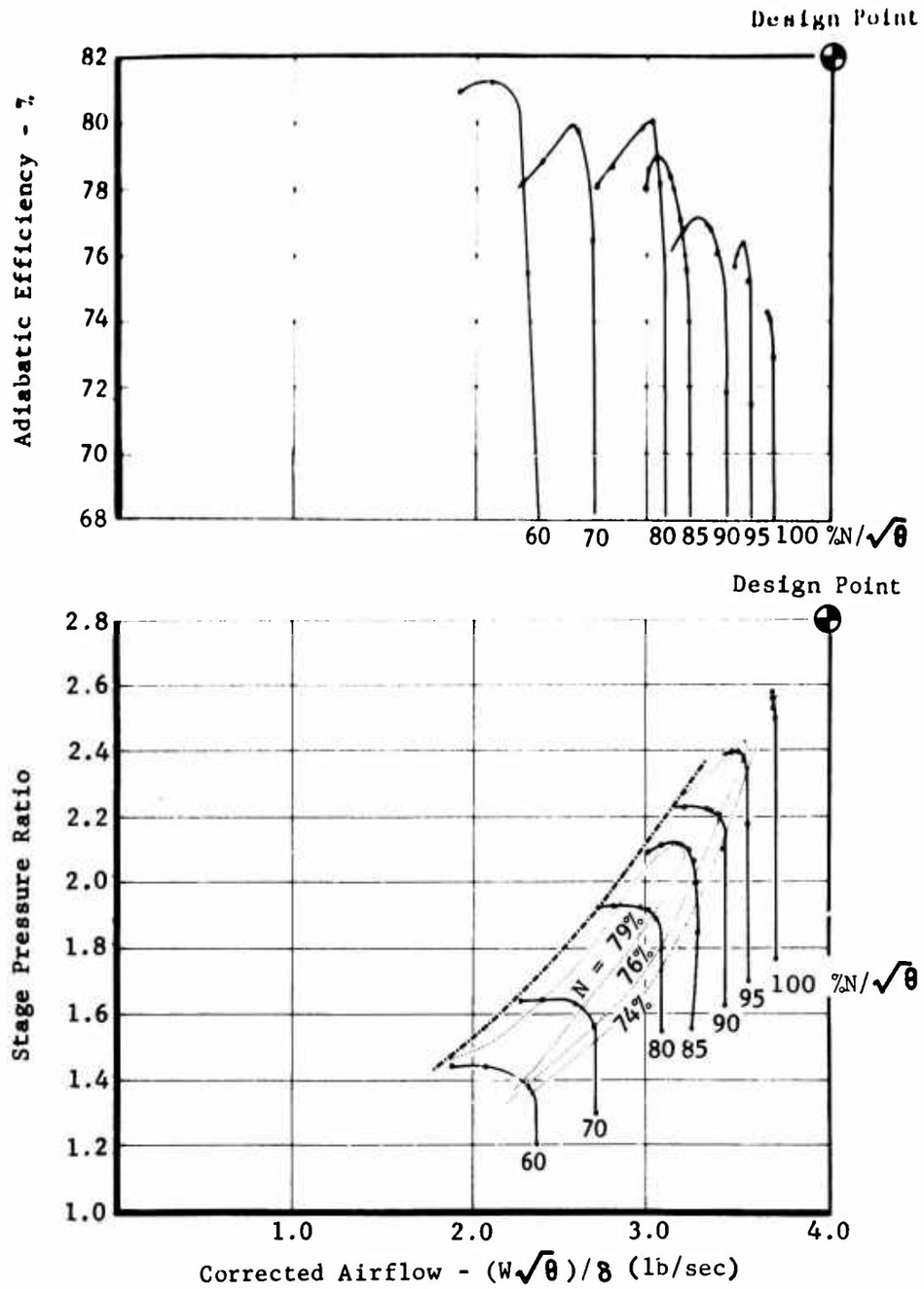

Figure 26. 2.8:1 Supersonic Compressor Test Stage Data, Build 8, Developed Airfoil IGV at -4° Setting.

Rotor Configuration 5, Stator Configuration 1

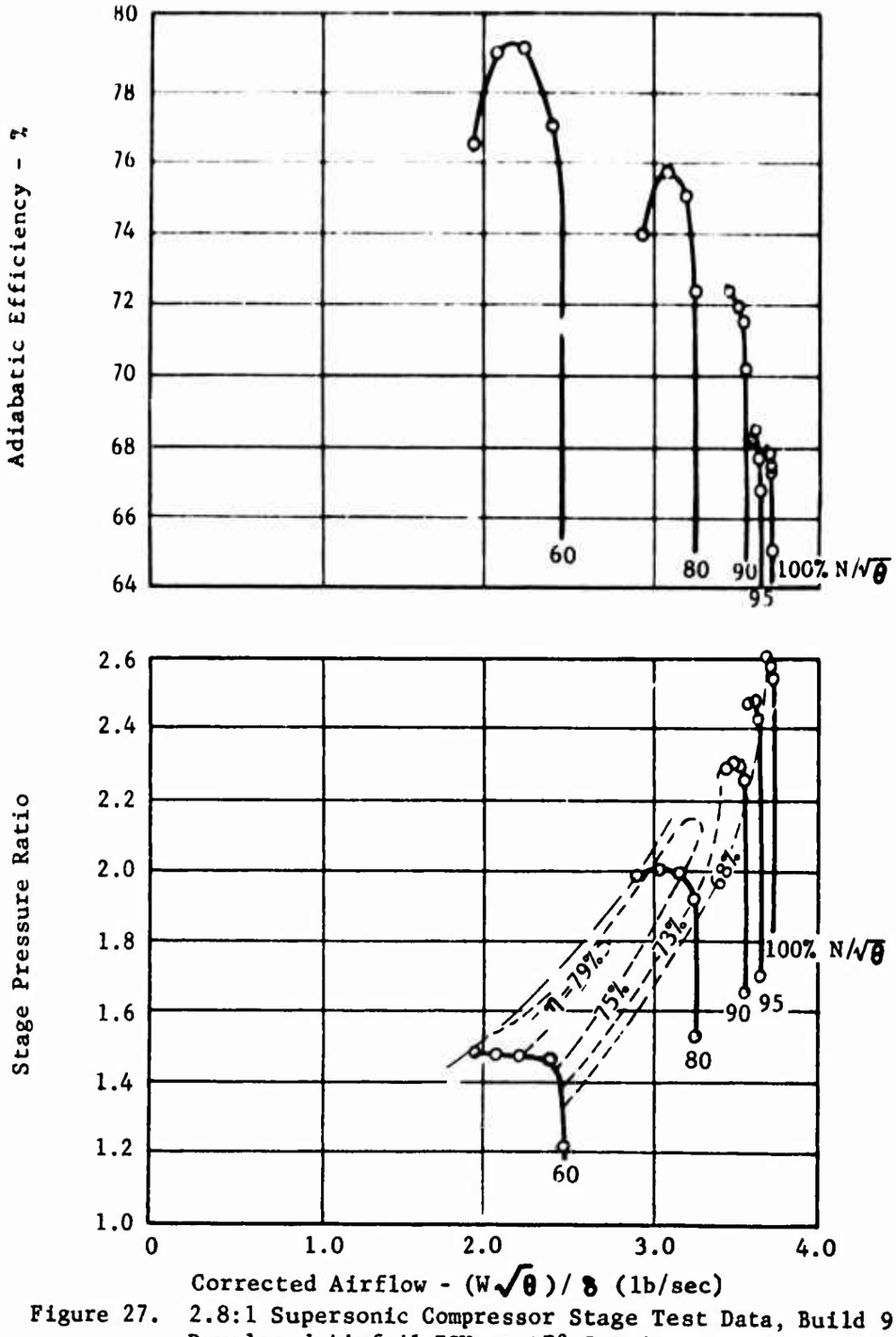

Figure 27. 2.8:1 Supersonic Compressor Stage Test Data, Build 9, Developed Airfoil IGV at +7° Setting.

TABLE V. STAGE PERFORMANCE DATA FOR BUILDS 7, 8, AND 9

	Percent Speed						
	50	60	70	80	90	95	100
Pressure Ratio:							
Predicted Peak at Design IGV Setting	-	1.41	1.60	1.84	2.26	2.56	2.80
Data Peak at Design IGV Setting	1.30	1.46	1.68	1.96	2.38	2.48	2.60*
Data Peak at -4^{o} IGV Setting	-	1.44*	1.64	1.92*	2.22*	2.40*	2.57*
Data Peak at $+7^{o}$ IGV Setting	-	1.48*	-	2.01*	2.30*	2.48*	2.60*
Efficiency:							
Predicted Peak at Design IGV Setting	-	83.3	-	82.7	82.5	-	82.2
Data Peak at Design IGV Setting	80.4	80.2	79.2	77.0	77.6	75.8	72.4*
Data Peak at -4^{o} IGV Setting	-	81.4*	80.0*	80.1*	77.0*	76.4*	74.4*
Data Peak at $+7^{o}$ IGV Setting	-	79.5*	-	75.8*	72.5*	68.5*	67.6*

* Data degraded by nicked leading edges.

Figure 28 presents the distribution of static pressure rise through the compressor at design speed for build 8. The results are typical for builds 7 and 9 also. The results show a departure from those of build 6A in the area of the rotor leading edge and aft of station 4. These results are discussed in the following sections on Inlet Guide Vane Performance and Exit Stator and Interconnecting Duct Performance respectively.

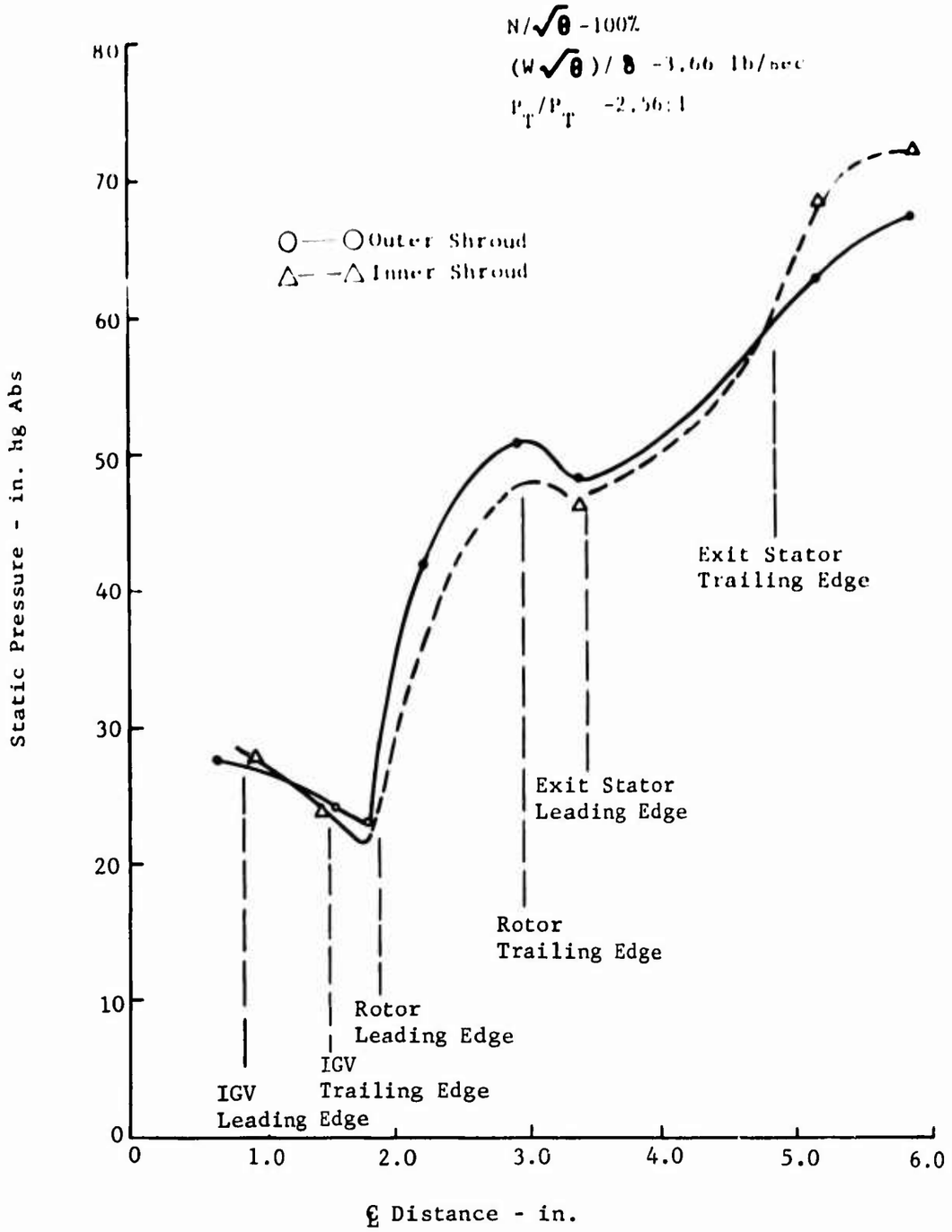

Figure 28. Buiid 8 Test Data, Static Pressure Distribution Versus Axial Distance Through Compressor.

Inlet Guide Vane Performance

A flow test of the developed airfoil IGV as an independent blade row was not conducted. The performance of this blade row has been evaluated by comparing the stage test data of builds 7, 8, and 9 (which included the developed airfoil IGV) to the data of builds 6 and 6A (which included the NACA 65 series IGV). Flow test of the NACA 65 series IGV indicated that at design setting, the design exit flow angle was met at the inner shroud but deviated increasingly with increasing radius up to 2 degrees low at the outer shroud. The comparison of the stage test pressure ratio versus corrected airflow relationship for constant speed lines indicates that a setting between -3 degrees and -4 degrees for the developed airfoil IGV is equivalent to the design setting for the NACA 65 series IGV. The design deviation was 6 degrees for the NACA 65 series vanes and 3 degrees for the developed airfoil. The developed airfoil, therefore, demonstrated 6 to 7 degrees less deviation. Based on the flow test results for the NACA 65 series vanes, the deviation of the developed airfoil is 0 to 1 degree.

The measured design speed static pressures at the IGV exit for build 8 are compared to the design values in Figure 29. The pressures are higher than the design value because the airflow is 7 percent low. Projecting the static pressure reduction which would accompany an airflow increase to the design value indicates that the design static pressure level would be met. The static pressures at the exit of the developed airfoil IGV are therefore in better agreement with the design than the results with the NACA 65 series vanes, and this result implies lower boundary layer thicknesses and smaller blade wakes.

The variation in part-speed performance between builds 7, 8, and 9 is much greater for a given change in IGV setting than that experienced in the rotor test phase. The developed airfoil vanes, therefore, provide a more positive response to a change in IGV setting than the NACA 65 series.

A comparison of the peak rotor efficiencies between builds 6A and 8 do not show a consistent trend as to the effect of the developed airfoil vanes. The data indicate that the nicks on the rotor blades may have degraded the efficiencies of build 8 by up to 2 points, in which case the performance with the developed vanes would show an improvement at most speeds.

A small static pressure decrease is indicated along the outer shroud between the IGV exit and the rotor leading edge (Figure 28) in builds 7, 8, and 9. This condition is attributed to a burr at the trailing edge of the IGV housing and the forward position of the rotor shroud relative to the rotor.

Rotor Performance

Figures 30, 31, and 32 are the experimental performance maps for the IGV and rotor at the design, -4-degree, and +7-degree IGV settings, respectively. The maximum design speed pressure ratio of 2.82:1 was demonstrated at the

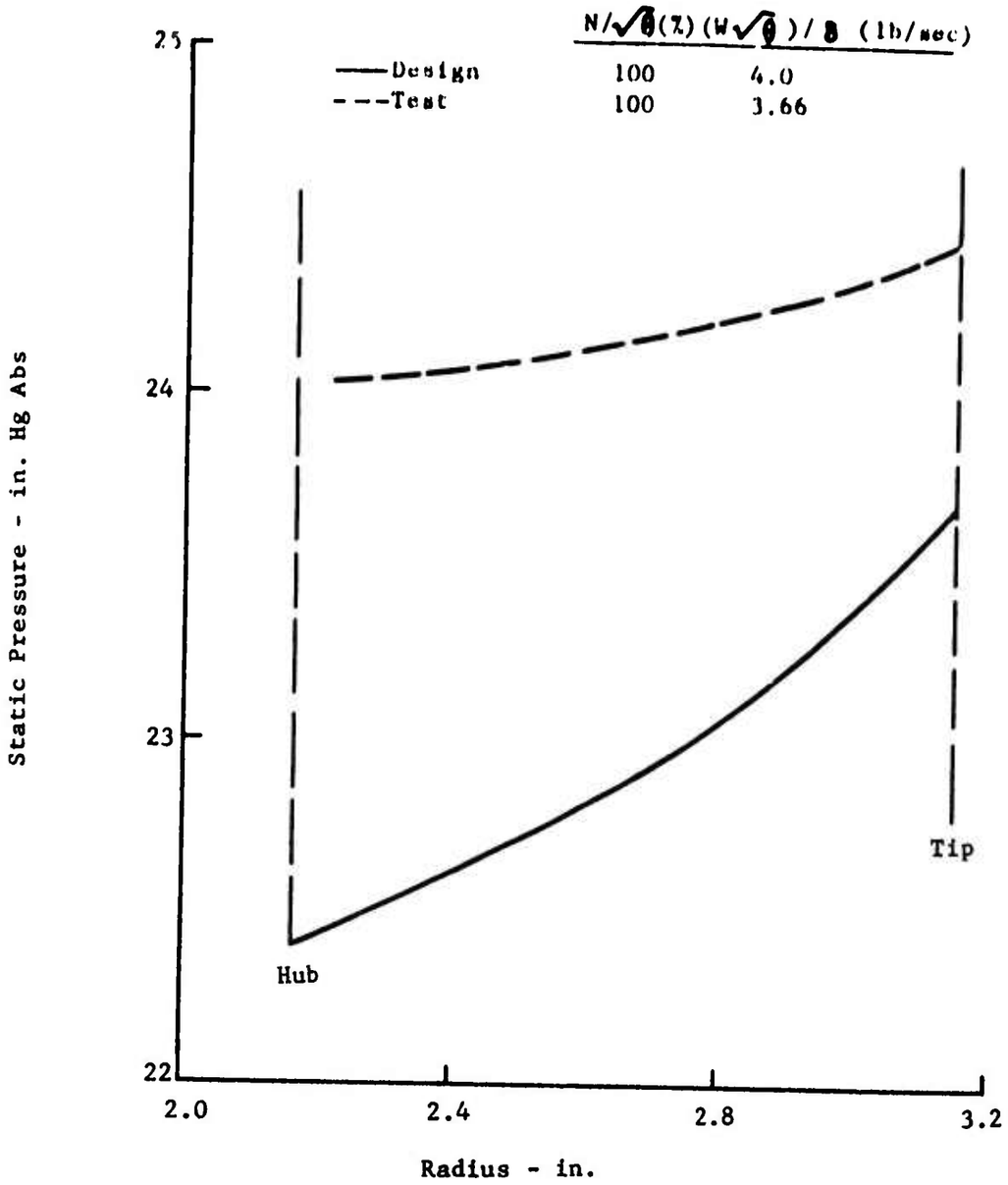

Figure 29. Build 8 Test Data, Static Pressure at IGV Trailing Edge Compared to Design.

Rotor Configuration 5, Stator Configuration 1

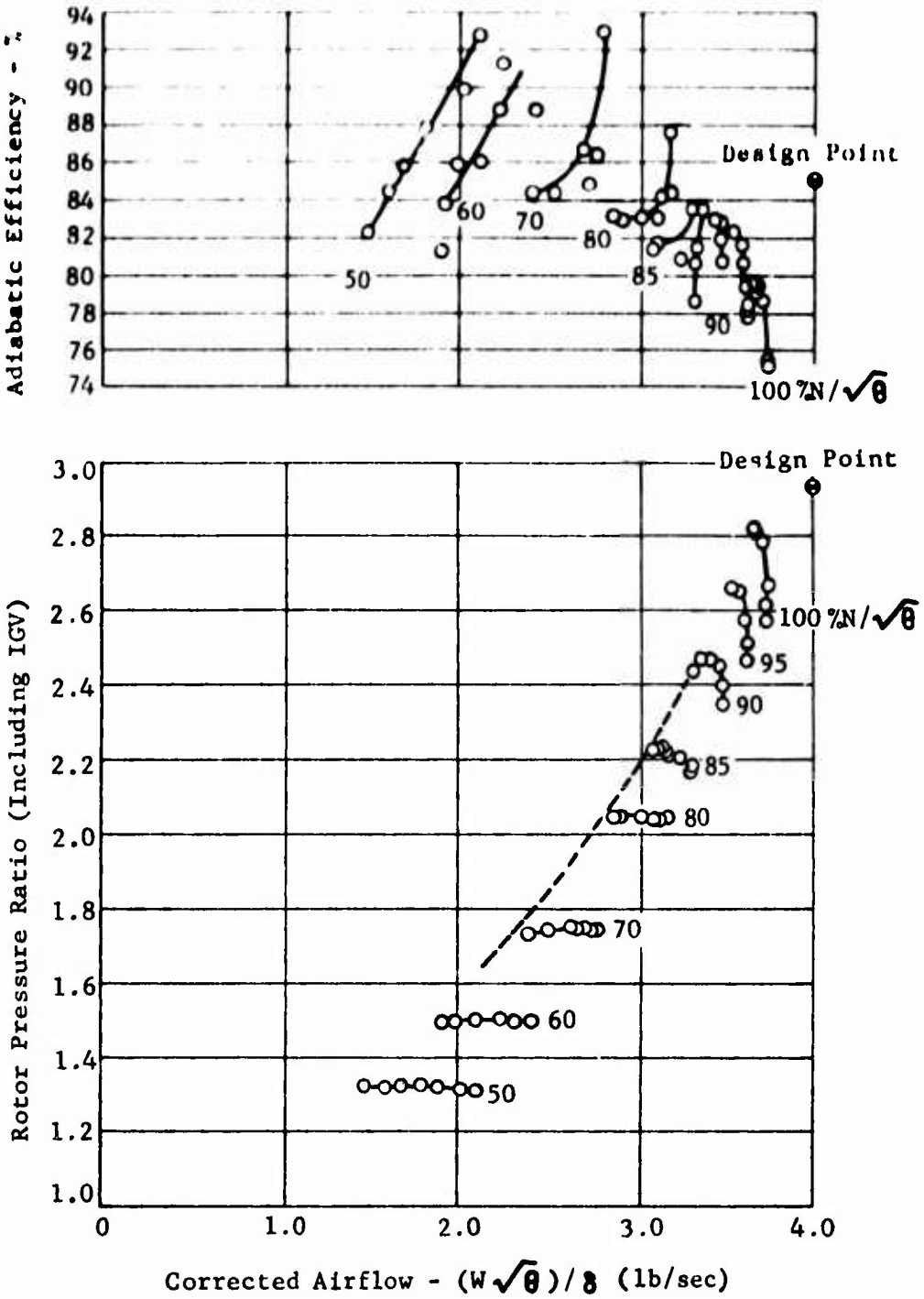

Figure 30. 2.8:1 Supersonic Compressor Stage Test, Build 7, Rotor Performance Data, Developed Airfoil IGV at Design Setting.

Rotor Configuration 5, Stator Configuration 1

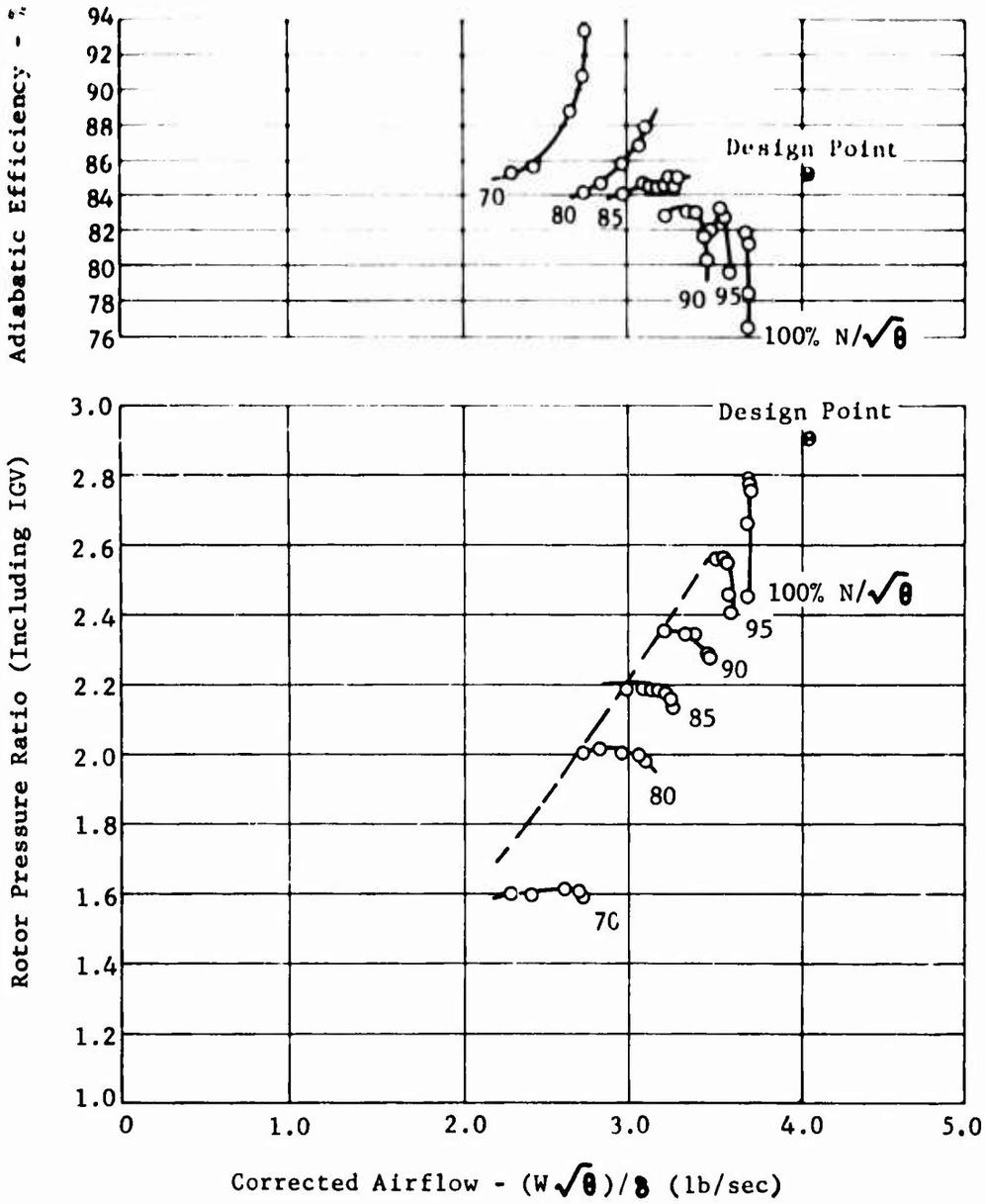

Figure 31. 2.8:1 Supersonic Compressor Stage Test, Build 8, Rotor Performance Data, Developed Airfoil IGV at -4° Setting.

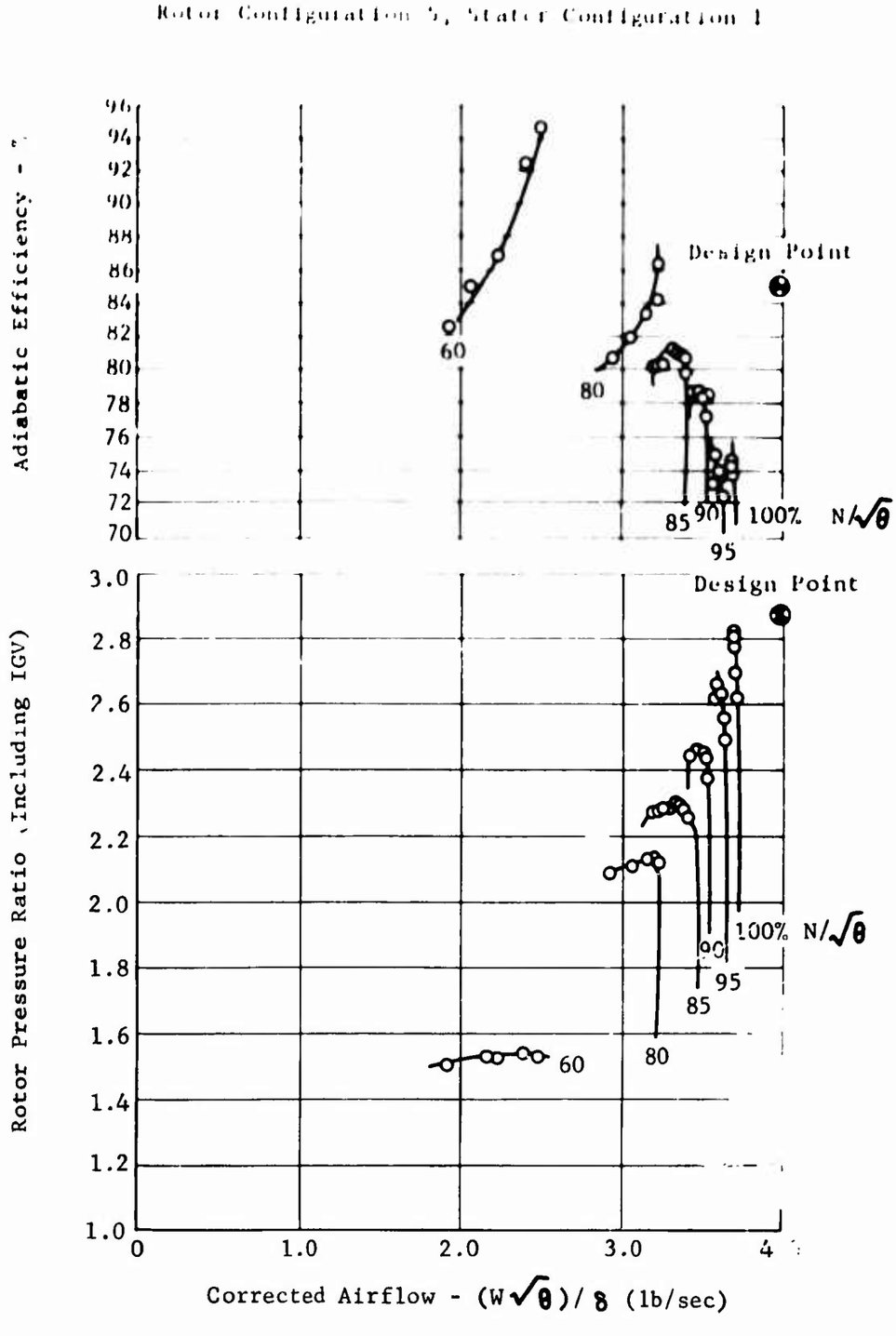

Figure 32. 2.8:1 Supersonic Compressor Stage Test, Build 9, Rotor Performance Data, Developed Airfoil IGV at +7° Setting.

design and +7-degree IGV settings. This pressure ratio was higher than that achieved in build 6A. The part-speed peak pressure ratios were highest at the +7-degree IGV setting and lowest at the -4-degree setting. The part-speed peak pressure ratios for the -4-degree setting were essentially the same as those of build 6A and were higher at the other two IGV settings. The efficiencies at the design and -4-degree settings were comparable to those of build 6A, while those at the +7-degree setting were lower.

The total pressures at the rotor exit were measured for all three hub, mean, and tip streamtubes in these builds. The hub and tip measurements were added to evaluate any change in exit profile due to the new guide vanes and to permit an evaluation of the section performance for the exit stator. The results indicate that with the new IGV, the tip streamtube pressure ratio has increased relative to the mean streamtube and is higher than the mean streamtube at peak pressure ratio, while the hub streamtube is still the highest.

The vector diagrams for the maximum pressure ratio point of build 8 are shown in Figure 33. The inlet vectors are consistent with those of build 6A and again confirm the design speed rotor incidence established in phase II. The exit vectors reflect higher exit Mach numbers than for build 6A. which is attributable to the lower level of the static pressures measured at station 4. The outer shroud static pressure decreased about 2.5 inches of mercury from the trailing edge of the rotor to station 4 in these builds (see Figure 28). This indicates that the flow along the extreme outer shroud reaccelerates from a Mach number of 0.87 at the rotor trailing edge to a Mach number of 0.92 at station 4. This reacceleration was believed to be associated with the relatively forward position of the rotor shroud with respect to the rotor and the gap at the rear of the shroud. Due to this change in axial position, the static pressure measurement at the rotor trailing edge is actually .060 inch upstream of the tip trailing edge instead of a few thousandths of an inch downstream, where the static pressure is probably a little higher. Figure 34 compares the rotor passage total pressure recovery at design speed peak pressure ratio with the design case. The results indicate that both the recovery at mid span and the average are below the design values. The hub is above, and the tip just at, its respective design value. The hub and tip recoveries did not deviate from the design as much as in the phase I data. The average design recovery was expected to be met when the design airflow was met, as in the case of build 3 of phase II.

Exit Stator and Interconnecting Duct Performance

Figure 35 shows the losses for the exit stator and interconnecting duct along constant speed lines as a function of stage pressure ratio for build 8. The minimum losses were generally higher than those for build 6A. The higher loss level is attributed to the reacceleration of the flow between the trailing edge of the rotor and the leading edge of the exit stator. As a result of the reacceleration, the Mach number at the stator entrance is higher and the flow angle is limited so that higher incidence angles are not achieved. As in the case of build 6A, the losses decrease to the

$N/\sqrt{\theta}$ = 100%
$(W\sqrt{\theta})/\delta$ = 3.66 lb/sec
Rotor P_T/P_T = 2.79:1

——— Test
– – – – Design

Tip Streamtube

γ_{in} = 3.01
γ_{out} = 2.81 in.

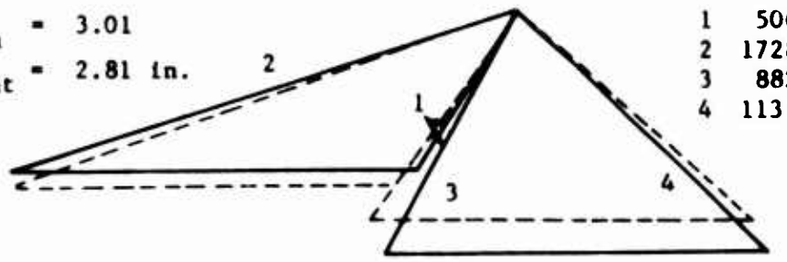

	V	a	M
1	506	29.0	.533
2	1728	73.0	1.592
3	882	28.5	.716
4	1131	46.5	.919

Mid Streamtube

γ_{in} = 2.71 in.
γ_{out} = 2.67 in.

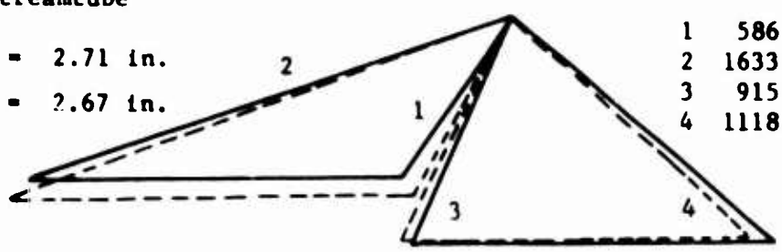

	V	a	M
1	586	31.2	.540
2	1633	72.1	1.505
3	915	21.3	.743
4	1118	49.5	.908

Hub Streamtube

γ_{in} = 2.36 in.
γ_{out} = 2.52 in.

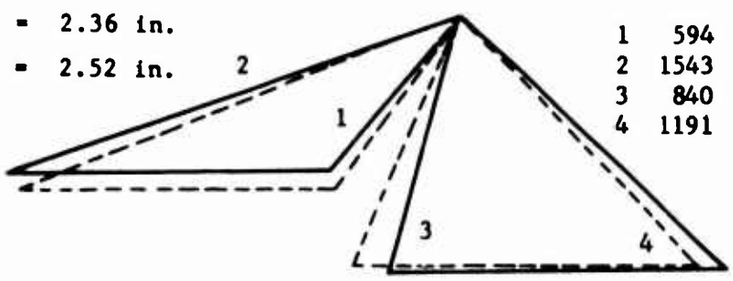

	V	a	M
1	594	35.3	.548
2	1543	71.7	1.423
3	840	16.4	.691
4	1191	47.4	.981

Figure 33. Build 8 Test Data, Vector Diagrams.

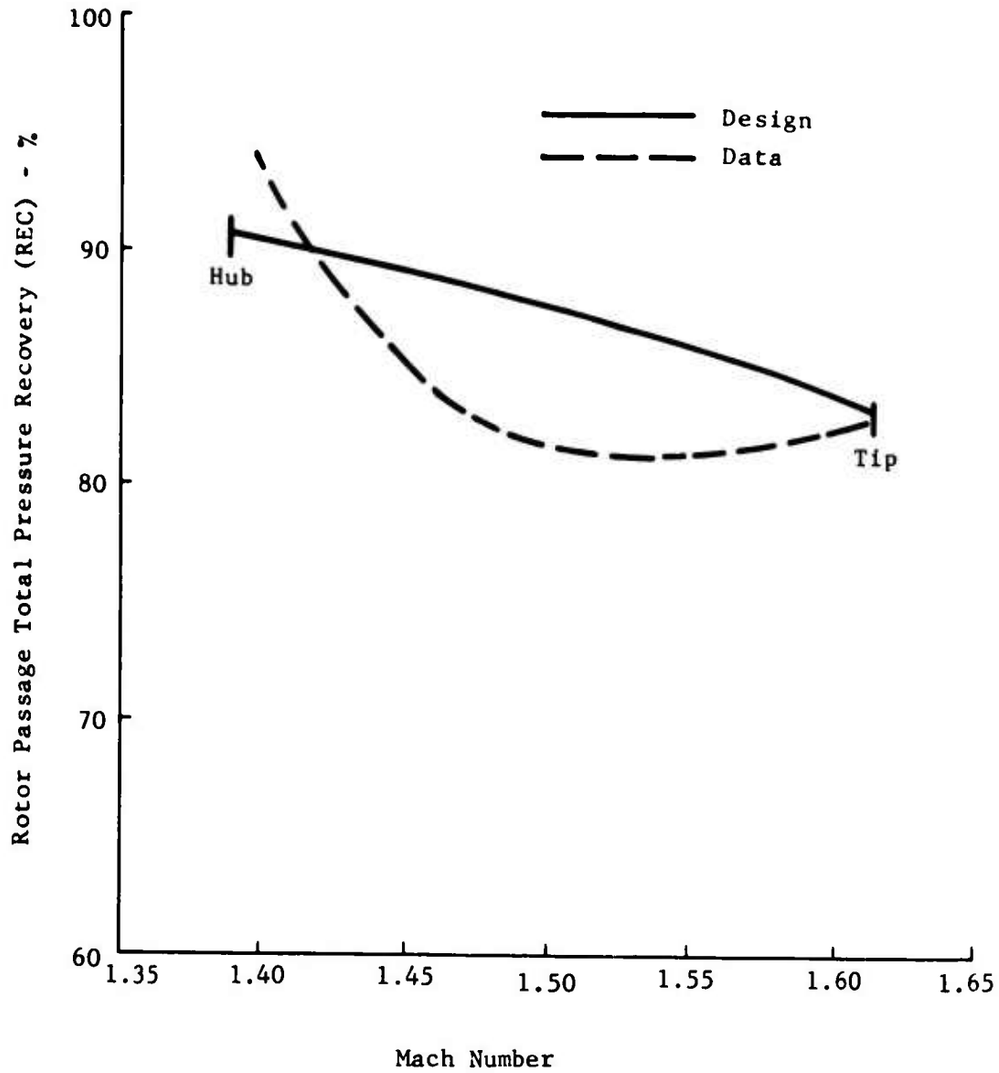

Figure 34. Build 8 Test Data, Rotor Passage Total Pressure Recovery for $N/\sqrt{\theta}$ =100%, $(W\sqrt{\theta})/\delta$ =3.661 lb/sec, and P_T/P_T =2.56:1.

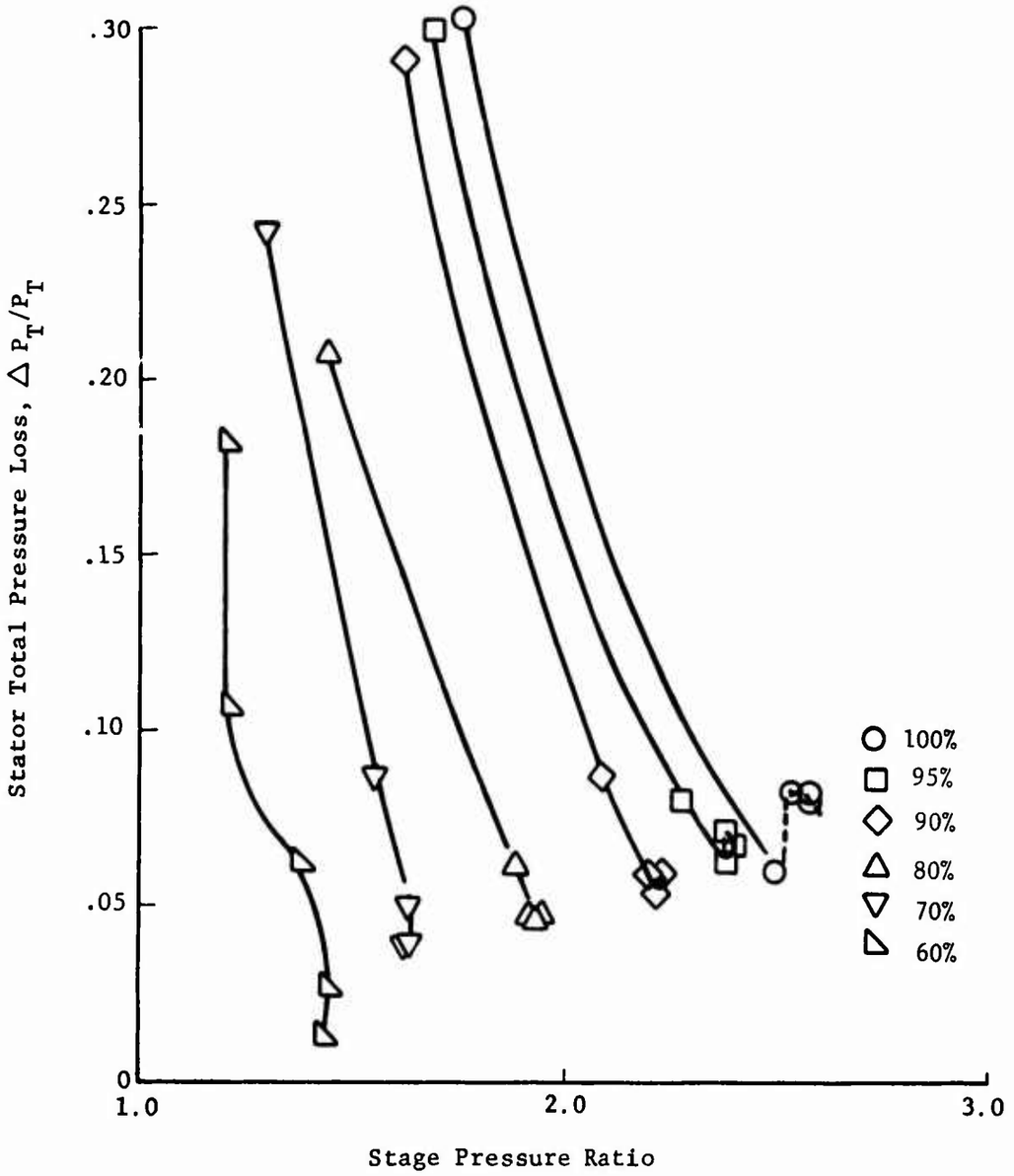

Figure 35. Build 8 Test Data, Pressure Loss for Exit Stator and Interconnecting Duct.

point of maximum throttling with the exception of a few points. The points which deviated from this trend are found to be associated with a condition where the stator entrance Mach number increases and the incidence angle decreases during the throttling to the last one or two most back-pressured points on a speed line. Figure 36 shows a compilation of the loss data for the speed range of 90 to 100 percent as a function of stator incidence for builds 7, 8, and 9. The results indicate that the minimum tip streamtube losses have met and surpassed the 3-percent design goal, while the hub and mid streamtubes have not. The data also indicate that none of the streamtubes have reached a minimum loss incidence, although the tip appears close. The mid streamtube appears to be at least 2 degrees away from the minimum loss incidence, and the hub streamtube appears to be at least 4 degrees short.

The radial profiles at the stage exit (station 5) are shown for the Mach number in Figure 37 and for the total pressure and temperature in Figure 38. These data are presented for the design speed peak pressure ratio for build 8 and are typical for builds 7 and 9, whose results are summarized in Table II. The total pressure profiles across the blade wakes for build 7 at design speed are shown for the peak pressure ratio point in Figure 39 and a part-throttle point in Figure 40. The maximum variation from the mean value is $\pm$5.0 percent at the peak pressure ratio. The amplitudes of the blade wakes are seen to decrease as the compressor is throttled. Figure 41 shows the profile at station 6 for the same part-throttle point. The mixing has reduced the amplitudes at the part-throttle point from 6.0 percent at station 5 to $\pm$2.5 percent at station 6. The average total pressures at the stage exit were determined as the average of the nine-element rake data. This average agreed with the traversing probe data.

The static pressures at the stage exit are lower for builds 7, 8, and 9 than for build 6A. This condition is attributed to the combination of the flow reacceleration at the rotor exit and the added blockage of the extra instrumentation at the rotor exit and the stage exit.

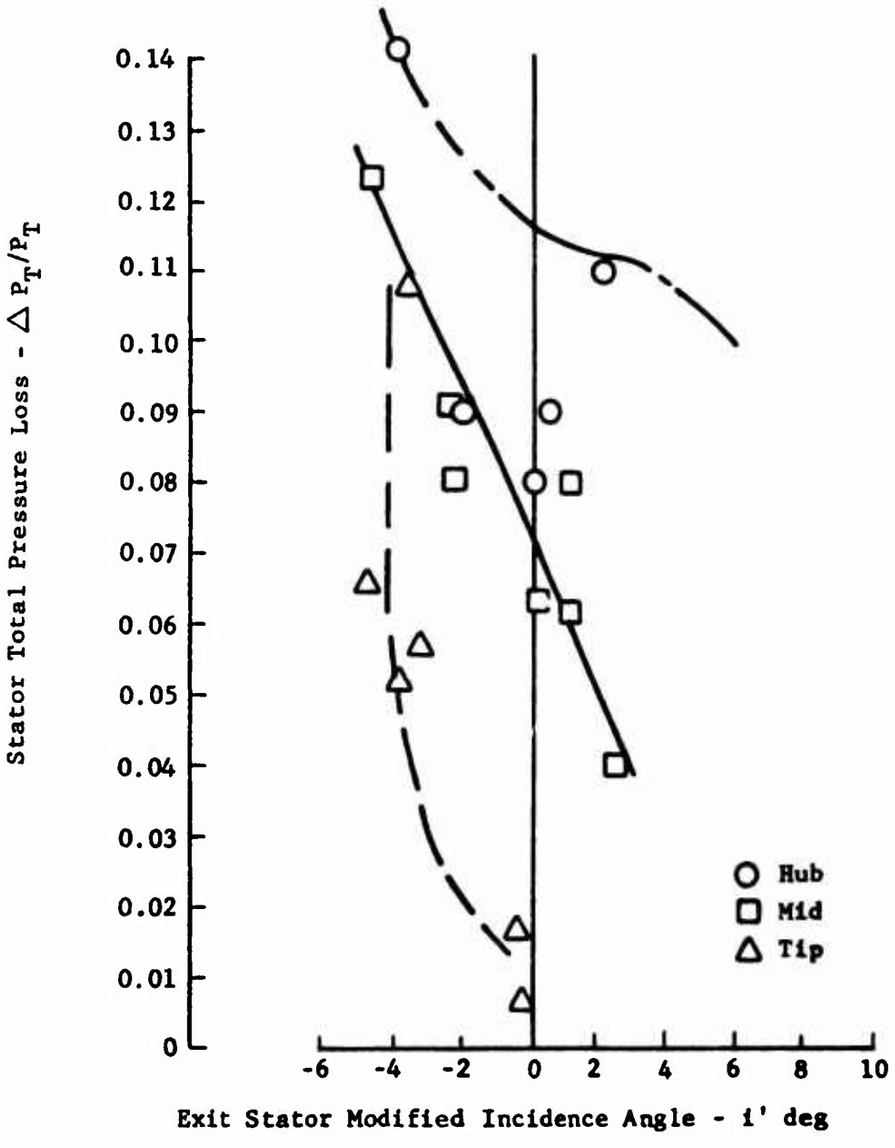

Figure 36. Builds 7,8, and 9 Test Data, Exit Stator and Duct Pressure Loss Versus Stator Incidence.

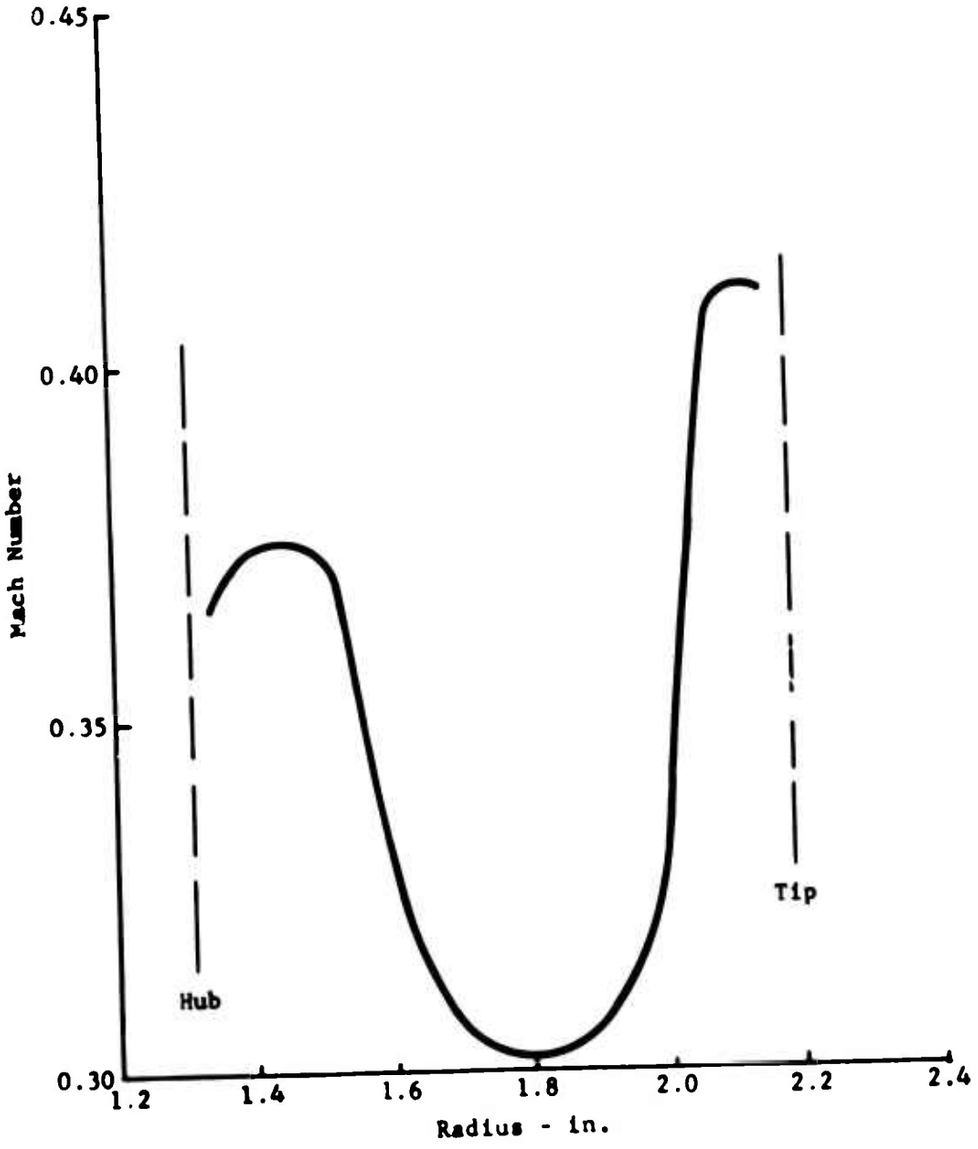

Figure 37. Build 8 Test Data, Mach Number Profile at Stage Exit Station 5 for $N/\sqrt{\theta}$=100%, $(W\sqrt{\theta})/\delta$ =3.661 lb/sec, and P_T/P_T =2.56:1.

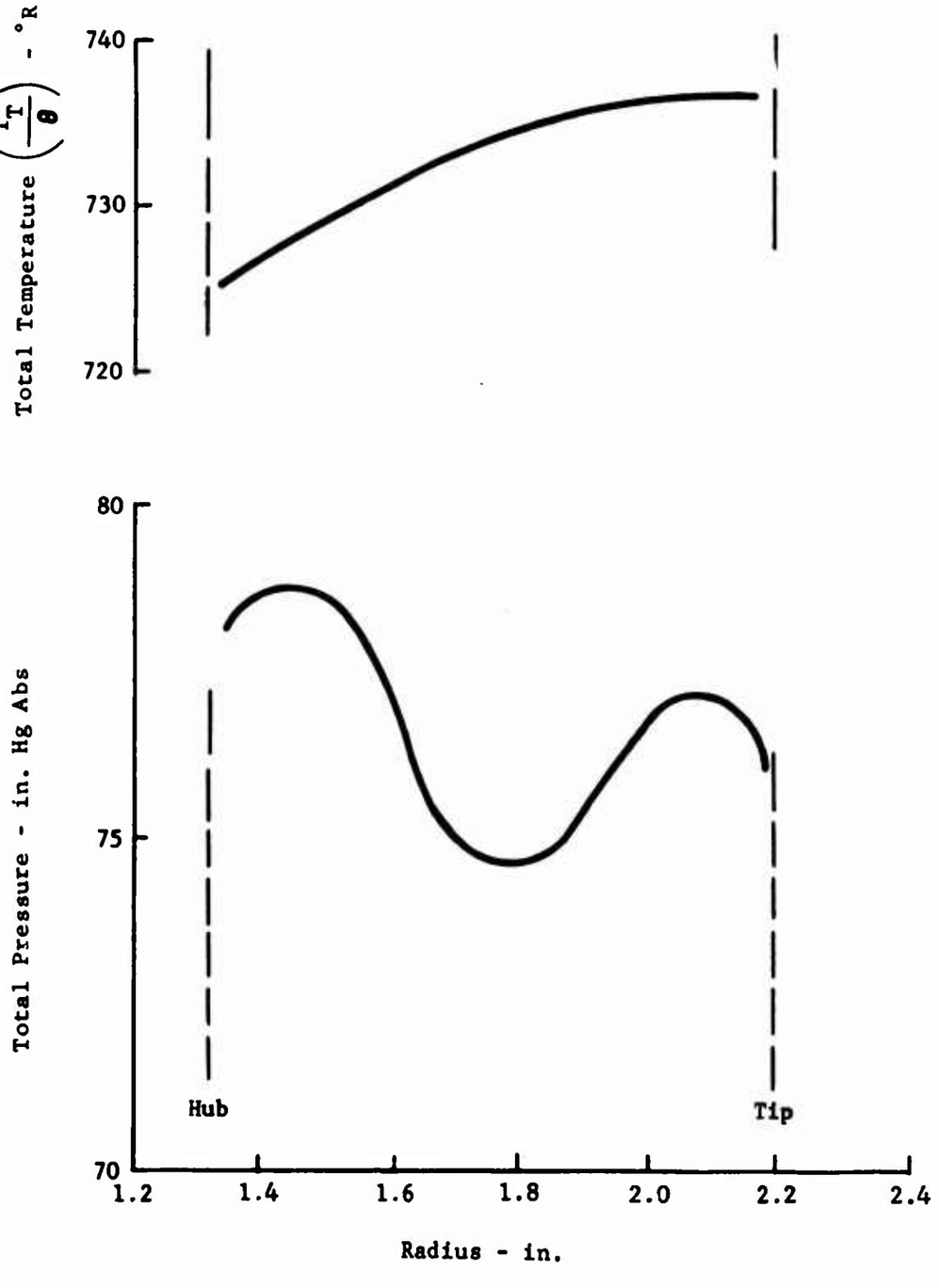

Figure 38. Build 8 Test Data, Temperature and Pressure Profiles at Stage Exit Station 5 for $N/\sqrt{\theta}$=100%, $(W\sqrt{\theta})/\delta$ =3.661 lb/sec, and P_T/P_T =2.56:1.

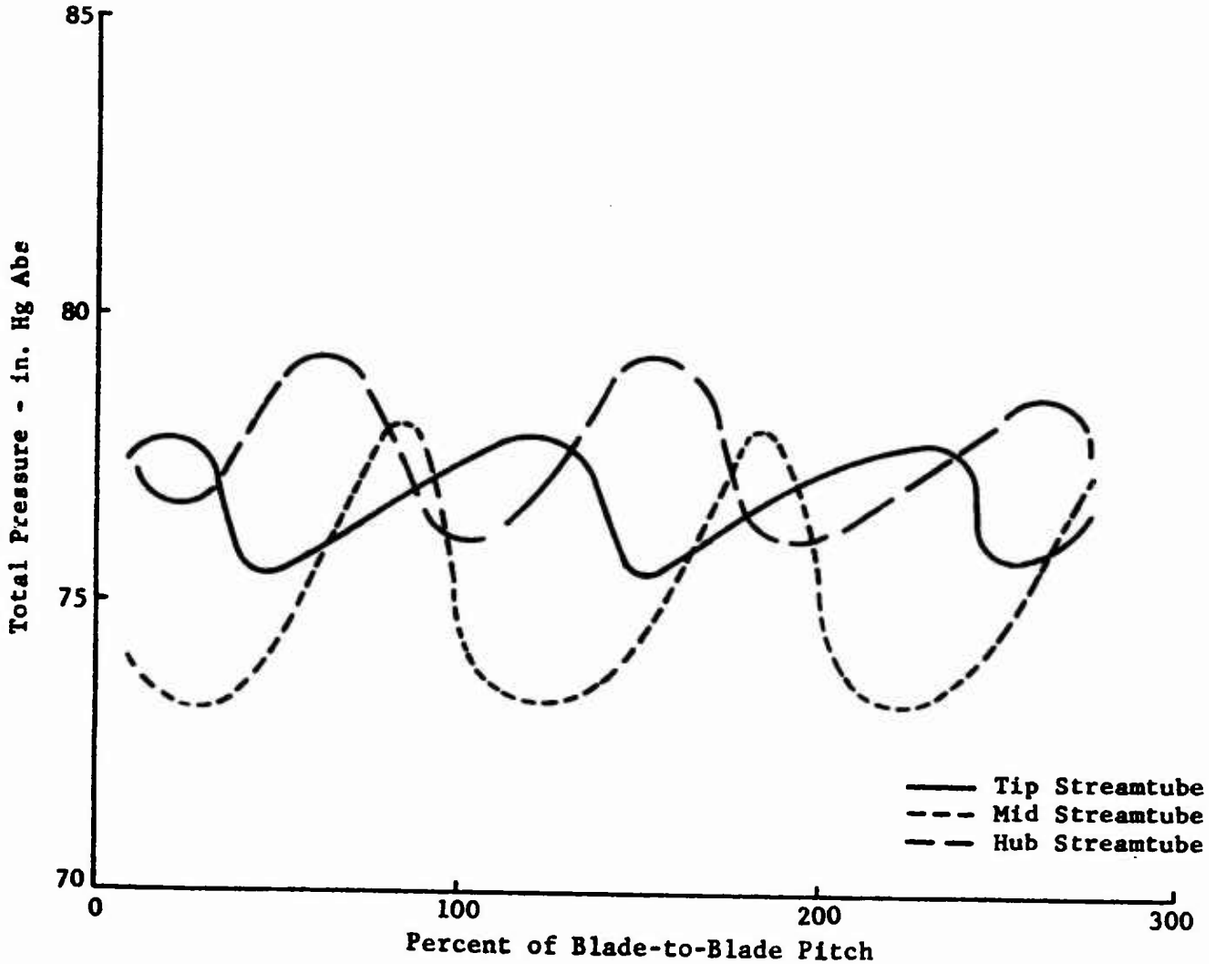

Figure 39. Build 7 Test Data, Total Pressure Profiles Across Blade Wakes at the Stage Exit Station 5 for $N/\sqrt{\theta}$=100%, $(W\sqrt{\theta})/\delta$ =3.70 lb/sec, and P_T/P_T =2.61:1.

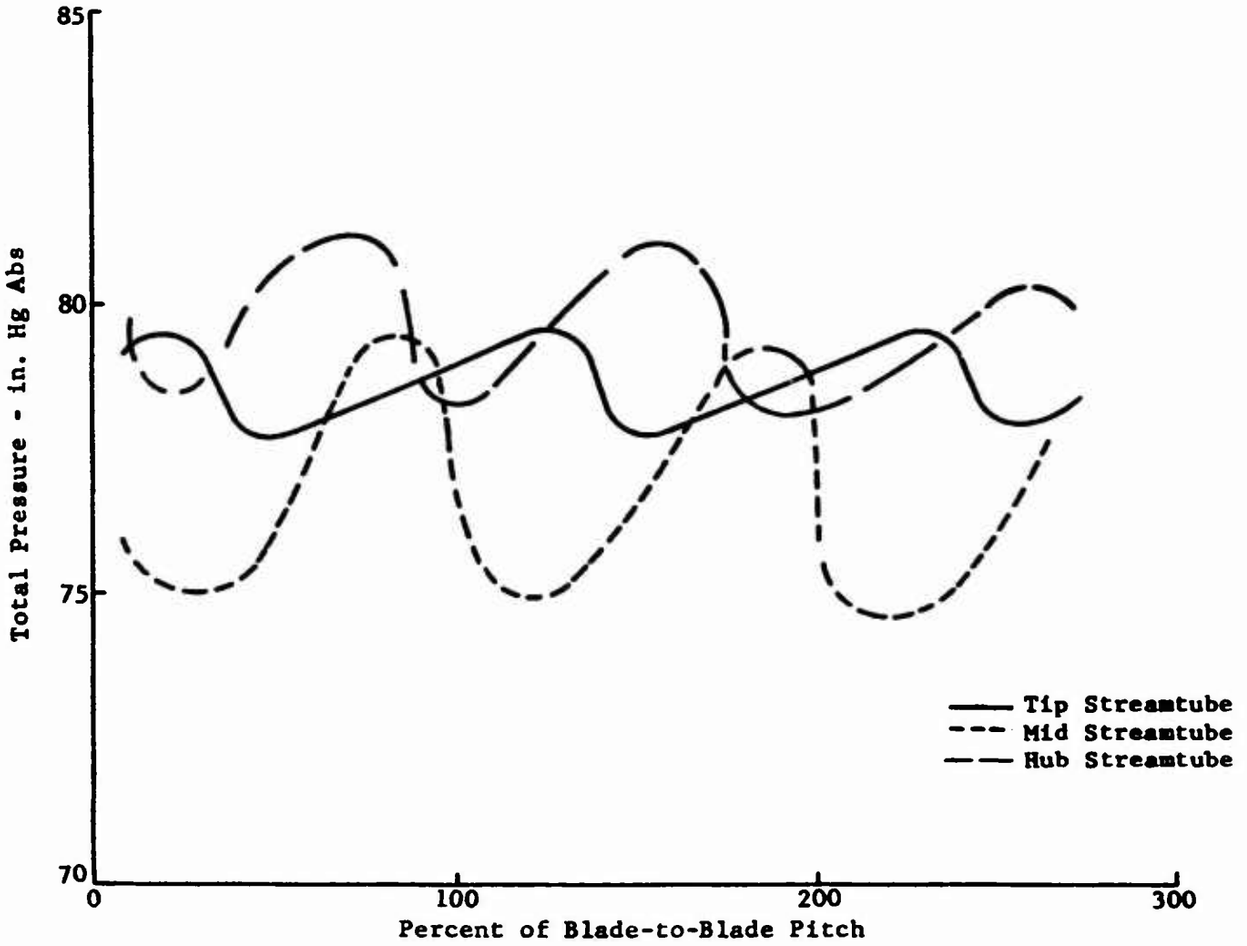

Figure 40. Build 7 Test Data, Total Pressure Profiles Across Blade Wakes at the Stage Exit Station 5 for $N/\sqrt{\theta}$=100%, $(W\sqrt{\theta})/\delta$ =3.71 lb/sec, and P_T/P_T =2.55:1.

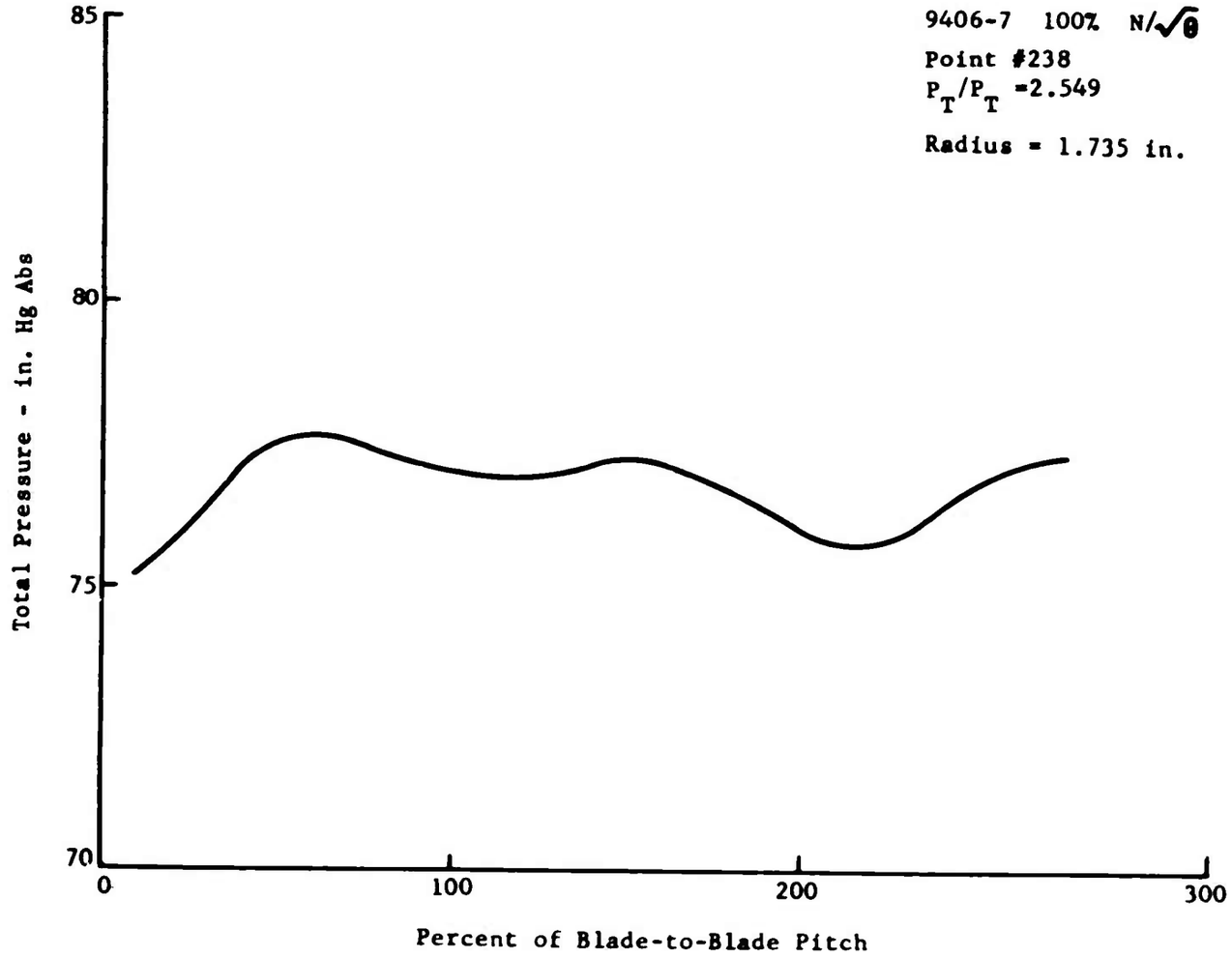

Figure 41. Build 7 Test Data, Total Pressure Profile Across the Mid Streamtube Blade Wakes at the Stage Exit Station 6 for $N/\sqrt{\theta}$ =100%, $(W\sqrt{\theta})/\delta$ =3.71 lb/sec, and P_T/P_T =2.55:1.

MODIFICATION OF STAGE DESIGN AND RETEST

Builds 10, 10A, 11, and 12 were tested under this task. The compressor configuration for these builds differed from builds 7, 8, and 9 in that (1) the burr was removed from the exit of the IGV housing, (2) the IGVs were reworked to vary to -7 degrees, (3) a new rotor was used which was modified to induce design airflow and had a correct tip diameter for proper positioning with respect to the shroud, and (4) the exit stator leading edge design was modified.

Builds 10 and 10A represented a -4-degree IGV setting. The IGV setting was changed to -7 degrees in build 11 and to design setting in build 12.

STAGE REDESIGN

The performance of each blade row in the tests of the previous builds was reviewed so as to establish the redesign necessary to correct the deficient areas.

Inlet Guide Vanes

The performance of the developed airfoil IGV assembly was superior to that of the NACA 65 series IGV, and therefore the former was included in the final configuration. The data indicated that the developed airfoil IGV worked as expected, and there was no evidence to indicate that a design modification would offer improved performance in this blade row. The removal of the burr at the exit of the IGV housing was one rework specified, and increasing the range of IGV settings to -7 degrees was the other. Removing the burr on the IGV housing together with the proper positioning between the rotor and the shroud was expected to correct the drop in static pressure from the IGV trailing edge to the rotor leading edge experienced in builds 7, 8, and 9. The provision for a -7-degree IGV setting was included since the -4-degree IGV setting in build 8 resulted in higher efficiencies than at the design setting in build 7, and the data from the 2:1 supersonic compressor program indicated that this direction might result in further performance gains.

Rotor

The results from the stage tests in builds 6, 7, 8, and 9 showed that the presence of the exit stator did not limit the airflow capacity of the rotor nor significantly affect the rotor performance; however, the circumferential uniformity was improved considerably. These tests also demonstrated that the desired tip clearance could be set without encountering a tip rub through design speed. The rotor tested in build 3 of phase II, which was fabricated to the configuration 2 specification, demonstrated the design airflow goal of 4.0 pounds per second with the NACA 65 series IGV. The airflow induction performance of the compressor at 100 percent speed is considered to be equal for both the newly developed IGV and the NACA 65 series IGV, and therefore the compressor was expected to meet the design airflow with the configuration 2 rotor and the developed airfoil IGV. The specified rotor leading edge expansion surface angle for configuration 2

is 1.6 degrees less than for configuration 1. The data from builds 3 through 9 indicated that the design rotor conditions would be met when the design airflow was induced and the circumferential profile was uniform. Based on these results, the configuration 2 rotor specification was defined. Any further redesign did not appear to be warranted. The same method of fabrication as used for rotor S/N 2 was followed, since there was little risk of sustaining damage to the leading edge as the result of a tip rub.

Exit Stator and Interconnecting Duct

The data from builds 7, 8, and 9 indicated that the incidence angle for minimum stator and duct losses at the hub was approximately 4 degrees higher than the original design value. The tip incidence for minimum loss was close to the design value, and the mid section value was halfway between the tip and the hub. The leading edge angle for the exit stator airfoils was redefined to decrease the angle at the hub by 5 degrees, and this angle change was to vary linearly along the span to 0 degrees at the tip. This redesign was based on meeting the rotor exit design conditions. No requirement for changes in the remainder of the stator or duct passage was evident from the data. It was concluded that the leading edge angle modification could be accomplished as a rework of the existing stator. This required the removal of the inner shroud in the leading edge area by machining it away to free the airfoils at the hub for twisting as required. After the twisting was completed, a replacement inner shroud piece was fabricated and tailored to mate with a slight interference fit at the blade ends.

The rotor shroud was lengthened to limit the gap at the trailing edge face to less than .005 inch (Figure 42). This rework, together with the proper positioning of the rotor relative to the shroud, was expected to correct the flow acceleration encountered in this area in builds 7, 8, and 9. The cone angle of the extended trailing edge portion was made 7 degrees less than the rest of the rotor shroud to match the contour of the exit stator outer shroud, which was also modified slightly to improve the flow path and to minimize the local annular convergence.

FABRICATION OF REDESIGN

Provision for varying the IGV angle to -7 degrees was made by removing a few thousandths of an inch from the ends of the blades at the inner shroud. The burr was also removed from the IGV housing.

The newly fabricated rotor (S/N 5) was first received without the leading edge expansion surface modification, as indicated by the inspection measurements. The compression surface angle was also measured at that time. The rotor was returned to the vendor for completion of the angle modification. Measurements of the corrected airfoils for the new rotor indicate that the leading edge expansion surface angles were 3/4 to 1 degree lower than the nominal specified. The compression surface was not machined during the correction of the airfoil, but the measurements indicated compression surface angles 3/4 to 1 degree lower than before the airfoil correction. This

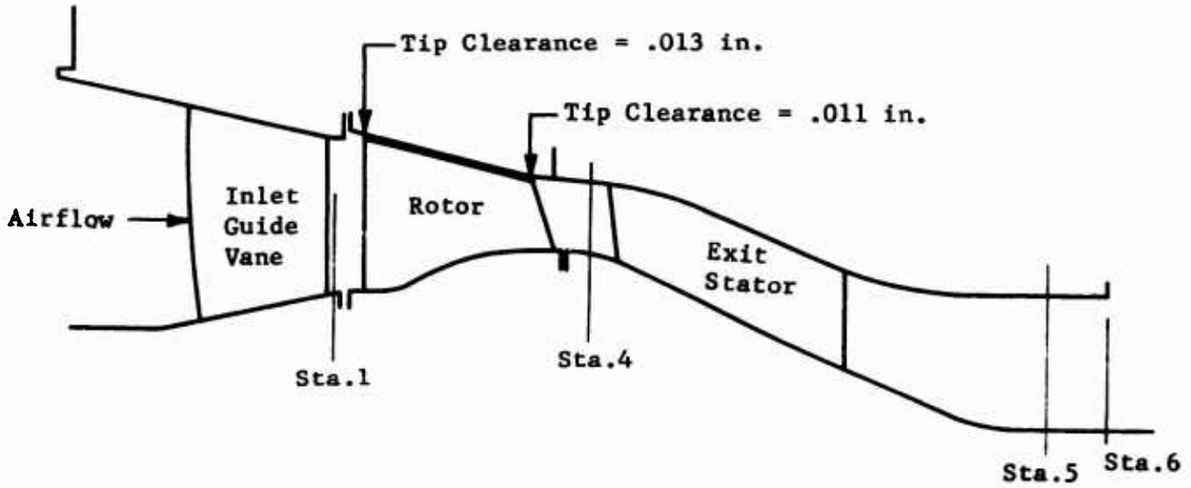

Figure 42. Flow Path for Builds 10, 10A, 11, and 12.

angle change could be attributed to either a change in the measuring reference during inspection or an actual shift of the leading edge as a result of the machining. In either case, the rotor was expected to induce the design airflow or higher in this test, thereby permitting the evaluation of the effect of increased airflow on performance as desired. The final tip grind of the rotor resulted in a leading edge radius of 3.1585 inches, which was well within the specified tolerance.

The exit stator leading edge changes were performed by making the dimensional change (.025 inch at the hub), which was calculated to meet the nominal 5-degree angle decrease at the hub. Figure 43 compares the measured expansion surface angles at the leading edge of the reworked stator vanes to those from the inspection prior to the rework. Final measurements indicate an angle decrease at the extreme hub of 10 to 11 degrees. A greater than nominal change was preferred rather than a smaller one in order to insure a change in the performance which could be measured and evaluated. The resultant change was acceptable in view of this consideration and the recognition that it is difficult to measure angle changes with a high degree of accuracy for these small dimensional changes.

TEST CONFIGURATION

The test configuration for build 10, which is shown in Figure 42, differs from build 8 by the redesign modifications discussed in the previous sections,including the change in the range of the IGV variation, the new rotor (S/N 5) with modified leading edge angle, the new extended rotor shroud, and the reworked exit stator. The rotor tip clearance was established at .013 inch at the leading edge and .011 inch at the trailing edge,with the rotor properly positioned with respect to the rotor shroud (Table I). The IGV setting was -4 degrees for build 10. Builds 11 and 12 differed from build 10 only by a change in IGV setting to -7 degrees and to design setting respectively.

INSTRUMENTATION

All the instrumentation included in builds 7, 8, and 9 was retained in builds 10, 11, and,12 and the instrumentation listed in Table VI was added.

The static pressures were added to investigate the flow velocities at the hub just at the leading edge of the exit stator and just inside the stator blade passage.

The unshielded thermocouples were added to investigate the validity of the stagnation thermocouple data. Test results from another program had indicated that the measurements from the stagnation thermocouples were readily distorted by impinging droplets of oil leading into the airflow while those from the unshielded thermocouples were not significantly affected under the same conditions.

The thermocouples at station 6 were also changed from the .040-inch wire used in builds 7, 8, and 9 to .060-inch wire for added strength.

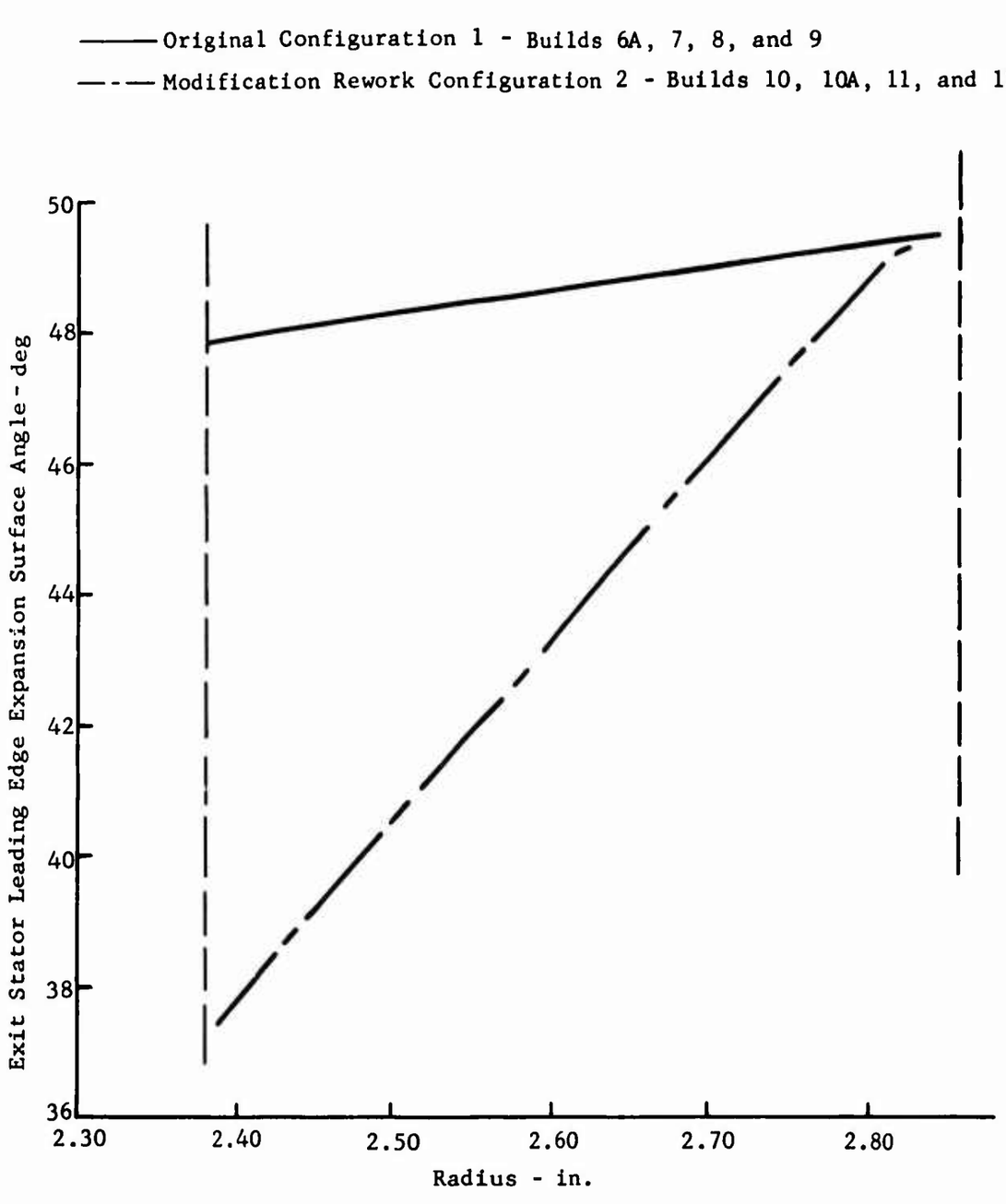

Figure 43. Measured Leading Edge Expansion Surface Angles of Reworked Exit Stators for Builds 10,11, and 12 Compared to the Original Exit Stator Configuration.

TABLE VI. INSTRUMENTATION ADDED TO BUILDS 10, 11, AND 12

Instrumentation	Location			Operating Range
	Axial	Circumferential (deg)	Radial Distance from Flow Path O.D. (in.)	
3 static pressures	.140 inch downstream of station 4	134 ,139 , 143	Flow Path I.D.	0 to 60 in. Hg. gage
2 static pressures	.20 inch downstream of stator L.E.	138 , 289	Flow Path I.D.	0 to 60 in. Hg. gage
1 four-element pitot rake $\alpha = 0^{o}$	station 6	240	.48, .74, .90, 1.16	0 to 60 in. Hg. gage
2 four-element unshielded IC thermos	station 6	80 , 140	.48, .74, .90, 1.16	50^{o}F to 500^{o}F

DESCRIPTION OF TEST

Testing of build 10 was initiated and progressed through 70 percent speed, where the vibration levels evidenced a loose clearance between a bearing race and the housing bore. The rig was disassembled, the condition corrected, and the rig reassembled as build 10A with no change in the compressor configuration. Testing was resumed and completed for all builds through 100 percent speed without mechanical difficulty. Points were obtained at 102 percent speed in build 10A and 101 percent speed in build 12. A total testing time of 45:55 and 229 data points were accumulated.

Post-test inspection of the rig revealed one slight nick on the leading edge of a rotor blade which was not considered to be significant. There was no evidence of a rotor tip rub on the shroud.

The surge line was investigated through 100 percent speed in all three builds.

TEST RESULTS

Stage Performance

The three stage-performance maps for each of the IGV settings of -4 degrees open, -7 degrees open, and design are Figures 44, 45, and 46 respectively. Table VII summarizes the demonstrated peak pressure ratio and efficiency at each speed.

TABLE VII. STAGE PERFORMANCE DATA FOR BUILDS 10, 11, AND 12

	Percent Speed						
	60	70	80	85	90	95	100
Stage Pressure Ratio:							
Predicted Peak @ Design IGV Setting	1.41	1.60	1.84	-	2.26	2.56	2.80
Data Peak @ Design IGV Setting	1.47	1.69	1.98	2.14	2.33	2.54	2.69
Data Peak @ -4° IGV Setting	1.45	1.66	1.94	2.10	2.28	2.45	2.62
Data Peak @ -7° IGV Setting	1.29	1.64	1.90	2.07	2.22	2.39	2.59
Stage Efficiency:							
Predicted Peak @ Design IGV Setting	83.3	-	82.7	-	82.5	-	82.2
Data Peak @ Design IGV Setting	81.5	79.2	78.0	76.2	75.4	75.9	73.8
Data Peak @ -4° IGV Setting	81.2	80.2	77.1	77.3	75.9	74.6	74.7
Data Peak @ -7° IGV Setting	82.5	79.5	80.0	78.1	76.7	75.6	74.8

The design speed corrected airflow for attached flow conditions at the rotor leading edge exceeded the design flow goal of 4.0 pounds per second at all three IGV settings. In each case the flow decreased slightly just prior to surge.

The peak stage pressure ratios at the -4-degree IGV setting (build 10A) were higher than for build 8 at all speeds. The increase in pressure ratio is attributed to the higher work input which accompanies the increased airflow. The build 10A peak stage efficiencies were generally within 1 point of those for build 8 at each respective speed, with no consistent trend of being higher or lower. The peak efficiencies for builds 10, 11, and 12 are

Rotor Configuration 6, Stator Configuration 2

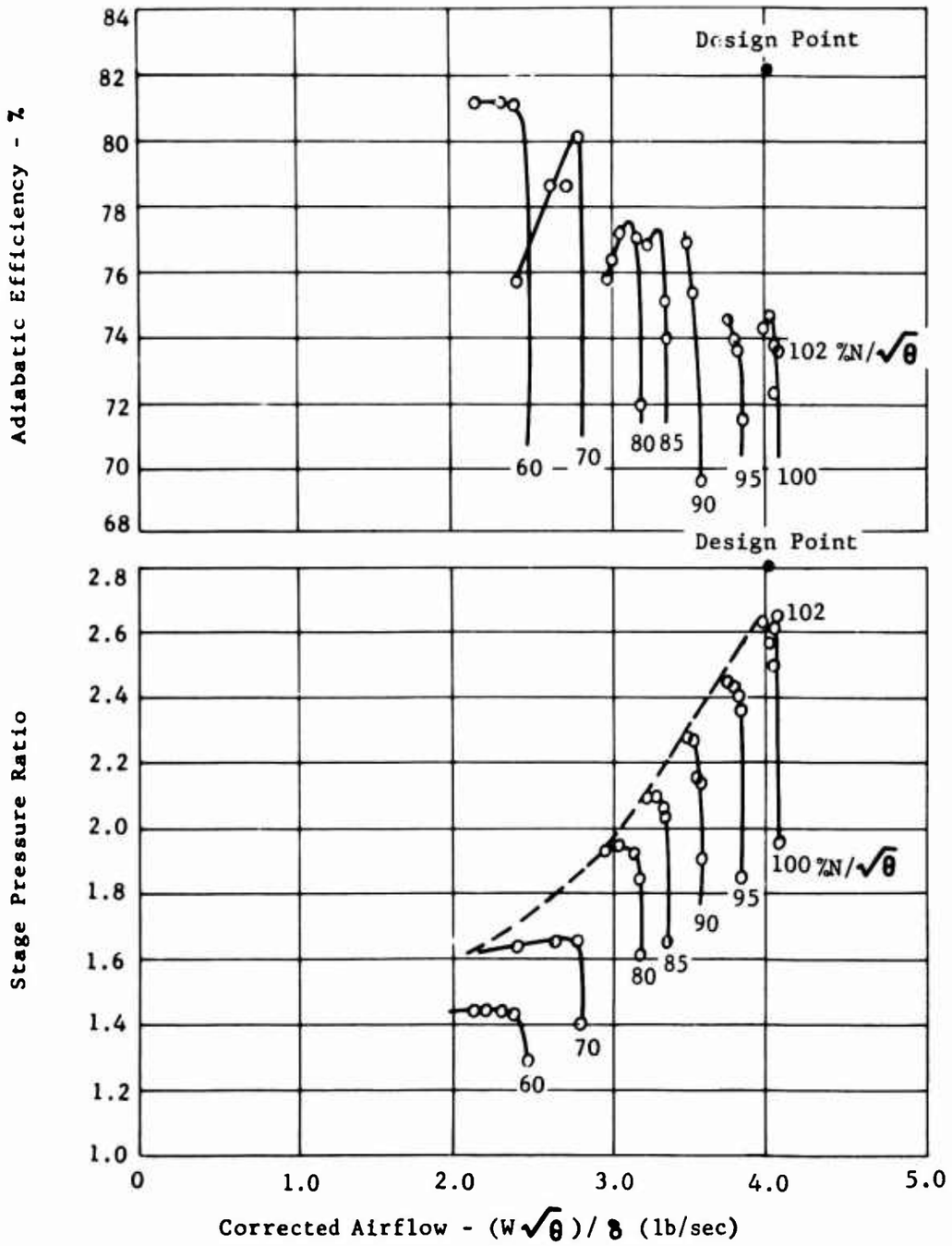

Figure 44. 2.8:1 Supersonic Compressor Test Stage Data, Build 10A, Developed Airfoil IGV at -4° Setting.

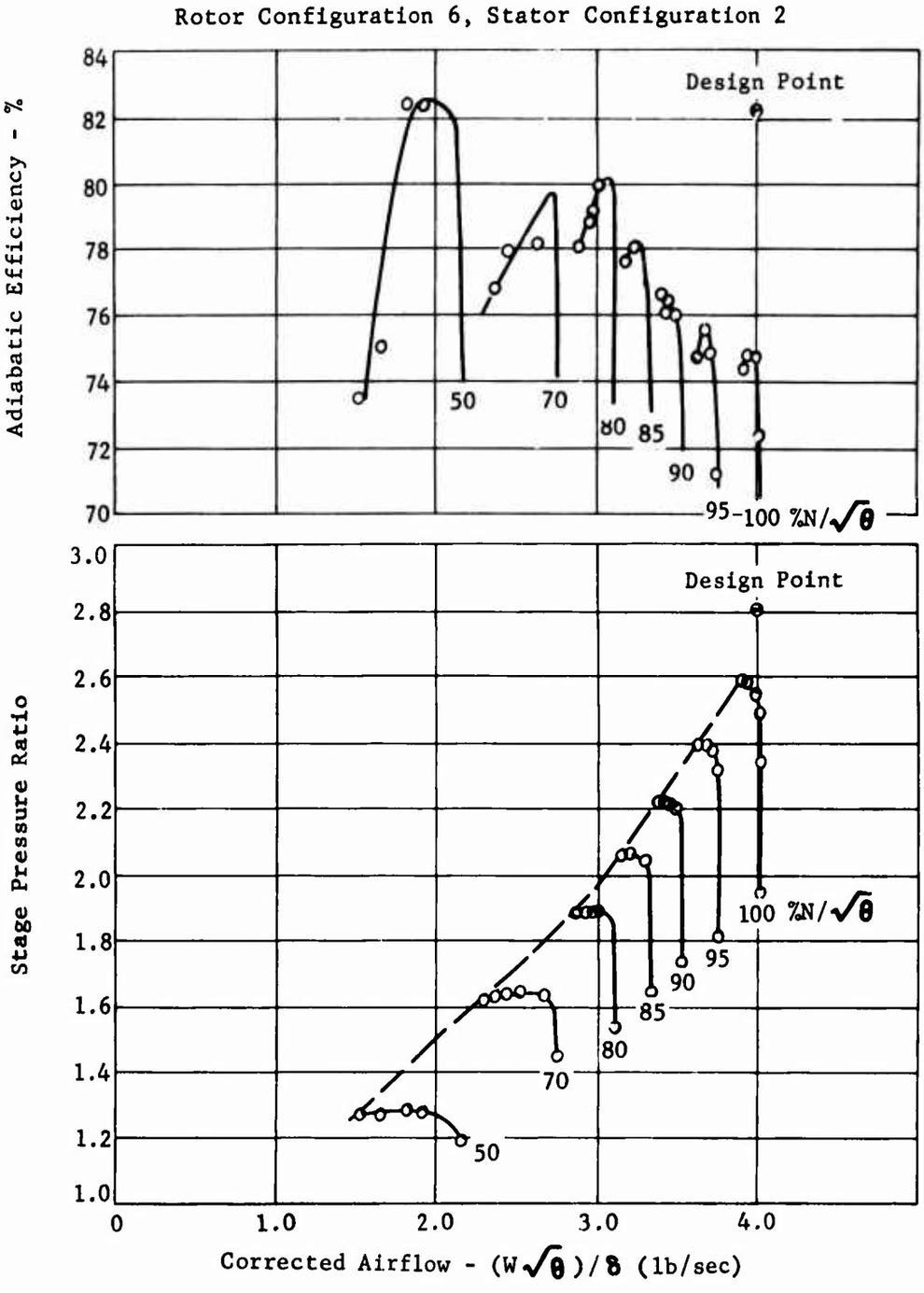

Figure 45. 2.8:1 Supersonic Compressor Test Stage Data, Build 11, Developed Airfoil IGV at -7° Setting.

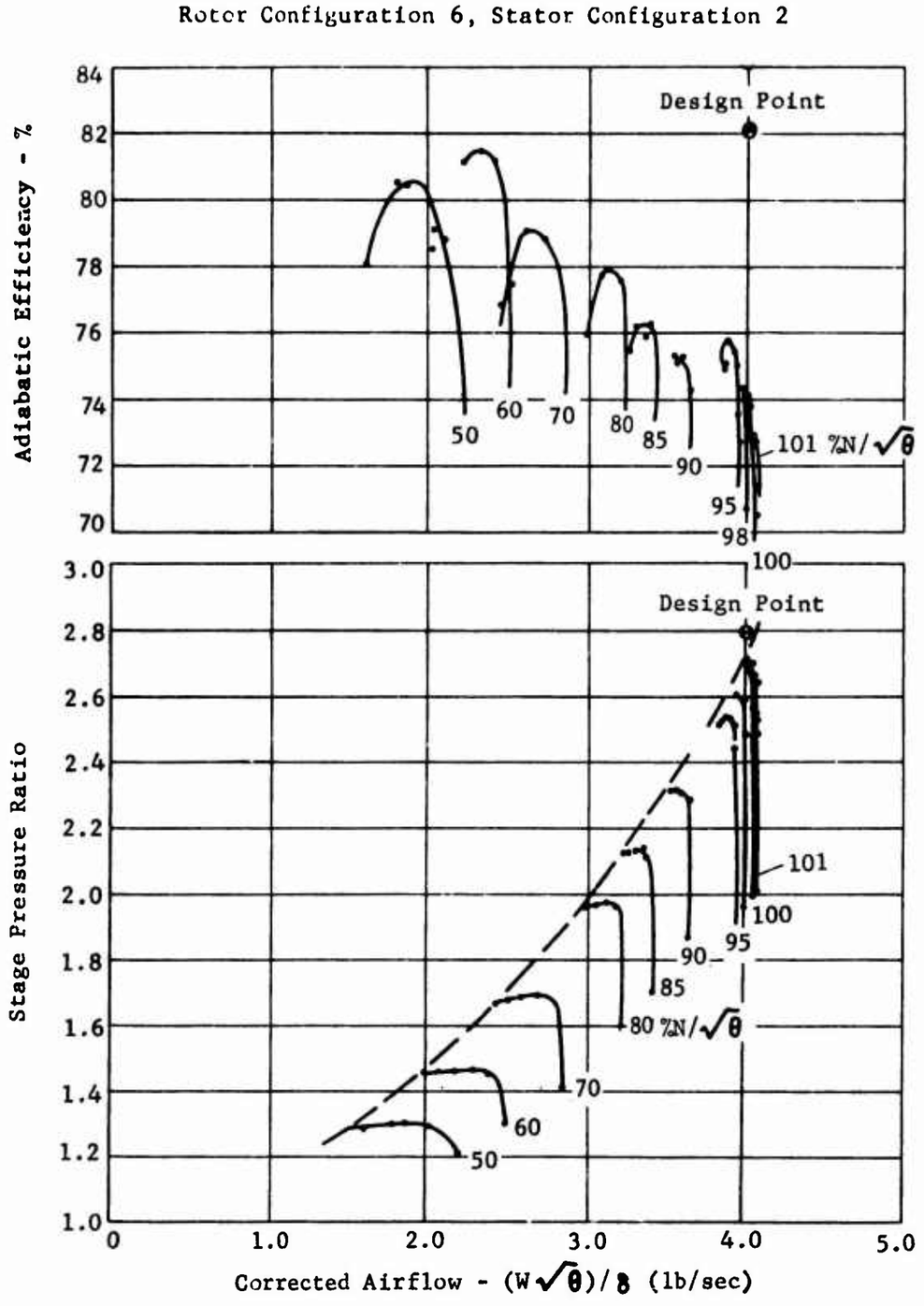

Figure 46. 2.8:1 Supersonic Compressor Test Stage Data, Build 12, Developed Airfoil IGV at Design Setting.

generally with n 1 point of each other at respective speeds, with only a couple of exceptions which differ up to 2.9 points. A maximum design speed stage pressure ratio of 2.69:1 was demonstrated in build 12 at an efficiency of 73.8 percent. The best design speed stage efficiency was 74.8 percent at a pressure ratio of 2.59:1.

An analysis of the stage performance indicates that the modified rotor has induced the design flow, and a further improvement in rotor performance has been measured to the point where the IGV and rotor have very nearly achieved all of their design goals, as discussed in the following sections. The major deficiency in the stage performance is in the higher than design losses of the exit stator and interconnecting duct. The results from this test did not show the desired reduction in stator and duct losses; however, the reacceleration between the rotor trailing edge and the stator leading edge was not eliminated or improved, and this condition may be the overriding factor in preventing a noticeable reduction in the stator and duct losses by adjustment of the stator incidence. Figure 47 shows the distribution of the static pressure through the compressor for build 10A, and it can be seen that the static pressure drop at the outer shroud between the rotor trailing edge and the stator leading edge is more extreme at the higher airflow than in build 8. The added static pressure measurements indicate that the static pressure at the hub shroud continues to decrease in the vicinity of the stator leading edge but begins to increase at a high rate just inside the blade passage. It is apparent that the rotor to shroud positioning and the gap at the rotor shroud trailing edge were not responsible for the acceleration in this area. Since the acceleration was not particularly severe prior to build 7, other changes between builds 6 and 7 were reviewed to find the probable cause. The two known changes which could have possibly effected the flow in this area are the substitutions of the developed airfoil IGV and the addition of two fixed pitot probes at the rotor exit. The static pressure measurements at the IGV exit show an improvement in flow conditions for the developed airfoil IGV. The static pressures along the rotor shroud for builds 7 through 12 show no significant deterioration relative to the data from build 6, and therefore the developed airfoil IGV does not appear to be responsible. The geometric blockage of the added pitot probes at the rotor exit was small enough that the probes were not expected to have had a significant effect. A local separation due to the probes, however, which amplifies the blockage effect could explain the acceleration. These probes are, therefore, the most probable cause of this acceleration.

The surge lines for builds 10, 11, and 12 show a characteristic versus airflow which is more nearly linear than predicted by a considerable amount. The surge line for build 12 shows a lower surge margin from the peak pressure ratio at design speed than for the predicted case; however, between 60 and 95 percent speed, the surge margin with respect to a potential operating line is far more favorable for the demonstrated data.

Inlet Guide Vane Performance

The measured static pressures at design speed for build 10A are compared to the design values in Figure 48. The corrected airflow is within 0.5

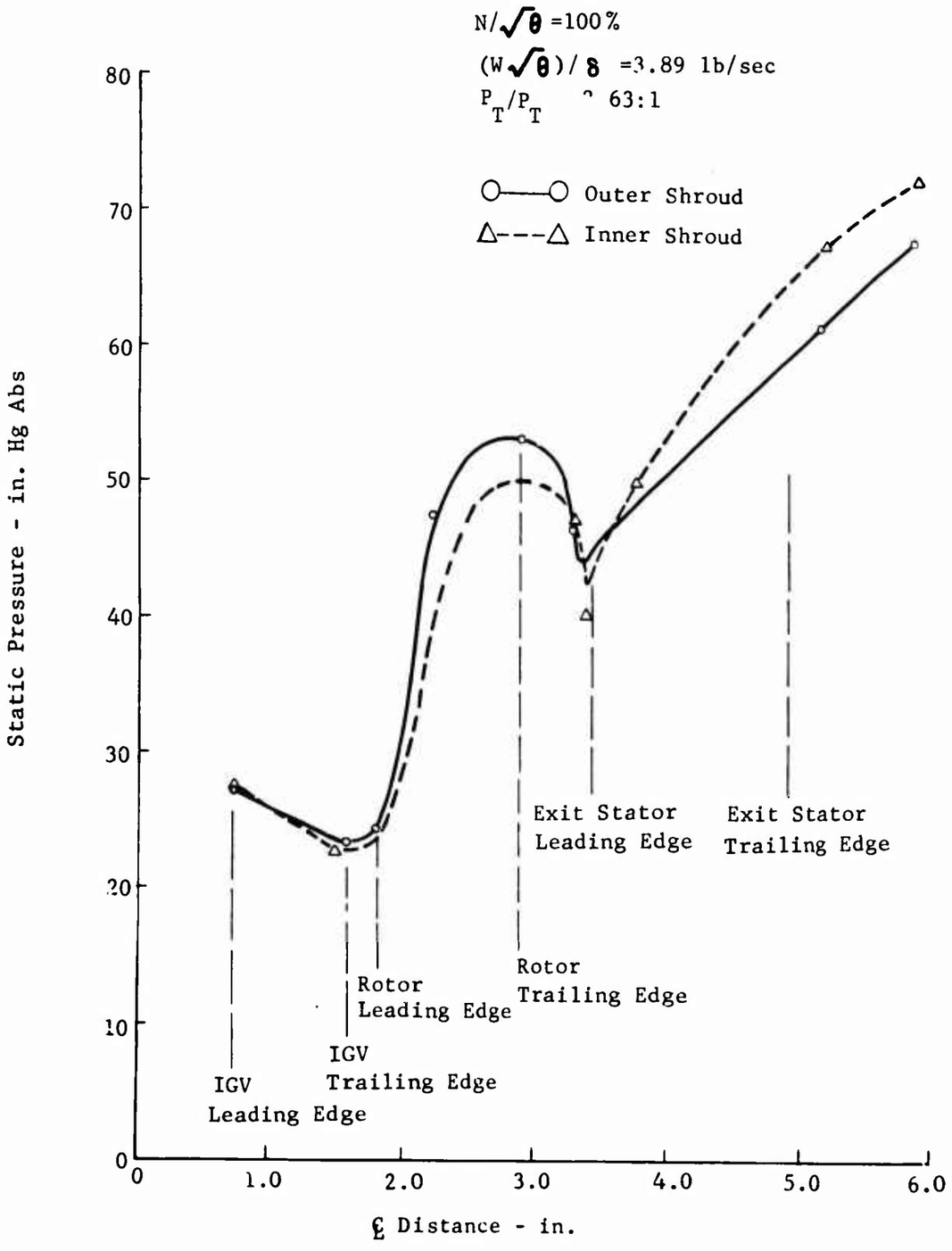

Figure 47. Build 10A Test Data, Static Pressure Distribution Versus Axial Distance Through Compressor.

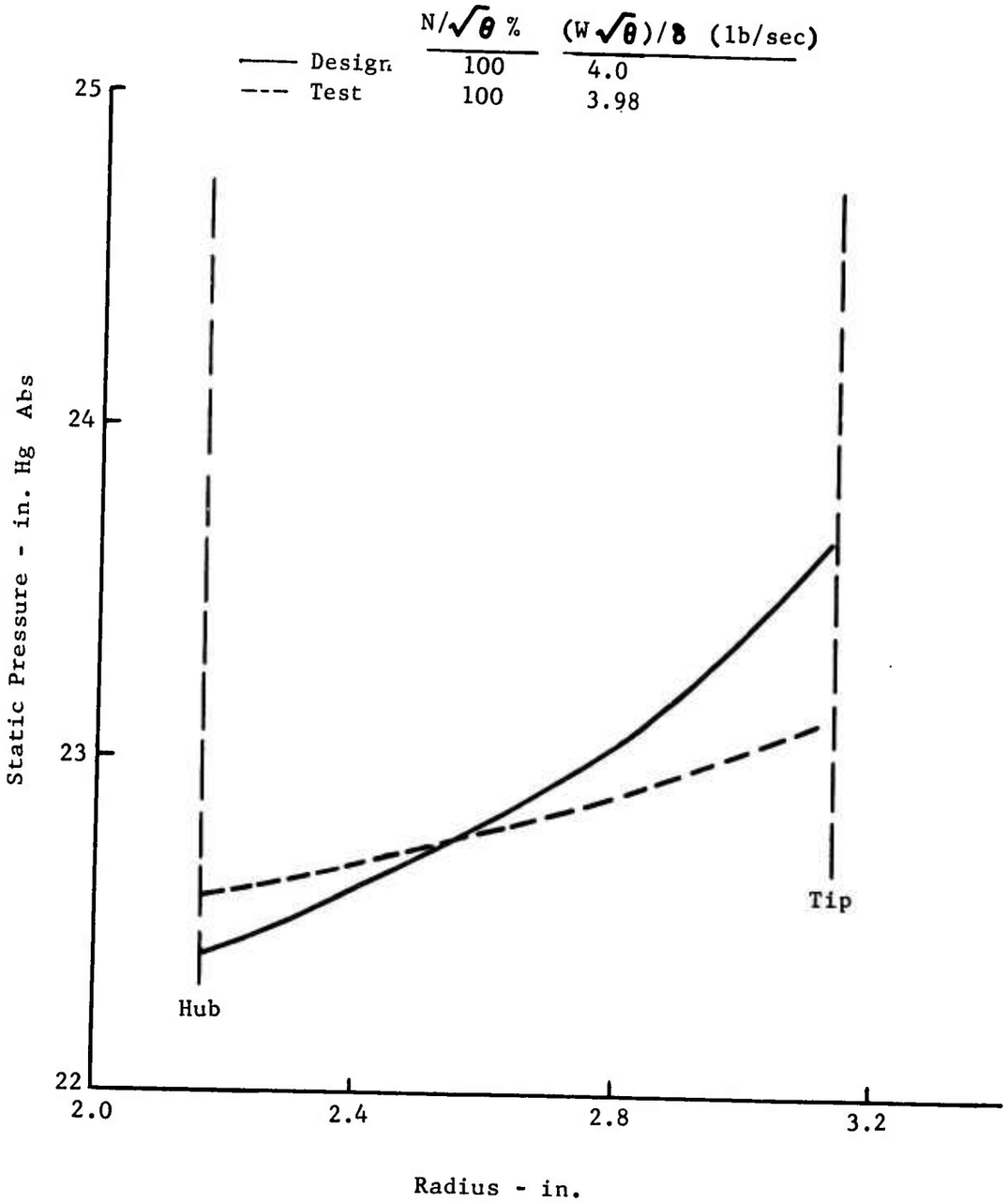

Figure 48. Build 10A Test Data, Static Pressure at IGV Trailing Edge Compared to Design.

percent of the design goal, and the mean static pressure for the test data is very close to the predicted value. The spread in pressure from the inner shroud to the outer shroud is lower for the test data than for the prediction, but this is probably attributable to the local radius of curvature at the shroud walls of the developed airfoil configuration, which is different from the original design.

The static pressure increases slightly at the outer shroud from the IGV trailing edge to the rotor leading edge (Figure 47). The removal of the burr and the proper positioning of the rotor to the shroud corrected the decrease in static pressure experienced in this area in builds 7, 8, and 9.

Rotor Performance

Figures 49, 50, and 51 are the rotor performance maps for builds 10A, 11, and 12. The best design speed rotor performance demonstrated was 2.85:1 pressure ratio at 83.9 percent efficiency, and 3.94 pounds per second airflow in build 11. This performance comes very close to the rotor goals of 2.89:1 pressure ratio, 85.2 percent efficiency, and 4.0 pounds per second airflow. The maximum rotor pressure ratio of 2.91:1 was achieved at the design IGV setting in build 12, but the efficiency was 80.7 percent.

The vector diagrams for build 11 are presented in Figure 52. The angle of the relative rotor inlet vector for this point indicates an average incidence of 3.4 degrees to the measured leading edge expansion surface. This test point is not on the vertical speed line characteristic, and therefore at some part of the leading edge there is a detached shock. On the vertical characteristic, where there is a fully attached shock, the incidence is 0.6 degree lower and is within $\pm$0.5 degree of the 2.3-degree value established in phase I.

The rotor exit absolute Mach numbers are based on the data measured at station 4 and are approximately sonic at the hub and near sonic at the tip. As in the case of builds 7, 8, and 9, the data indicate that the flow accelerates along the outer shroud from a Mach number of 0.85 at the rotor trailing edge to approximately 0.98 at station 4.

The rotor passage total pressure recoveries at the design speed peak pressure ratios for builds 10A and 11 are compared with the design values in Figure 53. The average value is below the goal in both cases. The recovery for build 11 is very close to the design and reflects an efficiency within two points of the design goal. The slightly lower Mach number range for build 11 is due to the lower airflow.

The rotor static pressure ratio is summarized in Table II. The peak design speed static pressure ratio along the outer shroud is in excess of 2.2:1 at the rotor trailing edge in all three builds (10A, 11, and 12), and a maximum of 2.34:1 was demonstrated in build 12 compared to a goal of 2.39:1. The station 4 values are lower at both the outer and inner shroud due to the flow acceleration aft of the trailing edge.

Rotor Configuration 6, Stator Configuration 2

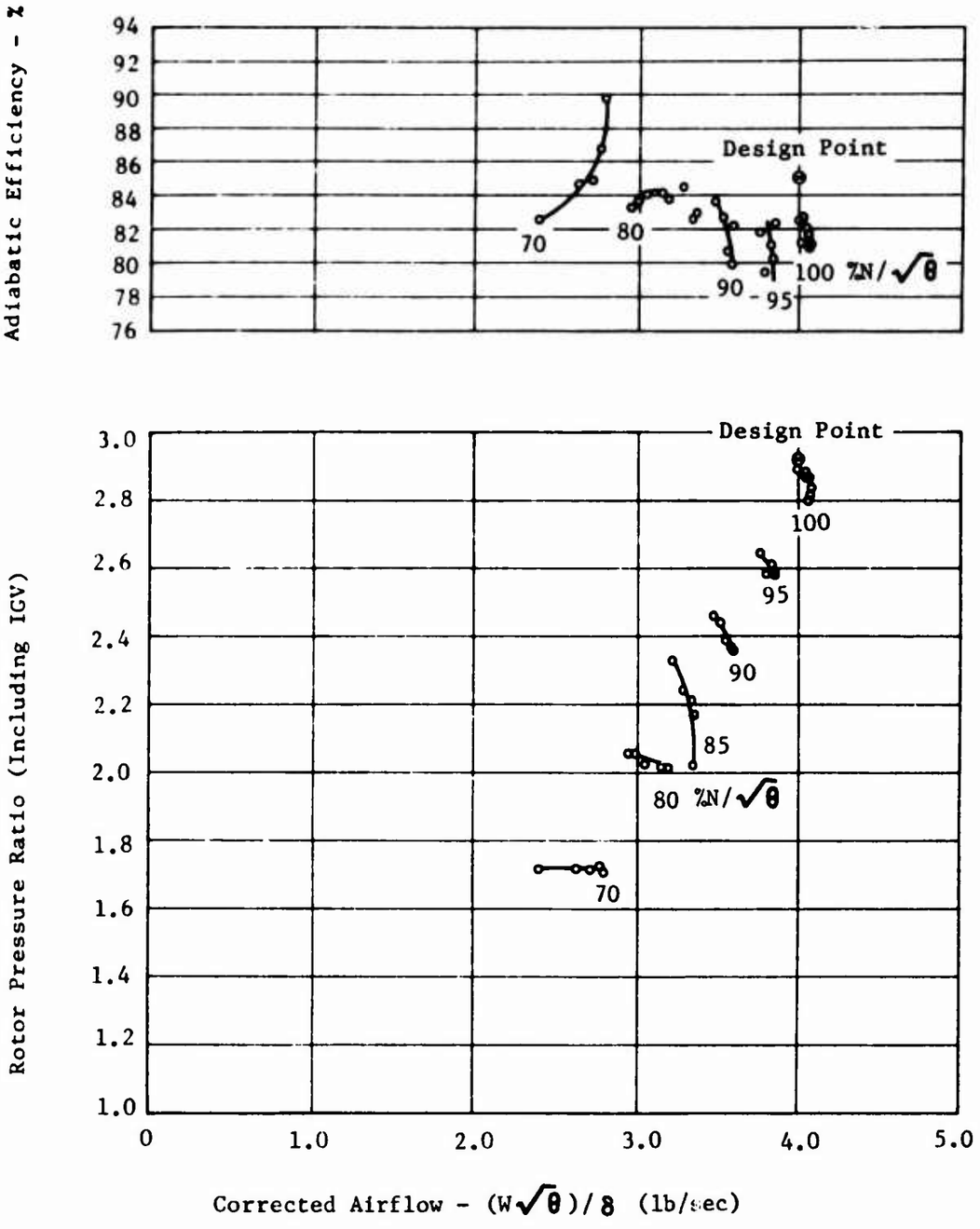

Figure 49. 2.8:1 Supersonic Compressor Stage Test, Build 10A Rotor Performance Data, Developed Airfoil IGV at -4° Setting.

Rotor Configuration 6, Stator Configuration 2

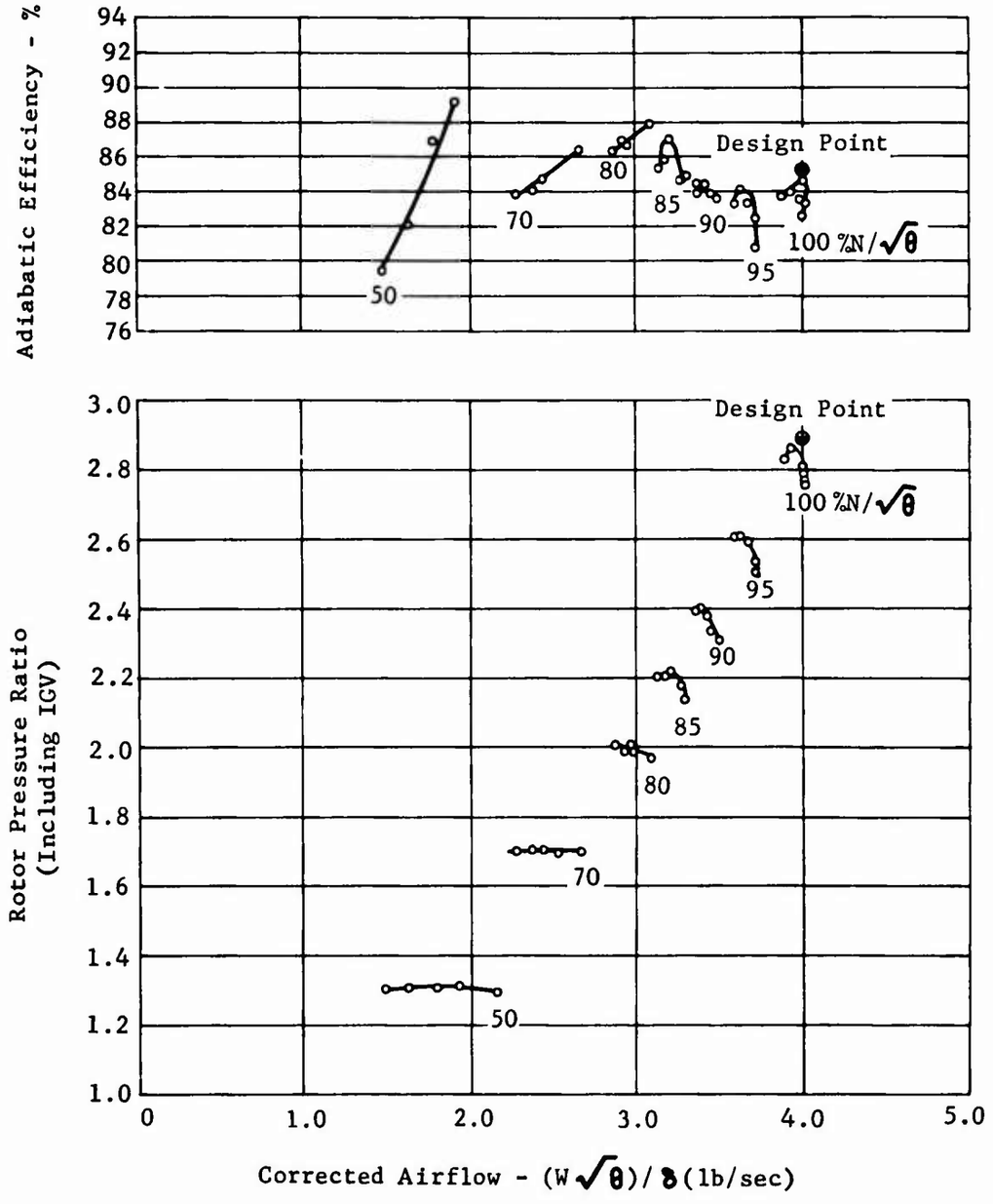

Figure 50. 2.8:1 Supersonic Compressor Stage Test, Build 11 Rotor Performance Data, Developed Airfoil IGV at -7° Setting.

Rotor Configuration 6, Stator Configuration 2

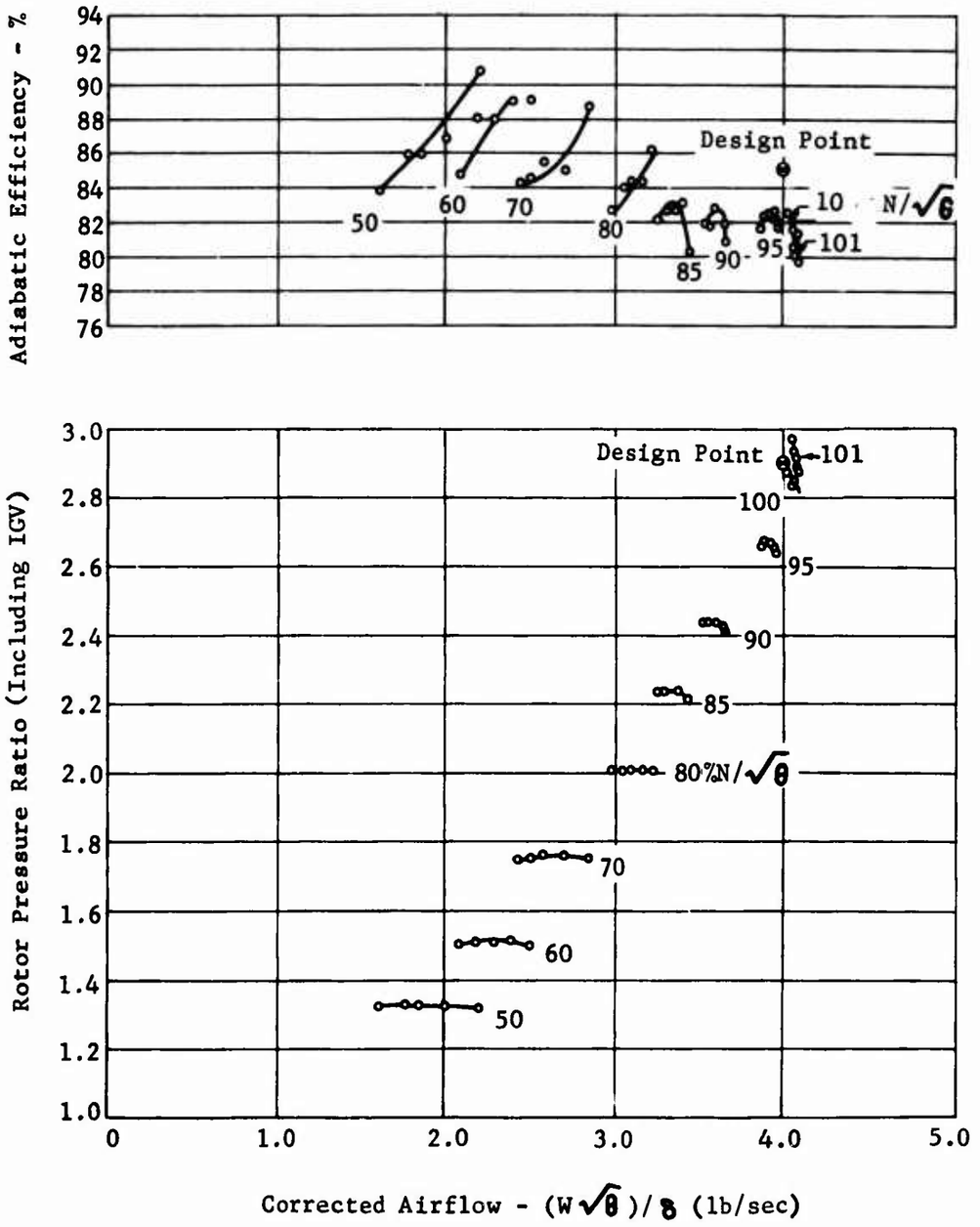

Figure 51. 2.8:1 Supersonic Compressor Stage Test, Build 12 Rotor Performance Data, Developed Airfoil IGV at Design Setting.

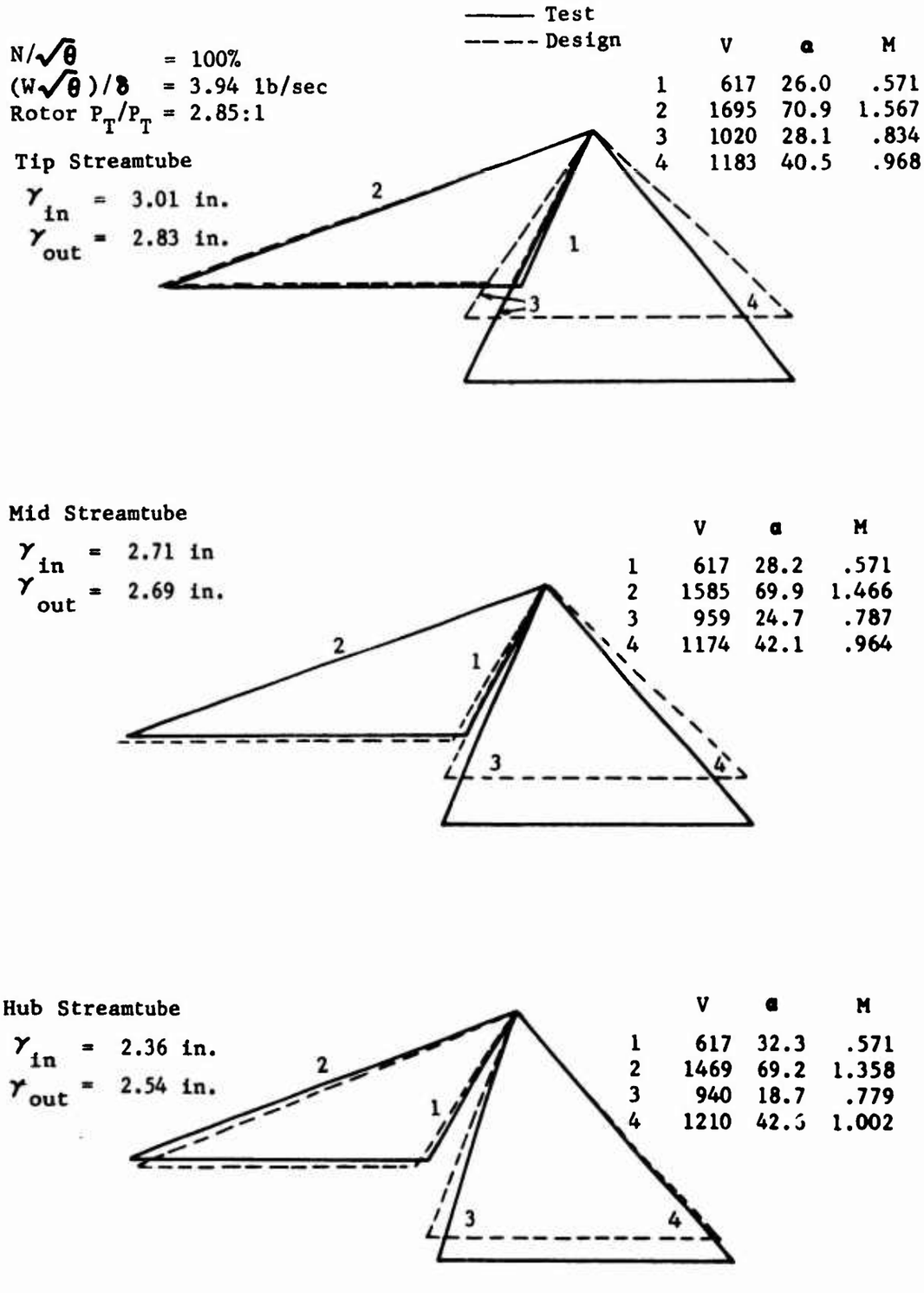

Figure 52. Build 11 Test Data, Vector Diagrams.

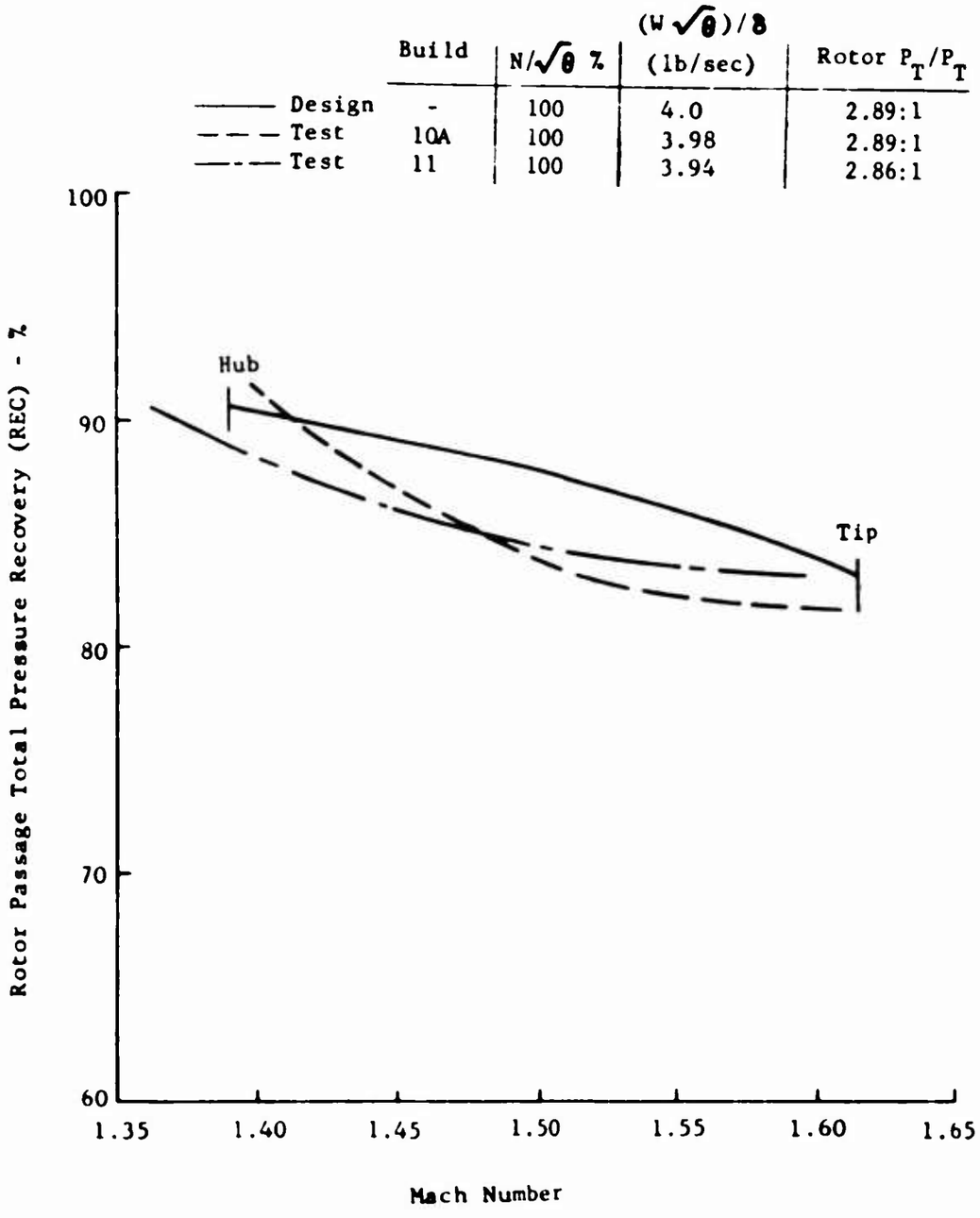

Figure 53. Builds 10A and 11 Test Data, Rotor Passage Total Pressure Recovery.

Exit Stator and Interconnecting Duct Performance

The exit stator and interconnecting duct pressure losses are shown in Figure 54. The results are similar to those of previous builds and do not exhibit a major improvement. The design speed losses at the hub, mid, and tip streamtube are shown in Figure 55 as a function of the stator incidence indicated by the flow angles computed at station 4. These results indicate that the losses have reached a minimum value at each section but are inconsistent with the results from builds 7, 8, and 9. It is known from the static pressure data that the flow continues to accelerate downstream of station 4, and consequently the flow angles computed at station 4 may provide a misleading variation in stator incidence. One inconsistency is that the loss data at the hub section in builds 7, 8, and 9 indicate that the minimum loss occurs at approximately +4 degrees incidence while the data for builds 10, 11, and 12 indicate that it may have occurred at a negative incidence. Another inconsistency is that the losses at the tip section reached as low as under 3 percent in builds 7, 8, and 9, while in builds 10, 11, and 12 they were above 6.5 percent. The inconsistencies and the lack of clear stator and duct loss characteristics are attributed to the conditions which cause the flow acceleration between the rotor and the exit stator. Due to these conditions, the effect of the exit stator modification is not apparent.

The design speed radial Mach number profile for the build 10A data measured at the stage exit (station 5) is shown in Figure 56. The Mach number level is higher than for builds 7, 8, and 9, which is attributed to the increased airflow and the blockage effects of the added instrumentation. The comparable total pressure and total temperature profiles are presented in Figure 57. Figure 58 shows the design speed total pressure profiles through the exit stator blade wakes at the stage exit. The variation in total pressure is $\pm$ 5 percent from the average. The mean total pressures of the blade wake profiles, as established at station 5 from the 9 element rakes, were from 0.5 to 1.0 percent higher than the numerical average of this rake data. These mean values were in agreement with the traversing probe data measured at station 6. The average total pressure at the stage exit was determined as the average of the mean values measured at the hub, mid, and tip sections.

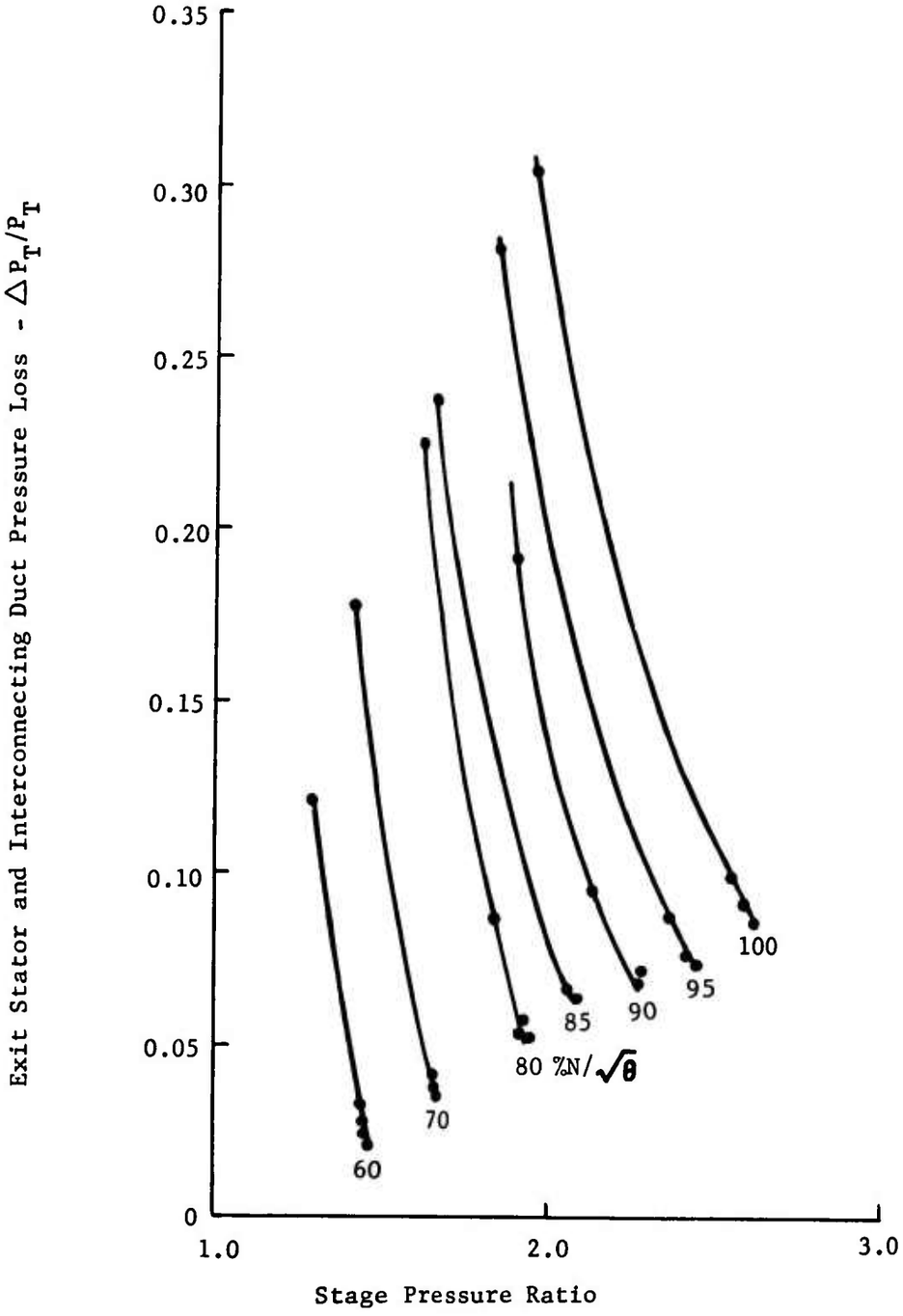

Figure 54. Build 10A test Data, Total Pressure Loss for Exit Stator and Interconnecting Duct.

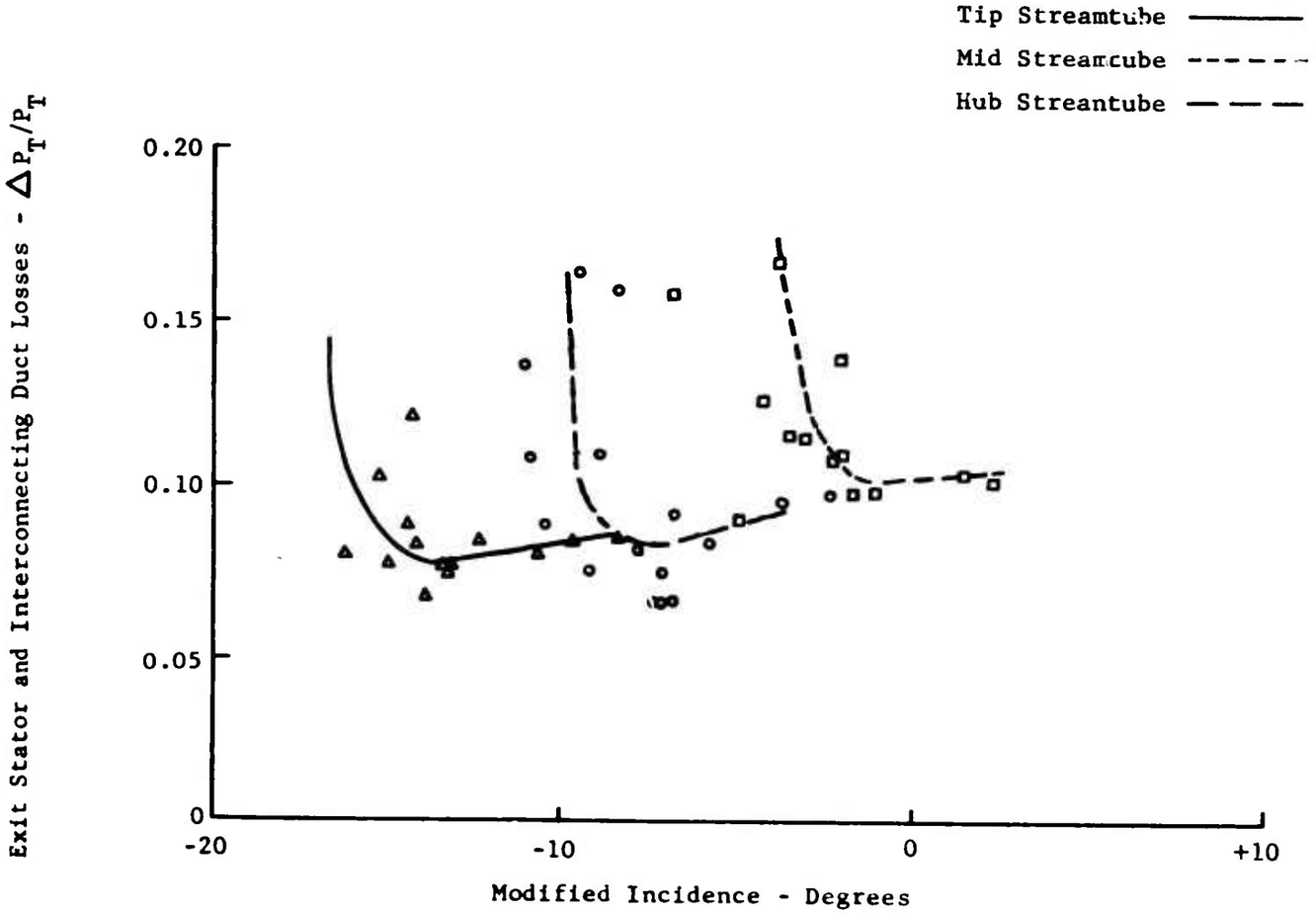

Figure 55. Builds 10A, 11, and 12 Test Data, Exit Stator and Interconnecting Duct Losses Indicated by Stator Entrance Data Measured at Station 4 for $N/\sqrt{\theta}$ = 100 Percent.

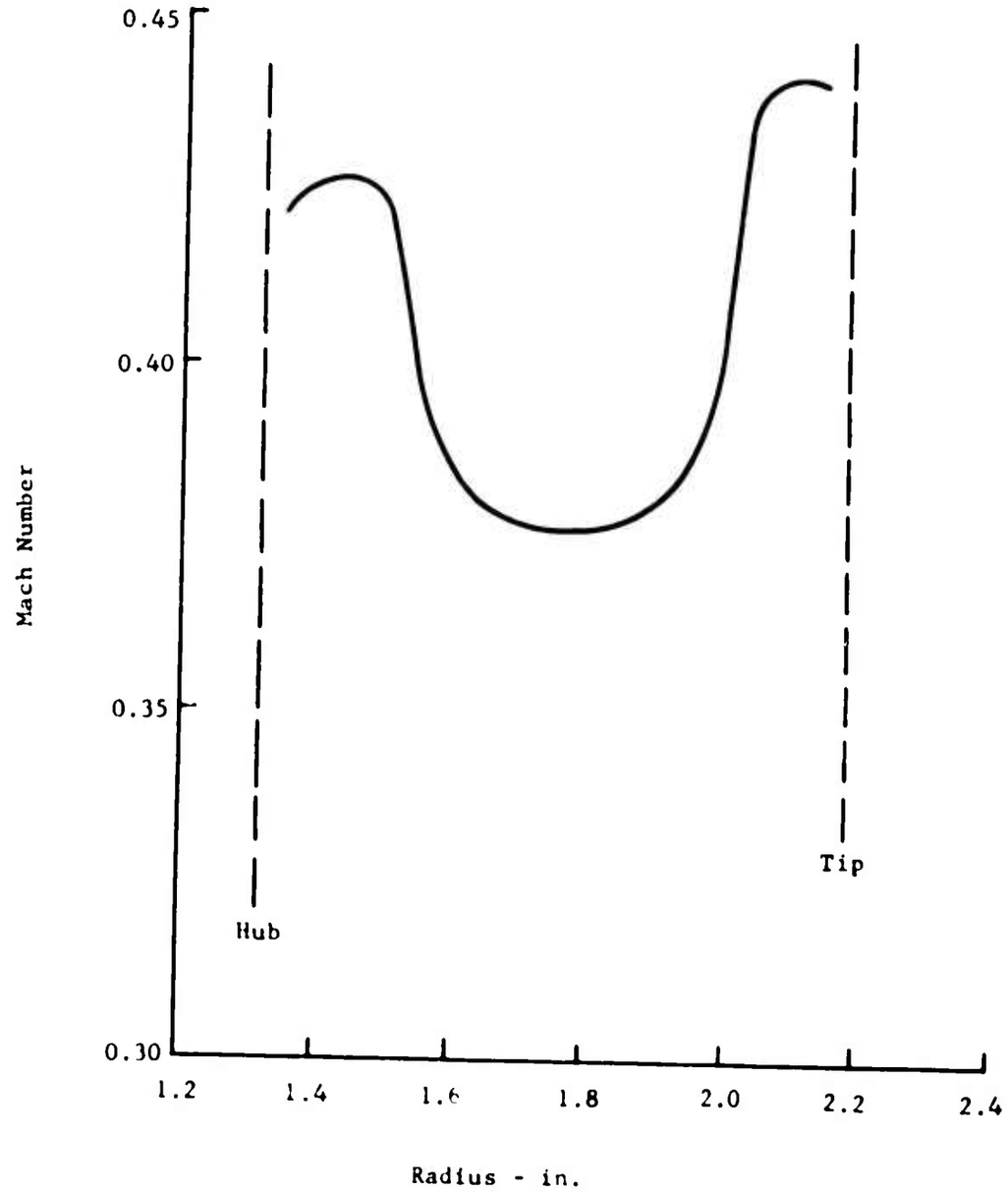

Figure 56. Build 10A Test Data, Mach Number Profile at Stage Exit Station 5 for $N/\sqrt{\theta}$ = 100 Percent, $(W\sqrt{\theta})/\delta$ = 3.98 lb/sec, and P_T/P_T = 2.63:1.

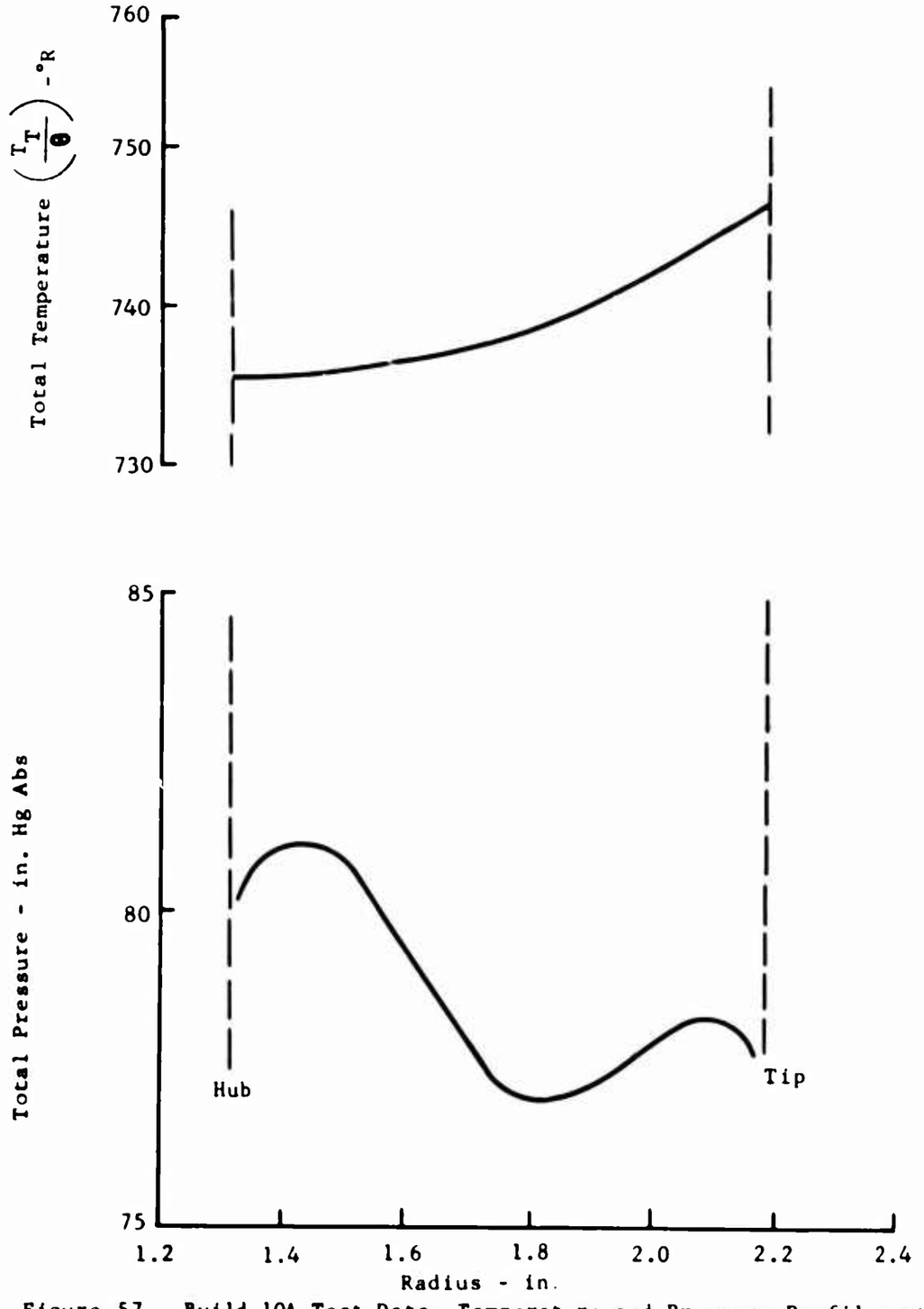

Figure 57. Build 10A Test Data, Temperature and Pressure Profiles at Stage Exit Station 5 for $N/\sqrt{\theta}$=100 Percent, $(W\sqrt{\theta})/\delta$ = 3.98 lb/sec, and P_T/P_T -2.63:1.

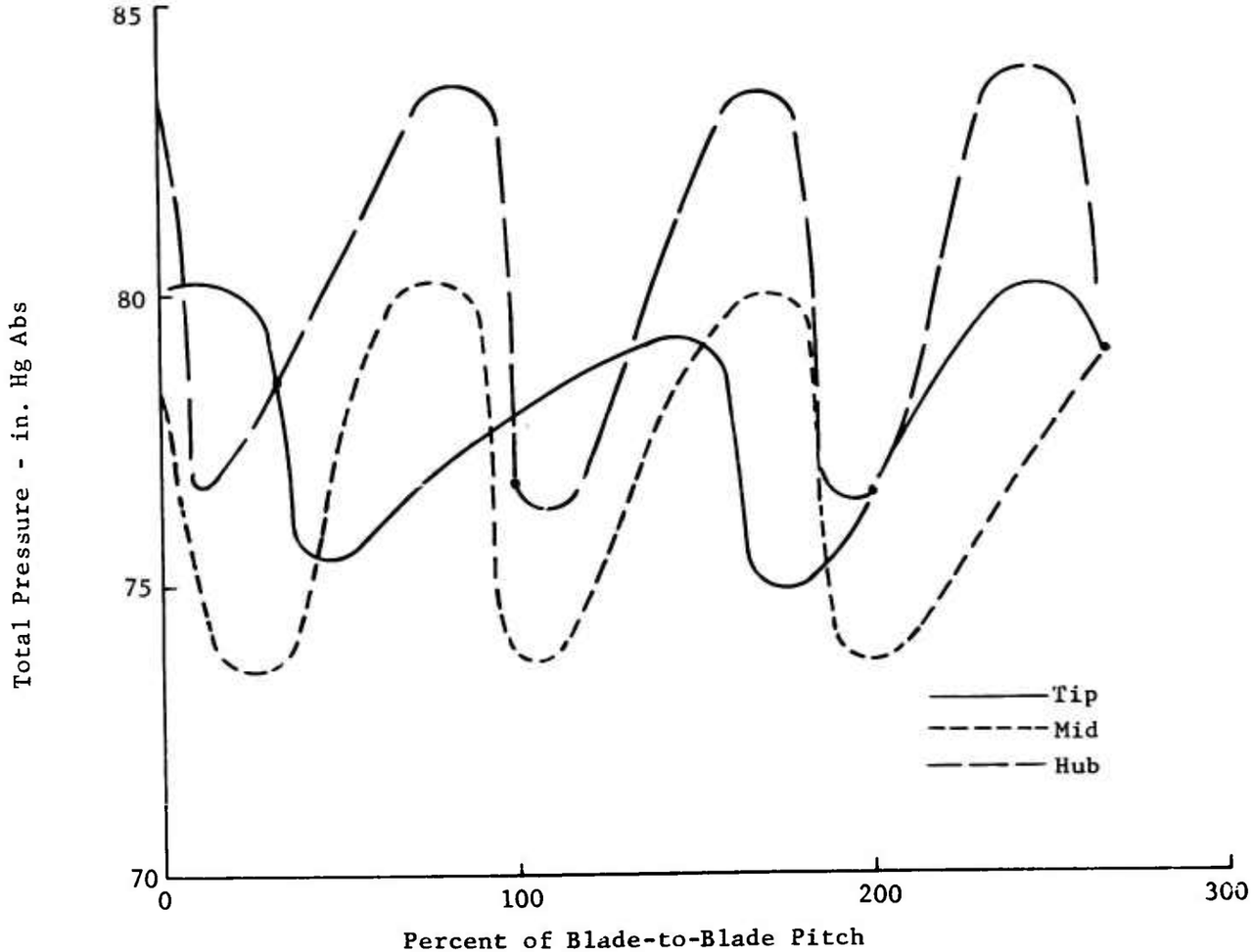

Figure 58. Build 10A Test Data Total Pressure Profile Through Blade Wakes at Stage Exit Station 5 for $N/\sqrt{\theta}$=100 Percent, $(W\sqrt{\theta})/\delta$ =3.98 lb/sec, and P_T/P_T =2.63:1.

REEVALUATION OF THE GAS GENERATOR CYCLE PERFORMANCE

An advanced gas generator engine configuration was defined in Volume I of this report, and its estimated performance for the predicted compressor maps was reported. The compressor for this engine consisted of the 2.8:1 supersonic axial stage and the Boeing RF-1 centrifugal stage.

Under the subject task, the stage performance map demonstrated in build 12 was substituted for the predicted 2.8:1 compressor map, and the engine performance was reevaluated. The performance for all of the other engine components was the same in this analysis as used in the phase I analysis. The peak stage efficiencies demonstrated in builds 10, 11, and 12 were for the most part within 1 point of each other at comparable speeds, and no one build exhibited superior efficiencies over the complete speed range. The build 12 map was expected to provide better part-speed performance and, therefore, was selected for this analysis even though the peak efficiency at design speed was 1 point lower than for build 11. The higher part-speed stage pressure ratios in build 12 were expected to result in better performance.

The engine performance with demonstrated axial stage compressor performance is compared to the results from the phase I analysis in Figure 59. The power at the 100 percent power point is 7.5 percent lower (726 compared to 785) for the demonstrated axial stage performance, and the specific fuel consumption is 6 percent higher (.457 compared to .431). This is due to the lower design speed stage pressure ratio of the demonstrated data (2.69:1 as compared to a predicted 2.8:1) and a lower demonstrated efficiency (73.8 percent compared to a predicted 82.2 percent). At 55 percent power the specific fuel consumption is only 2 percent higher for the case with the demonstrated axial stage performance. The 55 percent power component performance was analyzed to indicate the differences between the match points for the case with the demonstrated data and that with the predicted data. The results show that the overall compressor ratio is higher for the case with the demonstrated data (10.1:1 compared to 9.1:1), the compressor efficiency is lower (76.6 percent compared to 77.1 percent), and the turbine inlet temperature is 200°F lower. The axial stage operating lines are presented in Figure 60 for both the demonstrated data and the predicted data. The demonstrated data show surge-free operation over the full operating range, whereas the predicted data indicated operation in the surge region between 60 and 90 percent speed. This is due to the greater surge margin in the demonstrated data and the more favorable matching conditions. Two other advantages were indicated for the demonstrated data. One was a lower turbine temperature over the part-power operation (Figure 59), and the other was a reduction in the required power turbine stator area variation from 40 percent to 25 percent.

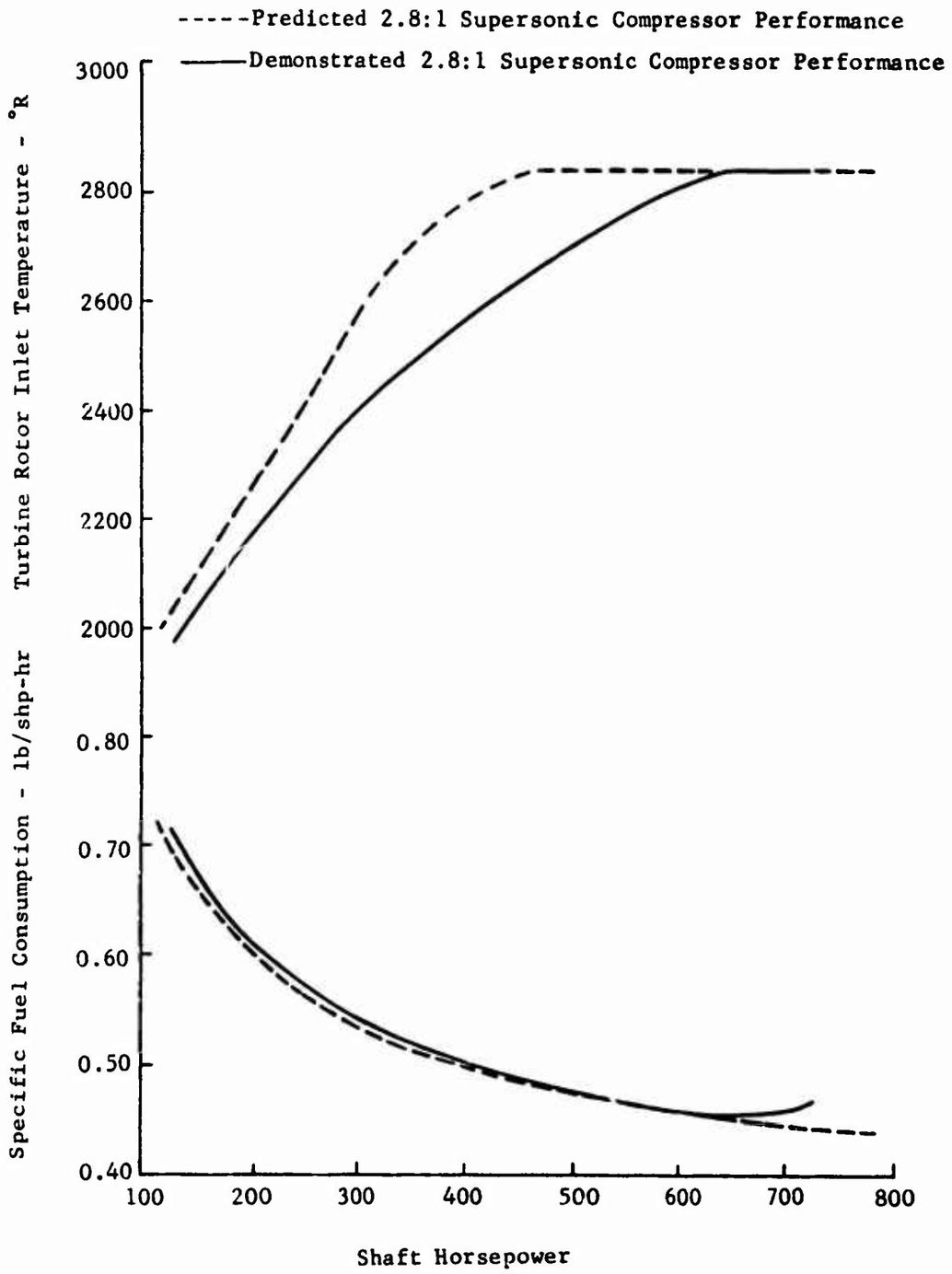

Figure 59. Estimated Engine Performance of Advanced Gas Generator, Results for the Demonstrated Axial Stage Compressor Map Compared With the Predicted.

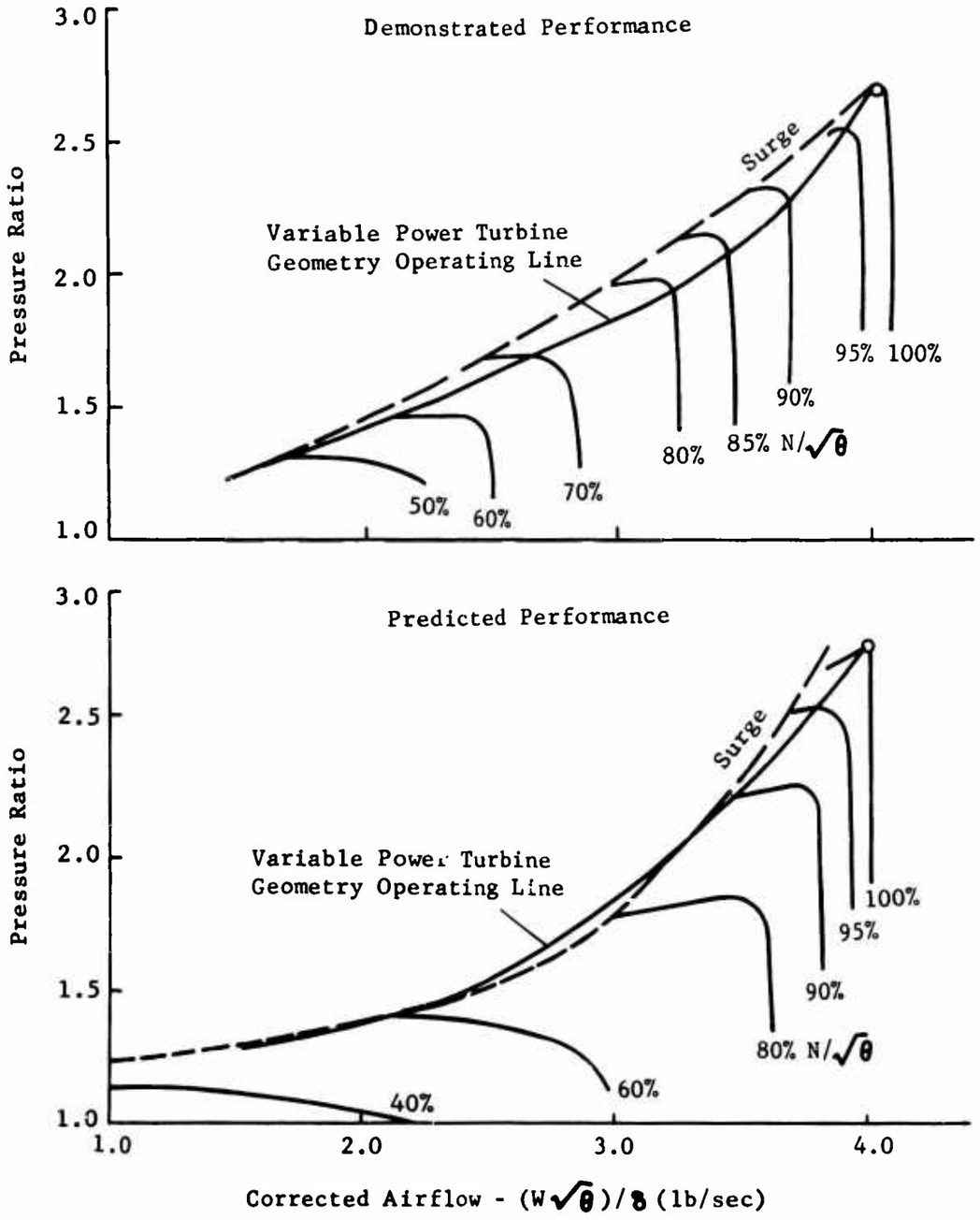

Figure 60. Operating Lines for Axial Boost Compressor Stage of the Advanced Gas Generator Comparing the Demonstrated Boost Stage Performance to the Predicted.

CONCLUSIONS

The analysis of the test results for the stage development phase led to the following conclusions:

1. The rotor and IGV performance demonstrated in this phase was within 1.5 percent of the pressure ratio goal, within 1.5 percent of the efficiency goal, and within 1 percent of the airflow goal and has therefore almost met design performance.

2. The rotor and IGV performance and flow induction capacity were not degraded or limited by the exit stator and interconnecting duct; however, the circumferential uniformity of the flow at the rotor exit was greatly improved by the stator.

3. The lowest demonstrated design speed pressure loss for the exit stator and interconnecting duct is 6.5 percent of the entering total pressure compared to a design goal of 3 percent; this represents the major deficiency in the stage performance.

4. A design speed pressure loss of less than 3 percent of the entering total pressure was measured at the tip section of the exit stator and interconnecting duct in build 9; this indicates that the design goal is feasible.

5. A flow acceleration from the trailing edge of the rotor to the leading edge of the stator prevented a demonstration of the minimum stator and duct losses. The fixed pitot probes are at least in part responsible for this acceleration. A test with no probes at the rotor exit should result in reduced stator and duct losses and improved stage performance.

6. The static pressure rise through the exit stator and interconnecting duct in build 8 indicated a conversion of 85 percent of the velocity head compared to a design goal of 90 percent.

7. The developed airfoil IGV met the design performance better than the NACA 65 series IGV and provided more positive flow control.

APPENDIX I

PHASE III TEST PLAN

OBJECTIVE

The objective of the stage development program is to evaluate the complete stage performance of the 2.8:1 single-stage supersonic compressor design through experimental testing, data analysis, and design modifications. The compressor stage consists of the inlet, inlet guide vanes, rotor, exit stators, and interconnecting duct which matches the inlet of the proposed second-stage centrifugal compressor. The stage performance goals are:

pressure ratio	2.8:1
adiabatic efficiency	82.2%
weight flow	4.0 lb/sec
design speed	50,700 rpm

The compressor rotor developed under Phase II of this program will be utilized in the stage testing.

APPROACH

The inlet guide vane performance for this compressor was established independent of the rotor by a flow test program using an external air supply. The combined inlet guide vane and rotor performance is being developed under Phase II of the program. This development involves experimental performance evaluation and rotor modification necessary to meet the design performance goals. Sufficient experimental data will be established on the finalized rotor configuration to provide the following combined inlet guide vane and rotor performance:

1. Compressor map between 40 and 100 percent speed at the optimum inlet guide vane setting.

2. Compressor maps between 70 and 100 percent speed at two other guide vane settings.

3. Rotor exit temperature, pressure, and flow angle radial traverse profiles at key performance points (peak pressure ratio, peak efficiency, etc.).

The design of the exit stators and interconnecting duct will be finalized based on the results of the Phase II test.

Testing of the complete compressor stage with the inlet guide vanes at design setting will be the initial step in the Phase III test program. Two builds are estimated for this series of tests. A compressor map will be developed between 40 and 100 percent speed for this configuration. Compressor maps for other inlet guide vane settings will be developed between 70 and 100 percent speed. Complete pressure and temperature data will be recorded during the testing.

The data points in the 90-to-100-percent speed range, which represent peak pressure ratio and peak efficiency, will be analyzed to establish vector diagrams that satisfy the experimental data. The experimental vector diagrams will be compared with the design conditions and previously measured inlet guide vane and rotor performance to pinpoint deficient area .

An advanced inlet guide vane will be designed, fabricated, and substituted for the NACA 65 se ies guide vanes. The stage test will be repeated as described above to evaluate the performance with the new guide vanes.

Based on the results of the data analysis, design modifications will be established. Where possible, these modifications will be incorporated in the compressor hardware by machining, blade bending, and similar means. Redesign and new procurement are planned in the event that the required modifications are beyond the limits of reworking the existing hardware. Another series of tests will be conducted and the data analyzed to evaluate the redesigned component or components in the same manner as the first test series. Two builds are estimated for this series.

An experimental map will be developed between 40 and 100 percent speed for the optimum stage configuration. Compressor maps for other inlet guide vane settings will be developed between 70 and 100 percent speed. Radial temperature and pressure profiles will be established at the exit plane of the interconnecting duct for key performance points.

TEST CONFIGURATION

Compressor

1. The compressor build will include the inlet guide vanes, the 2.8:1 pressure ratio rotor, the exit stators, and the interconnecting duct (Figure 61). The compressor will be mounted to and powered by the steam-driven Rover turbine on test stand WX25R.

2. The inlet guide vanes will be set in the zero position (design setting) initially, but repositioning may be required as indicated by the test results.

3. The rotor blade tip clearance will be set at the optimum value based on the Phase II test results. A rotor shroud with an abradable surface is tentatively planned for this testing, pending the final results of its application in the Phase II testing

4. An external air supply will be used to pressurize the cavity between the front oil seal and the rotor labyrinth seal. This pressurization serves to balance the axial forces on the rotor, thereby minimizing bearing loads and providing a pressure differential across the oil seal to eliminate oil leakage.

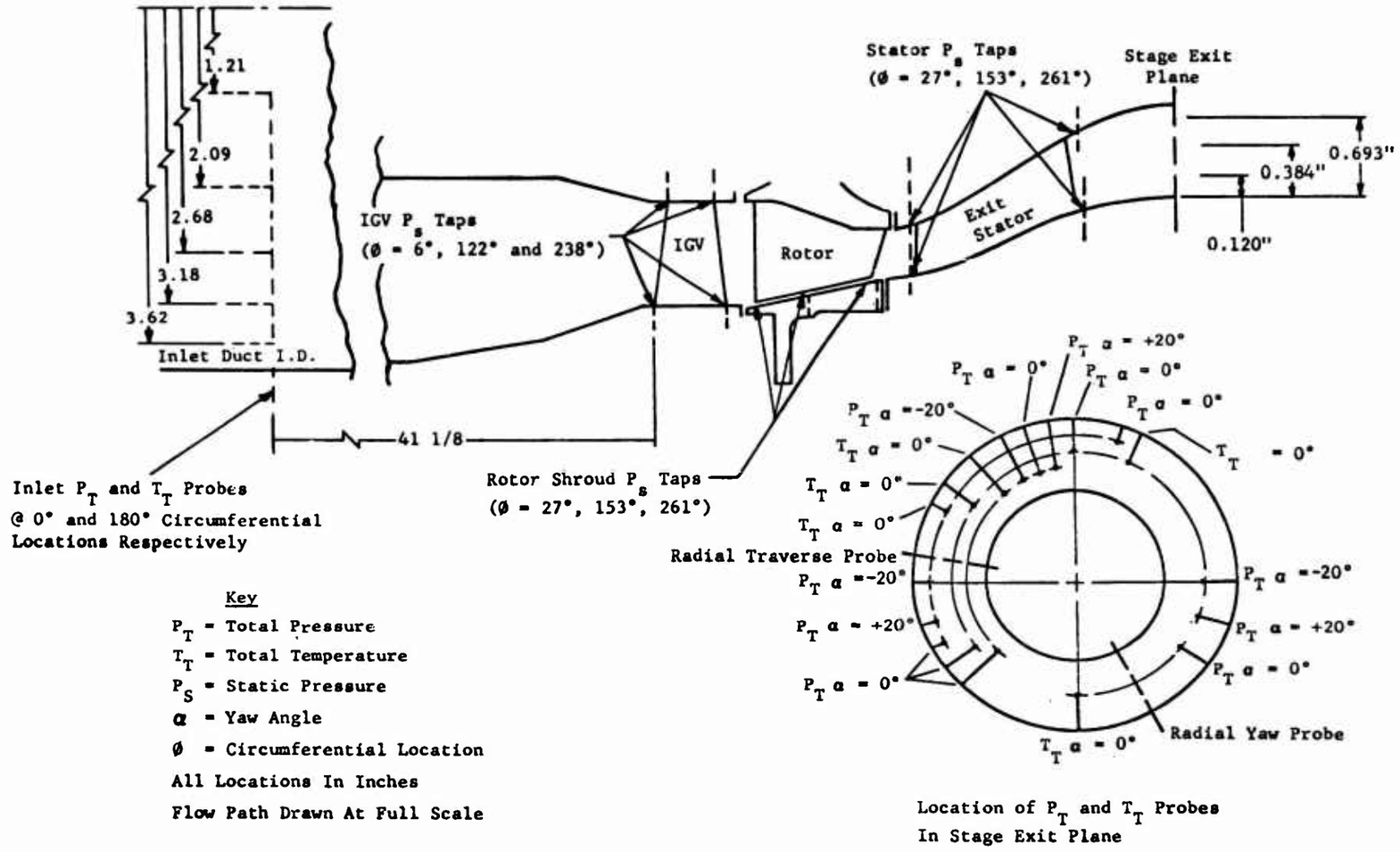

Figure 61. Schematic of Stage Test Pressure and Temperature Instrumentation.

Test Equipment

1. Air Inlet System - The air inlet system consists of an air filter, a calibrated air bottle, a convergent adapter, and approximately 7 feet of straight ducting.

2. Exit Air System - The compressor exit scroll is connected to a close-coupled valve with a divergent adapter. The exhaust air from the close-coupled valve is ducted and dumped into the vertical stack of the steam exhaust system.

3. Turbine Thrust Balance System - Pressurized air is supplied to the downstream side of the turbine balance piston to reduce the thrust load on the bearing. An automatic system maintains the air pressure equal to the stream pressure at the exit of the turbine stator.

4. Oil System - Oil is supplied from a pump to three inlet points on the compressor and turbine at a pressure of 300 psi. The inlet points feed (1) the compressor front bearing, (2) the compressor rear main bearing and turbine front main bearing, and (3) the turbine rear main bearing. The oil from the compressor front main bearing collects in the compressor sump, while the remaining oil collects in the turbine sump. The return oil from both sumps is scavenged with a common pump.

INSTRUMENTATION

Compressor Speed

A magnetic pickup is set to sense 12 lobes on the front compressor shaft nut. The signal is fed into an eput meter for direct rpm readout. The signal is also fed into an oscilloscope, and the rpm is periodically checked against a known frequency calibration signal.

Compressor Airflow

The pressure differential across a standard calibrated air bottle is measured on an inclinometer to determine the compressor airflow. The air bottle is located at the entrance of the compressor inlet air system.

Compressor Pressures

The compressor pressures to be measured include fixed total pressure probes, a traversing yaw probe, and static pressure taps. All of the pressures except those from the traversing probe are recorded on manometer banks, which are photographed. The data from the traversing probe are recorded on X-Y plotters. The locations and ranges of all pressures are detailed in Table VIII.

TABLE VIII. STAGE TEST INSTRUMENTATION

Instrumentation	Location			Operating Range	Quick-Look Board
	Axial	Circumf (deg)	Radial		
5 Inlet Totals (Pressures, Temperatures)	Inlet Duct	0, 180	1.21", 2.09" 2.68", 3.18", 3.62"	-60 to 0 in Hg gage	
Static Pressure in Labyrinth Cav.				-60 to 0 in Hg gage	
3 Statics	Leading Edge IGV	6, 122, 238	Flow Path OD	-60 to 0 in Hg gage	
3 Statics	Leading Edge IGV	6, 122, 238	Flow Path ID	-60 to 0 in Hg gage	
3 Statics	Trailing Edge IGV	6, 122, 238	Flow Path OD	-60 to 0 in Hg gage	1 pressure
3 Statics	Trailing Edge IGV	6, 122, 238	Flow Path ID	-60 to 0 in Hg gage	
3 Statics	Leading Edge-Rotor	40, 166, 274	Flow Path OD	-60 to 0 in Hg gage	
3 Statics	Mid Chord Rotor	27, 153 261	Flow Path OD	0 to 60 in Hg gage	
3 Statics	Trailing Edge-Rotor	14, 140, 248	Flow Path OD	0 to 60 in Hg gage	1 pressure
3 Statics	Leading Edge Exit Stator	27, 153, 261	Flow Path OD	0 to 60 in Hg gage	
3 Statics	Leading Edge Exit Stator	27, 153, 261	Flow Path ID	0 to 60 in Hg gage	
3 Statics	Trailing Edge Exit Stator	27, 153, 261	Flow Path OD	0 to 60 in Hg gage	
3 Statics	Trailing Edge Exit Stator	27, 153, 261	Flow Path ID	0 to 60 in Hg gage	
3 Statics	Stage Exit Plane	27, 153, 261	Flow Path OD	0 to 60 in Hg gage	
3 Statics	Stage Exit Plane	27, 153, 261	Flow Path ID	0 to 60 in Hg gage	
3 Pitot, θ = 0°	Stage Exit Plane	0., 126, 234	0.384" from Flow Path OD	0 to 60 in Hg gage	1 pressure
2 Pitot, θ = 0°	Stage Exit Plane	18, 243	0.120" from Flow Path OD	0 to 60 in Hg gage	1 pressure
2 Pitot, θ = 0°	Stage Exit Plane	225, 343	0.693" from Flow Path OD	0 to 60 in Hg gage	1 pressure
1 Pitot, θ = +20°	Stage Exit Plane	108	0.384" from Flow Path OD	0 to 60 in Hg gage	
1 Pitot, θ = -20°	Stage Exit Plane	90	0.384" from Flow Path OD	0 to 60 in Hg gage	1 Pressure
1 Pitot, θ = +20°	Stage Exit Plane	252	0.120" from Flow Path OD	0 to 60 in Hg gage	1 pressure
1 Pitot, θ = -20°	Stage Exit Plane	270	0.120" from Flow Path OD	0 to 60 in Hg gage	
1 Pitot, θ = +20°	Stage Exit Plane	351	0.693" from Flow Path OD	0 to 60 in Hg gage	
1 Pitot, θ = -20°	Stage Exit Plane	333	0.693" from Flow Path OD	0 to 60 in Hg gage	
3 Total Ic Therms θ = 0°	Stage Exit Plane	22, 180 304	0.384" from Flow Path OD	50°to 500°F	
1 Total Ic Therms θ = 0°	Stage Exit Plane	322	0.693" from Flow Path OD	50°to 500°F	
1 Total Ic Therms θ = 0°	Stage Exit Plane	288	0.120" from Flow Path OD	50°to 500°F	
Traversing Probe (Total Pressure) (Total Temperature) (Yaw Angle)	Stage Exit Plane	279	Variable	0 to 60 in Hg gage 50°to 500°F 30° to -30°	
Traversing Probe (Total Pressure) (Total Temperature) (Yaw Angle)	Stage Exit Plane	152	Variable	0 to 60 in Hg gage 50°to 500°F +30°to -30°	
Traversing Probe Variable (Total Pressure) (Total Temperature) (Pitch Angle)	Stage Exit Plane	Variable 300 -262	0.384" from Flow Path OD	0 to 60 in Hg gage 50°to 500°F +30°to -30°	

1. Inlet Total Pressure - The inlet total pressure is measured by a five-element total pressure rake located in the inlet ducting upstream of the compressor. The probe elements are located at the centers of equal areas along the zero-degree radial position from the duct centerline to the ID.

2. Stage Exit Total Pressure - The stage exit total pressure is measured with an array of fixed total probes and traversing yaw probes. These measurements are made at an axial station which represents the exit plane of the exit stators and interconnecting duct.

   The fixed total probes are positioned at yaw angles of 0°, + 20°, and -20° to cover the possible exit flow angle variation and at three radii which represent the hub, mean, and tip streamtubes. These fixed total probes are distributed uniformly at various circumferential locations.

   The traversing yaw probe senses and automatically aligns the probe along the flow yaw angle and is capable of a continuous traverse from the tip to the hub of the annular passage. During a traverse, the total pressure, yaw angle, and total temperature are recorded on X-Y plotters as a function of radius. Both radial and circumferential traverses will be made.

3. Static Pressures - Static pressure taps are located on the OD and ID of the flow path in the inlet section, at the leading and trailing edges of each of the blade rows, and at the exit plane of the interconnecting duct. Static taps are also located at the leading edge, mid chord, and trailing edge of the rotor shroud. These pressures are measured at each of three equally spaced circumferential locations.

Compressor Temperatures

The compressor temperature instrumentation includes fixed total temperature probes and a traversing total temperature probe. The fixed probe total temperatures are read out from a multiple selector Brown recorder, while the traversing probe temperature is recorded on an X-Y plotter. The detailed locations of the thermocouples are presented in Table VIII.

1. Inlet Total Temperature - The inlet temperature is measured by a five-element total temperature IC thermocouple rake which is located and spaced the same as the inlet total pressure rake.

2. Stage Exit Total Temperature - The stage exit total temperature is measured with an array of fixed total temperature thermocouples and a total temperature thermocouple on the traversing yaw probe. These measurements are made at an axial station which represents the exit plane of the interconnecting duct.

The yaw angles and streamtube locations of the thermocouples are the same as those described for the rotor exit total pressures. A switchbox arrangement permits recording of the exit temperature both as an absolute value and as a temperature rise with respect to the inlet temperature.

The traversing thermocouple is a part of the same traversing yaw probe described for the total pressure.

Vibration

Vibration pickups are located so as to record the vertical and horizontal vibrations at the front compressor support, turbine front support, and turbine rear support. The vibrations are recorded in units of acceleration (g's) since the displacement values are less than 0.1 mil.

Oil Temperatures and Pressures and Flow Rate

The oil temperature is recorded at the inlet and outlet of the compressor rig, and the temperature rise is monitored as an indication of satisfactory bearing operation. The oil flow rates to each of the three rig supply lines are monitored continuously. The pressure differential of calibrated orifices is measured to indicate the flow rates.

Steam Pressure

The steam pressure is recorded upstream of the control valve and at the inlet steam jacket for the turbine.

Blade Stresses

Provisions have been made to incorporate strain gauges on the compressor rotor blades. A slip-ring assembly is available, and an alternate design for incorporating this assembly in the compressor rig has been made. Strain gauges were not included in initial Phase II testing and are not planned for the Phase III testing unless flutter problems are encountered in Phase II.

PRETEST INSPECTIONS

Dimensional Inspection

Dimensional inspection of the hardware is performed prior to and during assembly to establish and check critical dimensions, clearances, and airfoil geometry.

Blade Natural Frequencies

The static natural vibrational frequency of the blades is measured by exciting the blades and calibrating their natural frequency against a known frequency on an oscilloscope. A microphone is used to sense the blade frequency. The result is compared to the predicted value, and the blade flutter analysis is reviewed.

Rotor Balancing

The compressor and turbine rotors and shaft assemblies are balanced to within .001 to .003 ounce-inches at 2500 rpm prior to assembly.

Magnaflux

The compressor rotor is given a Magnaflux inspection prior to assembly.

TEST PROCEDURES

Table IX presents the scheduled test points. The normal test procedure is as follows:

1. All subsystems (such as the oil system and the balance air systems) are started and checked for proper operation prior to opening the steam control valve and starting the compressor.

2. The steam control valve is activated and the compressor speed is brought slowly up to the first test speed with the close-coupled valve for the compressor air system in the wide-open position (maximum airflow). The vibration meter is monitored continuously throughout the test.

3. The inlet temperature is noted after it has stabilized, and the speed is then adjusted to the desired corrected speed ($N/\sqrt{\theta}$).

4. After all instruments are stabilized, a complete set of data is recorded, including a photograph of the manometer banks and full traverse from tip to hub with the traversing yaw probe.

5. A constant speed line is developed by closing the close-coupled valve while maintaining speed, until the next scheduled reduced weight flow is attained. Step 4 is then repeated. Four to five test points are planned for each speed line. The final test point on a given speed line is obtained by closing the close-coupled valve until compressor surge is audible. The weight flow at which surge is first detected is noted, and the close-coupled valve is opened until a weight flow slightly above surge is attained. This point is then taken as the last data point on the speed line.

6. The close-coupled valve is set wide open, and the compressor is then accelerated to the next highest speed. The process is repeated for each of the scheduled speed lines up to 100 percent speed. In the range of 90 to 100 percent speed, where the speed lines are expected to exhibit almost constant weight flow, the constant speed line is developed by closing the close-coupled valve to meet prescribed increments of increased pressure ratio rather than increments of reduced weight flow.

TABLE IX. SCHEDULED TEST POINTS

% Speed	$(W\sqrt{\theta})/\delta$	P/P
40	Wide-open throttle	
	2.0	
	1.5	
	1.2	
	Surge point	
60	Wide-open throttle	
	2.4	
	2.2	
	Surge point	
80	Wide-open throttle	
	3.2	
	2.1	
	Surge point	
90	Wide-open throttle	1.80
		2.1
		2.3
	Surge point	2.5
100	Wide-open throttle	2.08
		2.8
	Surge point	2.90

The above points are estimated based on predicted performance and are intended as a guide. Deviation from predicted performance may require adjustment of the data points to be run.

DATA PRESENTATION

Compressor Map

The standard compressor map in which the adiabatic efficiency and total-to-total pressure ratio are plotted against corrected weight flow for each of the corrected speed lines will be generated and compared to the predicted map. The predicted stage map is presented on Figure 13. This map will be based on the average compressor inlet conditions and the average stage exit conditions (measured at the exit plane of the interconnecting duct). The corrected conditions and efficiency are computed as follows:

$$\text{Corrected weight flow} = (Wa\sqrt{\theta})/\delta$$

where Wa = actual measured airflow in pounds per second

$$\sqrt{\theta} = \sqrt{\frac{T_{inlet}}{T_{reference}}}$$

T_{inlet} = average total temperature at the compressor inlet (°R)

$T_{reference}$ = 519°R

$$\delta = \frac{P_{T_{inlet}}}{P_{T_{reference}}}$$

$P_{T_{inlet}}$ = average inlet total pressure inches of mercury absolute

$P_{T_{reference}}$ = 29.92 inches of mercury absolute

$$\text{Corrected speed} = N/\sqrt{\theta}$$

where N = actual measured speed in revolutions per minute

$\sqrt{\theta}$ = same as above

$$\text{Percent speed} = \frac{(N/\sqrt{\theta} \text{ measured})}{(N/\sqrt{\theta} \text{ design})} \times 100$$

where $(N/\sqrt{\theta})$ measured = same as above

$(N/\sqrt{\theta})$ design = 50,700 rpm

Pressure ratio = P_{T_5} / P_{T_0}

where P_{T_5} = total pressure integrated from hub to tip of the velocity vector leaving the stage exit plane

P_{T_0} = integrated total pressure at the compressor inlet

$$\text{Adiabatic efficiency} = \frac{\Delta H'}{\Delta H} \times 100$$

where $\Delta H'$ = isentropic enthalpy rise for the measured pressure ratio (BTU/lb)

ΔH = actual enthalpy rise based on the average measured total temperature at the compressor inlet (T_{inlet}) and the total temperature of the stage exit velocity integrated from hub to tip (BTU/lb)

Stage Exit Conditions

The following stage exit parameters will be presented as a function of radius from hub to tip:

total pressure
total temperature
Mach number
flow angle with respect to axial

The circumferential pressure profile spanning two exit stator blades at the interconnecting duct exit plane will also be presented.

Vector Diagrams

The velocity vector diagrams representing the inlet and outlet conditions for the inlet guide vanes, rotor, and exit stator will be presented for three streamtube positions and will be compared to the design vector diagrams.

DATA ANALYSIS

A data analysis computer program will be used to construct the streamline paths, mass flow weight pressure ratio, efficiency, and vector diagrams which satisfy the test results. The inputs for this program are the measured inlet and outlet radial profiles of total pressure and total temperature, the measured weight flow, and the compressor geometry. The program computes a solution which satisfies these inputs and radial equilibrium for both tangential velocities and meridional streamline curvature. In addition to the parameters discussed above, numerous other parameters are calculated by the program, such as streamtube diffusion factors, loss coefficients, and incidence and deviation angles.

The data analysis will be run for key test points such as peak pressure ratios and peak efficiencies in the 90-to-100-percent speed range and for any other points which may give some insight into deficiencies in the design. In each case, adjustments will be made to the program inputs until the solution best satisfies all of the measured data (e.g., static pressures and total temperature and pressure profiles). This solution will then be used to analyze deficient areas and to determine which modifications will improve the performance. The compressor design techniques and empirical data will also be reevaluated based on these results.

APPENDIX II
2:1 SUPERSONIC COMPRESSOR

A company-sponsored program to develop a supersonic compressor stage with initial design goals of 2.08:1 pressure ratio, 79 percent adiabatic efficiency, and 4.0 pounds per second airflow was conducted concurrent with the development of the 2.8:1 compressor stage. The design data for the 2:1 compressor is presented in Appendix I of Volume I of this report.

The performance goals for the rotor and IGV for this stage were 2.13:1 pressure ratio and 81.2 percent efficiency. The design pressure ratio of 2.13:1 was met in the initial test of the 2:1 compressor, but the airflow was 11 percent low and the efficiency was 7 to 8 points low. In subsequent builds, the leading edge thickness of the rotor blades, which was from .015 to .020 inch in the first build, was reduced to .005 to .010 inch and the rotor leading edge expansion surface angle was reduced 2.5 degrees. The concentricity of the rotor to the tip shroud was also improved, and the static tip clearance was reduced to .011 to .012 inch, which is projected to provide a .001 to .002-inch dynamic tip clearance at 100 percent speed. The final configuration tested in the rotor development phase produced a 2.15:1 pressure ratio at 82 percent adiabatic efficiency and an airflow 4 percent less than the 4.0-pounds-per-second goal. The airflow was only 2.5 percent below the goal at a 2.09:1 pressure ratio. The average values of rotor exit flow absolute Mach number and angle at these operating points were 0.64 and 45 degrees compared to the goals of 0.53 and 43 degrees respectively. The average static pressure ratio measured across the rotor was 2.06:1 compared to the design value of 2.3:1. The peak rotor passage recoveries demonstrated at design speed for the 2:1 compressor are compared in Figure 62 to the 2.8:1 compressor data and to the design values. Although the hub and tip effects are more extreme than anticipated in the design, the average values agree with the predicted values and the results of the two compressors agree very well. One interesting observation is that the peak passage recoveries for the two compressor rotors have remained essentially constant at approximately the same relative inlet Mach numbers even though the 2.8:1 rotor has a much higher camber and a somewhat higher passage area ratio. This data supports the use of the Mach number recovery curve as a rotor loss design criterion for this type of supersonic compressor when solidity, passage area ratio, and area schedule meet the passage criteria.

The initial stage performance goals for the 2:1 stage were established for an exit stator which would turn the flow to an axial direction at the stage exit. During the course of the program, the plan was changed and the exit stator was designed to match a centrifugal second stage. The stator requirements for this stator were to turn the flow a nominal 18 degrees and to decelerate the flow from the .53 design Mach number to .45. The stage exit annulus area was at a smaller mean diameter than at the rotor exit; therefore, an "S" duct flow path was required. The stage performance goal for the final exit stator and duct design was 2.1:1 pressure ratio at an efficiency of 81 percent. The exit stator and duct loss was estimated to be .8 percent of the total pressure.

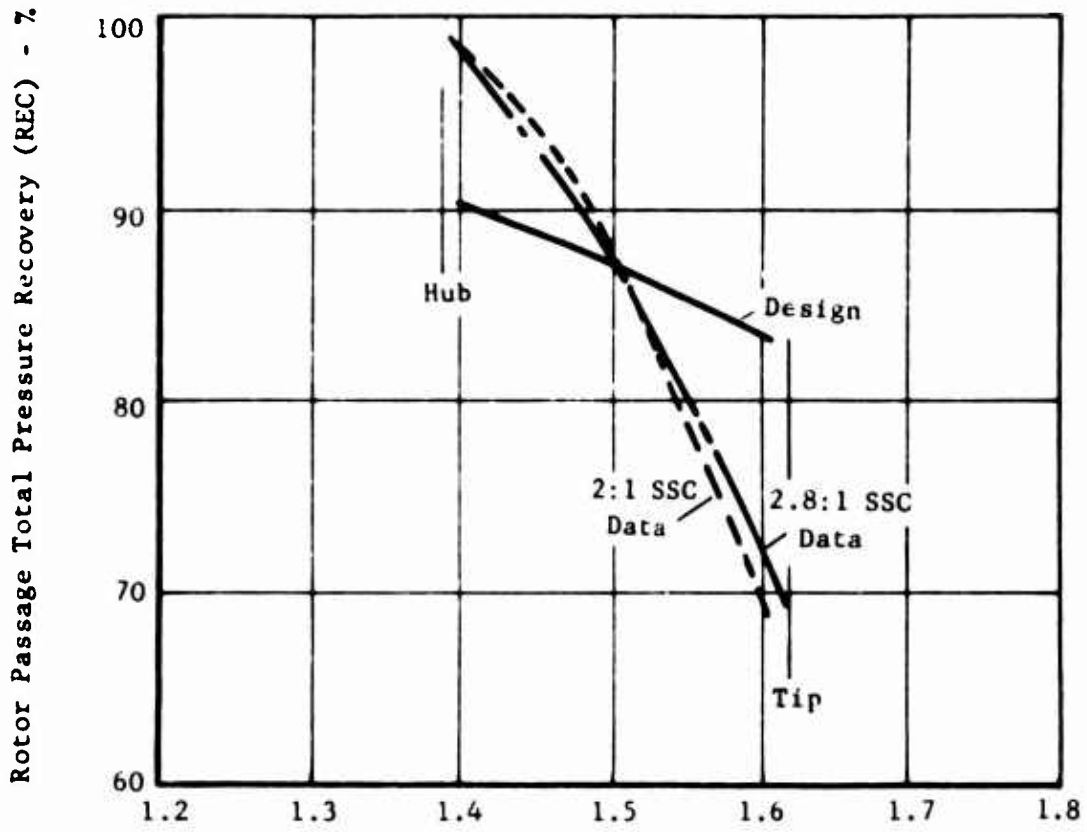

Figure 62. Demonstrated Rotor Passage Total Pressure Recovery for 2:1 and 2.8:1 Compressors Compared to Design Case.

As in the case of the 2.8:1 compressor, the exit stator vanes and integral interstage connecting duct, which forms the passage transition from the rotor exit to the smaller annulus at the centrifugal stage inlet, were designed as a continuous subsonic passage using diffuser criteria. The stator blades were located between the initial and final turns of the meridional "S" duct shape.

Initial stage tests were performed with the NACA 65 series guide vanes which were replaced by the developed airfoil guide vanes in the latter tests. The performance data presented in Figures 63 and 64 are from tests with the developed guide vanes. It was found that the induced airflow and pressure ratio capability with the developed vanes at a -4-degree setting was comparable to that of the NACA 65 series vanes at their design setting. The rotor test data for the design setting are therefore considered to be representative of the -4-degree configuration of the stage test data, which is consistent with the results from the 2.8:1 compressor.

The significant results from the stage data are: (1) the maximum induced airflow at 100 percent speed is not changed by the addition of the exit stator and interconnecting duct; (2) the best stage efficiency was achieved with the guide vanes set at -10 degrees producing at design speed a 2.05:1 stage pressure ratio with 78 percent efficiency;and (3) the highest design speed stage pressure ratio of 2.08:1 with 76 percent efficiency was produced at the guide vane setting of -4 degrees.

The compressor rotor used in these tests was made to the same specifications as the rotor used to develop the final rotor test performance; however, the resultant leading edges of the rotor for the stage test were some .005 inch thicker. The thicker leading edges are considered to be the cause of approximately 2 points degradation in measured rotor efficiency from the rotor test to the stage test. The rotor static pressure ratio increased to 2.16:1, and the exit Mach number reduced to 0.58 in the stage test; this could be explained by the nearly uniform circumferential performance profile.

The combined exit stator and interstage duct losses are shown in Figure 65. The minimum average loss at design speed is 1.6 percent. The hub and tip losses are seen to be higher than the mid-span losses,which at the minimum value met the design goal. The minimum loss for each of the three sections does not occur at the same operating point,suggesting some mismatch of optimum incidence along the span. A static pressure rise equal to 27 percent of the inlet velocity head was measured,which is higher than the design value. This is possible even though the stator exit Mach number is slightly above design,because the rotor static pressure rise was below its design goal and was partially recovered in the stator.

Certain hardware defects such as etch marks on the airfoil surfaces, which resulted from an improper brazing procedure, and a reflex in the airfoil contour along the hub streamline blade section are considered to have contributed significantly to the losses. It is believed that the stator

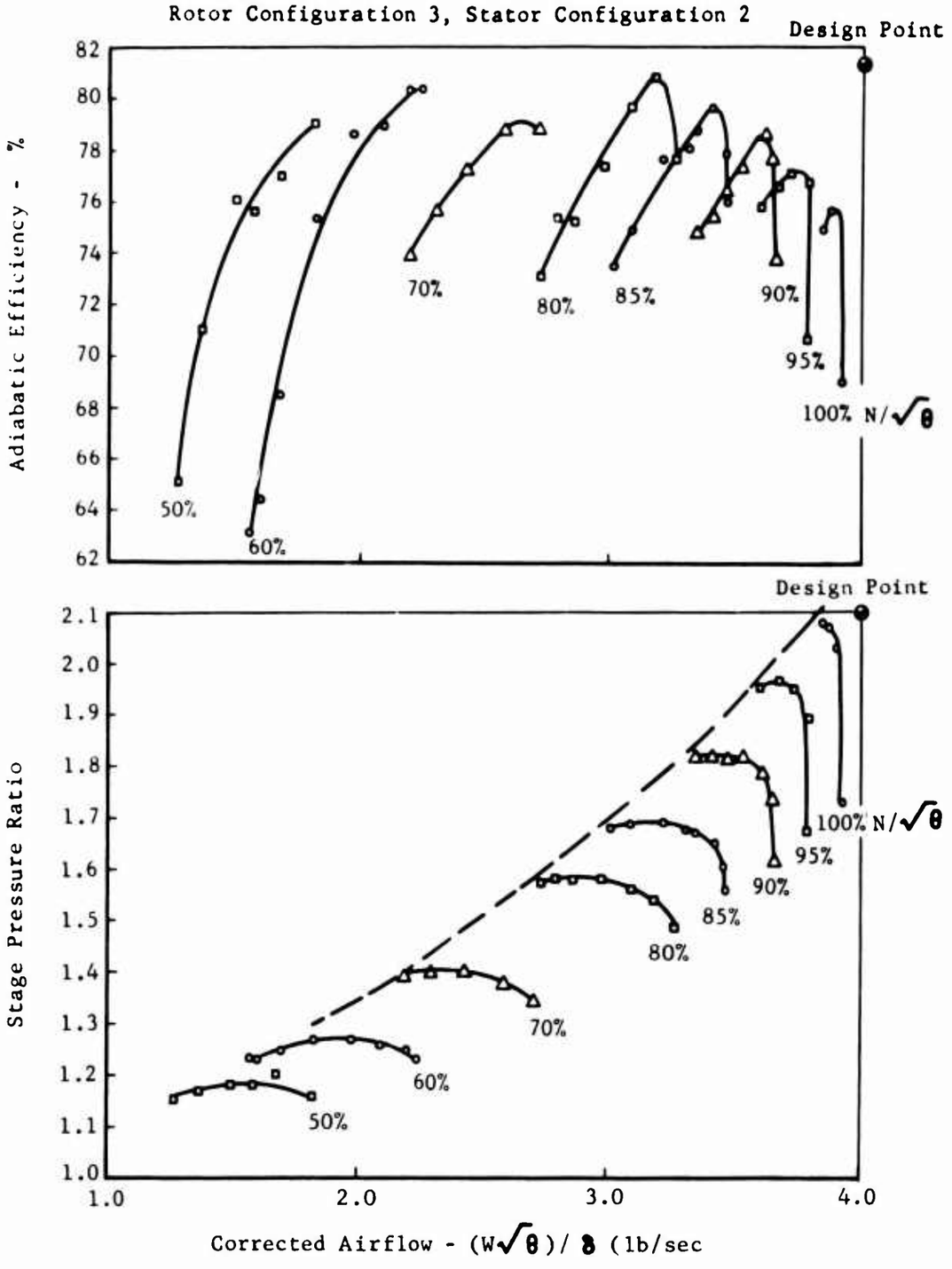

Figure 63. 2:1 Supersonic Compressor Stage Test Performance Map, Developed Airfoil IGV at -4° Setting.

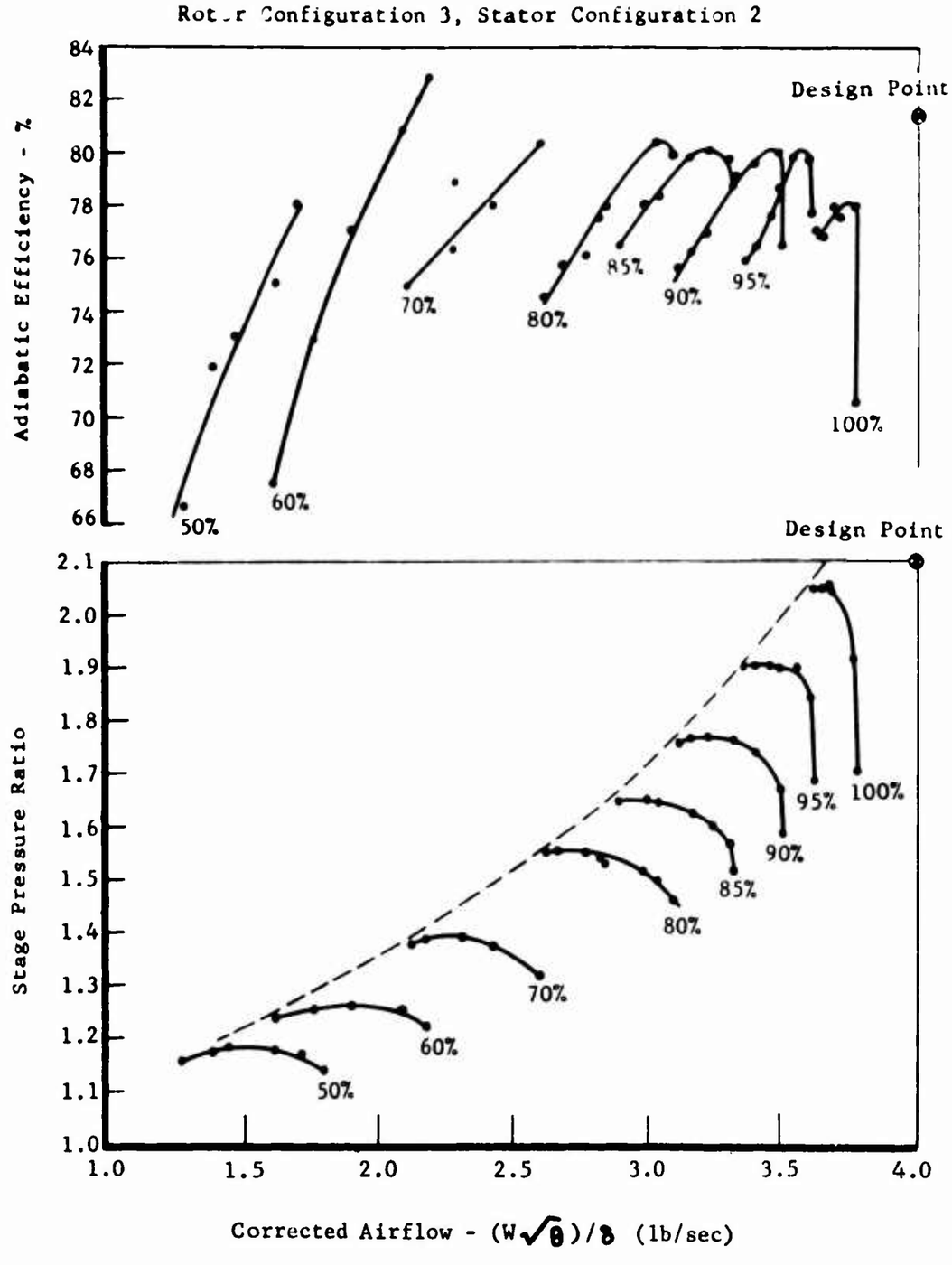

Figure. 64. 2:1 Supersonic Compressor Stage Test Performance Map, Developed Airfoil IGV at -10 Setting.

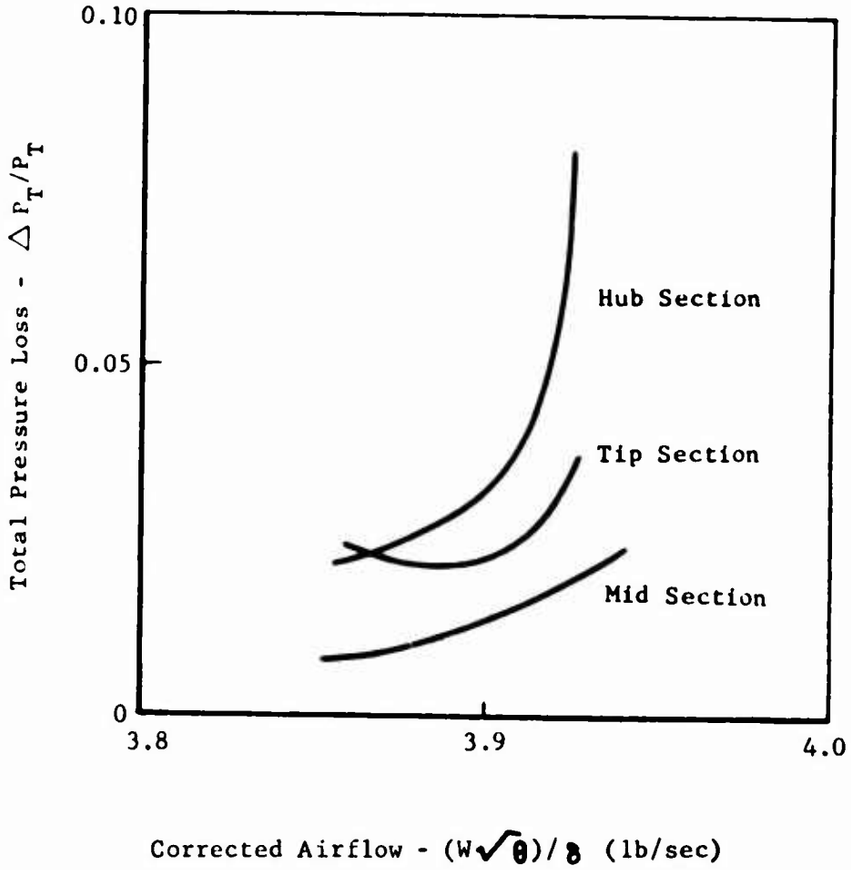

Figure 65. 2:1 Supersonic Compressor Test Data, Exit Stator and Interconnecting Duct Pressure Loss.

loss goals and the overall stage performance goals can be met with the correction of the hardware defects and further development to optimize the aerodynamic matching.

Unclassified
Security Classification

DOCUMENT CONTROL DATA - R & D

(Security classification of title, body of abstract and indexing annotation must be entered when the overall report is classified)

1. ORIGINATING ACTIVITY (Corporate author)	2a. REPORT SECURITY CLASSIFICATION
Curtiss-Wright Corporation Wood-Ridge, New Jersey 07075	Unclassified
	2b. GROUP

3. REPORT TITLE

Single Stage Axial Compressor Component Development for Small Gas Turbine Engines
Volume III - Supersonic Compressor Stage Development

4. DESCRIPTIVE NOTES (Type of report and inclusive dates)

Final Report Volume III January 1967 - December 1968

5. AUTHOR(S) (First name, middle initial, last name)

Charles H. Muller, Leslie R. Cox

6. REPORT DATE	7a. TOTAL NO. OF PAGES	7b. NO. OF REFS
June 1969	125	2

8a. CONTRACT OR GRANT NO.	9a. ORIGINATOR'S REPORT NUMBER(S)
DA44-177-AMC-392(T) b. PROJECT NO. Task 1G162203D14413 c.	USAAVLABS Technical Report 68-90C
	9b. OTHER REPORT NO(S) (Any other numbers that may be assigned this report) Curtiss-Wright 68-050166.F

"This document is subject to special export controls, and each transmittal to foreign governments or foreign nationals may be made only with prior approval of US Army Aviation Material Laboratories, Fort Eustis, Va. 23604."

11. SUPPLEMENTARY NOTES	12. SPONSORING MILITARY ACTIVITY
Volume III of a 3-volume report	U.S. Army Aviation Materiel Laboratories Fort Eustis, Virginia

13. ABSTRACT

This report describes the development of the complete stage for the 2.8:1 supersonic axial compressor design. The performance of the overall stage including the exit stators and interconnecting duct was evaluated through experimental testing with the rotor and inlet guide vanes developed under the previous phase of this program. The experimental results are analyzed and compared with the design data and criteria for each of the blade rows as well as the overall stage. The demonstrated rotor performance improved from that measured in the rotor development phase and nearly met the design goals. The demonstrated performance of the exit stator and interconnecting duct was very encouraging but requires further development to meet the design goals. The overall demonstrated stage performance was 2.62:1 pressure ratio at 74.7 percent adiabatic efficiency.

DD FORM 1 NOV 68 1473 REPLACES DD FORM 1473, 1 JAN 64, WHICH IS OBSOLETE FOR ARMY USE.

Unclassified
Security Classification

14 KEY WORDS	LINK A		LINK B		LINK C	
	ROLE	WT	ROLE	WT	ROLE	WT
Compressor Research and Development						
Supersonic Compressors						
Small Gas Turbine Technology						